BRNO UNIVERSITY OF TECHNOLOGY

VYSOKÉ UČENÍ TECHNICKÉ V BRNĚ

FACULTY OF ELECTRICAL ENGINEERING AND COMMUNICATION

FAKULTA ELEKTROTECHNIKY
A KOMUNIKAČNÍCH TECHNOLOGIÍ

DEPARTMENT OF TELECOMMUNICATIONS

ÚSTAV TELEKOMUNIKACÍ

MAPPING AND ANALYZING SIGNAL COVERAGE IN 4G/5G MOBILE NETWORKS

MAPPING AND ANALYZING SIGNAL COVERAGE IN 4G/5G MOBILE NETWORKS

MASTER'S THESIS
DIPLOMOVÁ PRÁCE

AUTHOR
AUTOR PRÁCE

Bc. Michal Baránek

SUPERVISOR
VEDOUCÍ PRÁCE

doc. Ing. Ladislav Polák, Ph.D.

BRNO 2024

BRNO UNIVERSITY OF TECHNOLOGY
FACULTY OF ELECTRICAL ENGINEERING AND COMMUNICATION

Master's Thesis

Master's study programme **Communications and Networking (Double-Degree)**

Department of Telecommunications

Student: Bc. Michal Baránek ***ID:*** 219836

Year of study: 2 ***Academic year:*** 2023/24

TITLE OF THESIS:

Mapping and analyzing signal coverage in 4G/5G mobile networks

INSTRUCTION:

In the theoretical part of the work, present an overview of the principles and capabilities associated with the measurement, mapping, and coverage analysis in 4G/5G mobile networks. Develop a portable measurement setup employing appropriate hardware and software tools to assess coverage in both indoor and outdoor environments. Propose a procedure for long-term collection and processing of data. Conduct a review of algorithms applicable to the collected data, aiming to construct a coverage map for the measured area. In the experimental part of the work, carry out extensive measurement campaigns to evaluate indoor and outdoor coverage by a mobile signal, considering various transmission and environmental conditions (e.g., the impact of the time of day on network load). Perform a quantitative analysis of the coverage in 4G/5G mobile networks based on the collected data. Prepare a laboratory assignment focused on analyzing the coverage of 4G/5G mobile networks and provide a sample solution for the proposed task.

REFERENCE:

[1] RAIDA, Vaclav, Philipp SVOBODA a Markus RUPP. Real World Performance of LTE Downlink in a Static Dense Urban Scenario - An Open Dataset. In: GLOBECOM 2020 - 2020 IEEE Global Communications Conference [online]. IEEE, 2020, s. 1-6 [cit. 2023-05-13]. ISBN 978-1-7281-8298-8. Dostupné z: doi:10.1109/GLOBECOM42002.2020.9348204

[2] EL-SALEH, Ayman A. and et al. Measurements and Analyses of 4G/5G Mobile Broadband Networks: An Overview and a Case Study. Wireless Communications and Mobile Computing [online]. 2023, 1-24 [cit. 2023-05-13]. ISSN 1530-8677. Dostupné z: doi:10.1155/2023/6205689

Assignment deadline: 5. 2. 2024 ***Submission deadline:*** 21. 5. 2024

Head of thesis: doc. Ing. Ladislav Polák, Ph.D.

Co-supervisor: Olga Galinina

doc. Ing. Jiří Hošek, Ph.D.
Chair of study program board

ABSTRACT

This thesis addresses the enhanced measurement of signal coverage, capacity, and reliability in mobile networks, particularly with the growing prevalence of 4G and 5G technologies. Given the escalating importance of these networks in everyday activities, there arises a demand for open-source solutions to evaluate and enhance their performance effectively. The objective of the research, provided in this thesis, is to analyze gathered data to pinpoint areas necessitating network enhancements and to develop open-source software and hardware solutions for extracting essential performance metrics (KPIs) from 4G/5G networks. The proposed system offers an interface for assessing network performance and signal coverage, enabling cost-efficient measurements across diverse environments.

KEYWORDS

coverage mapping, fourth-generation (4G), fifth-generation (5G), key performance indicators (KPIs), mobile networks, machine learning (ML), interpolation, data analysis

BARÁNEK, Michal. *Mapping and analyzing of signal coverage of 4G/5G mobile networks*. Master's Thesis. Brno: Brno University of Technology, Faculty of Electrical Engineering and Communication, Department of Telecommunications, 2024. Advised by doc. Ing. Ladislav Polák, Ph.D.

Author's Declaration

Author:	Bc. Michal Baránek
Author's ID:	219836
Paper type:	Master's Thesis
Academic year:	2023/24
Topic:	Mapping and analyzing of signal coverage of 4G/5G mobile networks

I declare that I have written this paper independently, under the guidance of the advisor and using exclusively the technical references and other sources of information cited in the paper and listed in the comprehensive bibliography at the end of the paper.

As the author, I furthermore declare that, with respect to the creation of this paper, I have not infringed any copyright or violated anyone's personal and/or ownership rights. In this context, I am fully aware of the consequences of breaking Regulation § 11 of the Copyright Act No. 121/2000 Coll. of the Czech Republic, as amended, and of any breach of rights related to intellectual property or introduced within amendments to relevant Acts such as the Intellectual Property Act or the Criminal Code, Act No. 40/2009 Coll. of the Czech Republic, Section 2, Head VI, Part 4.

Brno .....

.....
author's signature*

*The author signs only in the printed version.

ACKNOWLEDGEMENT

I would like to express my sincere gratitude to Doc. Ing. Ladislav Polák, Ph.D., for his invaluable guidance and support throughout the entire research process. His insightful comments, constructive feedback, and unwavering commitment to excellence have played a crucial role in shaping this thesis. I am truly fortunate to have had such a dedicated and knowledgeable mentor.

I would also like to extend my heartfelt thanks to Ing. Jan Kufa, Ph.D., who served as a technical consultant for this work. His expertise and thoughtful input greatly enhanced the technical aspects of the research. His willingness to share his knowledge and provide valuable insights has been instrumental in the development of this thesis.

Additionally, I am deeply grateful to my co-supervisor, Olga Galinina, Ph.D., for her support and valuable guidance.

I appreciate the collaborative efforts of all my mentors, whose mentorship and technical guidance have been a source of inspiration. Their contributions have significantly enriched the quality of this work, and I am thankful for the opportunity to benefit from their wisdom and expertise.

Contents

List of Figures

List of Tables

Introduction

The exponential growth in the number of mobile users has brought the buzzwords '4G' and '5G' into people's everyday lives. As these networks gain popularity, understanding aspects such as signal coverage, capacity, and reliability becomes crucial for performance optimization and seamless connectivity. Thus, this thesis delves into the complex world of mobile network coverage analysis, focusing on the extensively utilized 4G and rapidly expanding 5G technologies.

The core of this work lies in the experimental evaluation of indoor and outdoor coverage provided by mobile networks, considering various transmission and environmental conditions. We meticulously designed a novel measurement setup comprising a 4G/5G module, a processing unit, and a custom-built application for controlling and configuring measurements. This setup, independent of any third-party application, grants us flexibility and allows for individual settings of visualization and data manipulation. We conducted extensive measurement campaigns, encompassing both static indoor and mobile outdoor tests. Static indoor tests focused on assessing network performance within a university dormitory, examining the impact of time of day and occupancy levels on network load and signal quality. Mobile outdoor measurements, utilizing various modes of transportation, spanned a significant area of the city of Brno, capturing real-world coverage scenarios across different LTE bands and 5G NR NSA Band 78.

We performed a quantitative analysis of the collected data, employing various processing methods and algorithms to extract valuable insights. We explored the use of machine learning algorithms to predict future network load based on historical data, demonstrating the potential of these techniques for proactive network management. Furthermore, we employed different interpolation methods to estimate the coverage maps for each measured band. We meticulously compared these methods, evaluating their strengths and weaknesses, and compared our estimated coverage maps with official estimates provided by the Czech Telecommunication Office (CTO).

This comprehensive analysis allowed us to unveil interesting patterns in network performance, highlighting the dynamic nature of coverage influenced by various factors, such as time of day, network load, building structures, mode of transportation, and the inherent propagation characteristics of different frequency bands. We identified areas with consistently good coverage, as well as those with signal degradation and potential outages. This nuanced understanding of coverage dynamics provides valuable insights for network operators, enabling them to optimize network performance, prioritize resource allocation, and enhance the quality of service for users.

The thesis is organized into six main chapters. The first chapter provides a brief overview of 4G and 5G mobile networks, focusing on the Physical Layer (PHY) and the Radio Access Network (RAN). We delve into the architecture of these networks, discuss key aspects, and examine the coverage provided by different Mobile Network Operators (MNOs) in the Czech Republic. The second chapter explores the characteristics of indoor and outdoor measurement environments, highlighting the unique challenges posed by each and their impact on signal propagation. We discuss urban, suburban, and rural areas, as well as positioning technologies used in these environments. The third chapter details the measurement setup, encompassing the methodology employed, the data collection process, the selection of the 4G/5G module and processing unit, energy-saving options, the development of a custom-built application for measurement configuration and control, the visualization of collected data, and introducing the Coverage Analysis tool we developed using the Dash framework. We present the functionality of the tool, highlighting its user-friendly interface, interactive maps, filtering capabilities, and graphical representations of signal metrics. The fourth chapter delves into the processing methods and algorithms used for data analysis, providing a brief overview of machine learning algorithms and their potential for network performance prediction. We introduce the Linear Regression and XGBoost models, demonstrating their application in forecasting network load based on historical data. Furthermore, we discuss different interpolation methods and their suitability for estimating coverage maps. The sixth chapter presents a detailed analysis of the collected data, examining both static indoor and mobile outdoor measurements conducted in 4G LTE and 5G NR NSA technologies. We explore the performance characteristics of individual LTE bands and 5G NR NSA Band 78, highlighting significant findings, notable patterns, and areas requiring optimization. We compare our estimated coverage maps with official estimates, identifying any discrepancies and potential explanations for observed differences.

This thesis addresses the following research questions:

- What are the key differences in signal propagation characteristics between the various LTE bands deployed in the Brno (Czech Republic), and how do these differences impact coverage estimation?
- How do different interpolation methods perform in estimating LTE and 5G NR NSA coverage, and which method is the most suitable for this task?
- What key insights can be gained from analyzing the static and mobile measurement data regarding LTE and 5G NR NSA network performance in Brno?

These research questions are explored throughout the entire work and specifically addressed in the Conclusion.

1 Mobile Networks

Nowadays, mobile networks have become an integral aspect of the daily lives of the majority of the global population. Within cellular mobile networks, the fundamental concept involves dividing large areas into smaller cells. Each cell has its own base station and devices (e.g., user equipment – UE) connect to the closest station within their current location. As users move about and transition between cells, the network ensures their uninterrupted connection by linking them to the most appropriate nearby base station. Through these approaches and technologies, continuous and seamless connectivity for mobile devices is assured.

This chapter offers a brief overview of the extensively utilized fourth-generation (4G) and the rapidly expanding fifth-generation (5G) mobile networks. The focus is primarily on introducing the initial segment of the network, specifically the Physical Layer (PHY) in conjunction with the Radio Access Network (RAN).

First of all, it is essential to grasp the organizational framework that among others manages the evolution of mobile networks. The 3rd Generation Partnership Project (3GPP) embodies a collaborative effort among seven telecommunications organizations. Collectively, they wield significant influence in shaping the landscape of contemporary mobile communication, tasked with defining and advancing 3GPP technologies. These specifications cover various aspects of cellular telecommunications, serving as the bedrock for mobile networks. Furthermore, they enable smooth integration with non-3GPP networks, ensuring seamless connectivity across different technologies [1]. The 3GPP organization divides its efforts into releases, a strategic approach that helps to adopt new technologies and guarantees interoperability of network components and devices from diverse vendors. Fig. 1.1 illustrates the evolution of 4G and 5G mobile communication standards in terms of available releases.

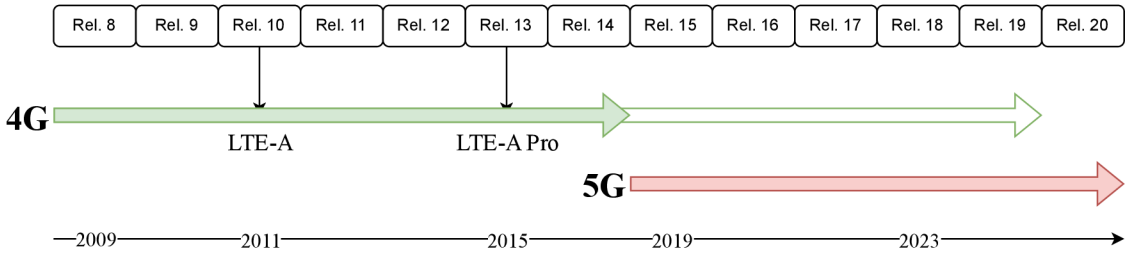

Fig. 1.1: 3GPP Release Timeline

1.1 4G Mobile Networks

As can be seen from Fig. 1.1, the Long-Term Evolution (LTE) technology, as detailed in 3GPP Release 8, made its commercial debut in late 2009, ushering a phase of rapid global expansion in commercial networks. The advancements within LTE are systematically categorized into distinct releases by 3GPP [2].

The first set of enhancements was introduced in 3GPP Release 9, with notable improvements following in 3GPP Rel. 10, widely known as LTE-Advanced (LTE-A). Compared to LTE, LTE-A brings about significant improvements: it elevates the peak data rate to 1 Gbps (a theoretical value) in both directions, manages more simultaneously active subscribers, standardizes private femtocells, and introduces beamforming techniques and various other functionalities [3].

The last member of the 4G family was introduced by 3GPP in October 2015 with Release 13, recognized as LTE-A Pro or the 4.5G network. The LTE-A Pro technology introduced substantial enhancements in data speed, network efficiency, and capacity. Achieving speeds up to 1.2 Gbps through a combination of carrier aggregation (CA), utilization of unlicensed radio frequency (RF) bands, a 4×4 Multiple Input Multiple Output (MIMO) antenna setup, and an upgraded 256-QAM modulation scheme. The primary objective of LTE-A Pro is to address the increasing data consumption and the evolving challenges in the resource management challenges brought by emerging applications, for example, Internet-of-Things (IoT) [4], [5].

1.1.1 Architecture

Every mobile cellular network consists of two fundamental parts. The first part includes the PHY layer and RAN. The RAN section coordinates transmissions, assigns channels, and performs other coordination functions. The second one is the core network (CN), which interlinks all access networks. It provides global services such as authentication, roaming, and billing, while also establishing connections to external networks like the Internet [3]. Fig. 1.2 captures a simplified illustration of the LTE network and its fundamental elements. The network is structured into two primary components: the Evolved Universal Terrestrial Radio Access Network (E-UTRAN) and the Evolved Packet Core (EPC), as depicted in Fig. 1.2. E-UTRAN is responsible for supervising the radio interface between the UE and the network. Conversely, EPC handles the coordination of calls and data routing between the UE and external networks.

In contrast to conventional 3GPP networks, an LTE network adopts a unified architectural structure by combining Radio Network Controller (RNC) nodes and

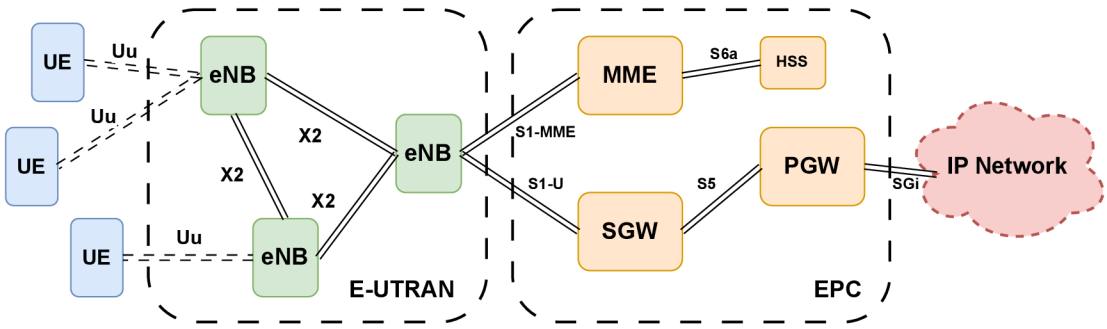

Fig. 1.2: Architecture of LTE network

NodeB nodes into E-UTRAN NodeB (eNodeB) nodes. These eNodeB nodes handle circuit switching at the base stations, streamlining the network, reducing system latency, and minimizing costs associated with establishment and maintenance [6]. Hence, LTE primarily relies on an IP-based core network. The use of an all-IP network architecture significantly simplifies the design and operation of the LTE air interface, the radio network, and the core [7].

Fig. 1.2 shows the connections (via interface) among various network elements. These connections include interface *Uu* linking UEs to eNBs, *X2* interconnecting eNBs, *S1-MME* connecting eNBs to the Mobility Management Entity (MME), *S6a* linking the MME to the Home Subscriber Server (HSS), *S1-U* ensures linking eNBs to the Serving Gateway (SGW) responsible for the routing of data traffic between UEs through the *S5* connection to the Packet Data Network Gateway (PGW), and *SGi* link connecting to the other IP networks, such as the Internet. In the 4G networks, UEs encompass different kinds of devices, including mobile phones, smart terminals, multimedia devices, and streaming devices [6].

1.1.2 Key aspects

The 4G network technology, represented by LTE, employs different modulation schemes for downlink (DL) and uplink (UL) communications. The Orthogonal Frequency Division Multiple Access (OFDMA) is used in DL and Single-carrier FDMA (SC-FDMA), due to its advantage of having a low Peak-to-Average Power Ratio (PAPR), is employed in UL [8].

LTE supports various bandwidths ranging from 1.4 MHz to 20 MHz, with commonly used channels having bandwidths of 10, 15, and 20 MHz. The operating frequencies can be from 700 MHz to 2.7 GHz. LTE enables to provide a cell radius of up to 100 km, accommodates user mobility at speeds up to 500 km/h, and offers a theoretical peak DL rate of 300 Mbps or 1.2 Gbps with LTE-A or LTE-A Pro, respectively. The air interface offers options like Frequency Division Duplex (FDD),

Table 1.1: LTE Categories and Performance Parameters [7]

UE Category	**4**	**6**	**9**	**12**	**18**
Max DL Datarate with CA (Mbit/s)	150	300	450	600	1200
Typical Number of Aggregated Carriers (DL)	1	2	3	4	5
Max UL Datarate (Mbit/s)	50	50	50	100	125
Typical Number of Aggregated Carriers (UL)	1	1	1	2	2
Number of Receive Antennas	2	2	2	2	4
Number of MIMO DL Streams	2	2	2	2	4
Support for 64-QAM in UL	No	No	No	No	Yes

which separates DL and UL transmission by frequency, or Time Division Duplex (TDD) which separates DL and UL transmissions through time slots. In the Czech Republic, FDD is the primary choice due to fewer synchronization issues, although TDD offers greater flexibility. Additional improvements, including CA allowing the bundling of up to five carriers, MIMO transmission, beamforming, and other enhancements, contribute to a more reliable and efficient utilization of resources. LTE ensures Quality of Service (QoS) guarantees, lower wireless network delays, higher cell edge bit rates, and backward compatibility [7], [9]. The maximum DL data rate is significantly influenced by the selected UE category. There are 20 LTE UE categories, each characterized by diverse parameters and performance levels. For a clearer understanding of these UE categories, a summary of selected categories is provided in Table 1.1.

1.1.3 Coverage of 4G networks in Czech Republic

In the Czech Republic, three major Mobile Network Operators (MNOs), namely O2, T-Mobile, and Vodafone, provide comprehensive mobile signal-based coverage across the country. The coverage of the 4G network varies depending on the specific RF band. 4G technology in the Czech Republic mainly relies on four RF bands: Band 20 (800 MHz), Band 3 (1800 MHz), Band 1 (2100 MHz), and Band 7 (2600 MHz). Bands 1, 3, and 7 are strategically utilized as capacitive layers in high-traffic urban areas, such as big cities, ensuring robust coverage and high-speed data transfer rates. Band 20 operates as the backbone, excelling in providing broader coverage in less populated and rural regions.Fig. 1.3 illustrates the detailed allocation of RF spectrum bandwidth in units of MHz for each MNO.

Another MNO (virtual MNOs are not considered), namely Nordic Telecom, operates on Band 78 (3600 MHz). However, it is not as prominent as the three major MNOs mentioned earlier. An exception, not depicted in Fig. 1.3, is O2, which also provides 4G services on Band 78.

Fig. 1.4 shows the territorial coverage of the 4G network according to the MNO. The blue color signifies robust outdoor coverage, while the light blue color denotes basic outdoor coverage, and areas without coverage are uncolored. These coverage maps are based on measurements conducted by the Czech Telecommunication Office (CTO) [11]. The coverage provided by all MNOs is robust.

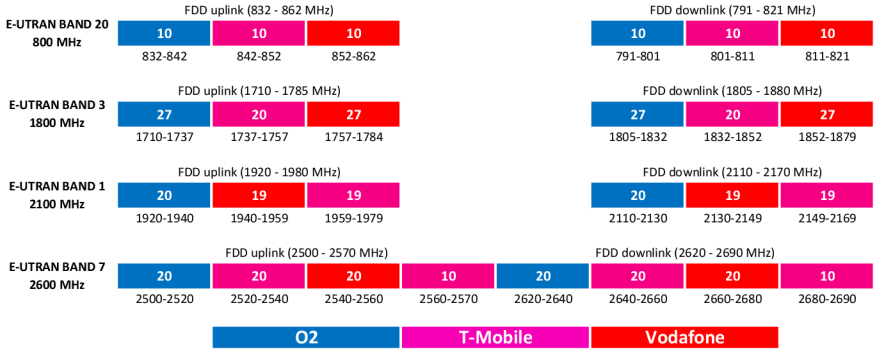

Fig. 1.3: Spectrum division of LTE bands by MNOs in the Czech Republic (*valid to: 25.11.2023*) [10]

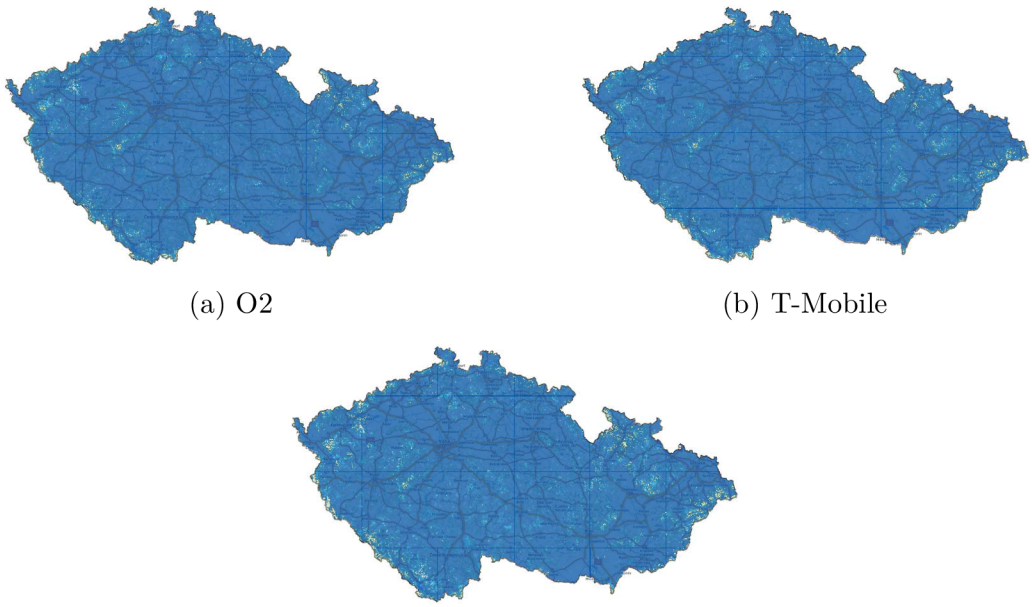

(a) O2

(b) T-Mobile

(c) Vodafone

Fig. 1.4: The 4G coverage (all bands) by MNOs in the Czech Republic (*valid to: 25.11.2023*) [11]

1.2 5G Mobile Networks

The demand for faster data transfer speeds, enhanced efficiency, and simplified network architecture has accelerated the development of 5G technologies. At the core of 5G technology is the 5G New Radio (NR), introduced in Release 15, as it is visible in Fig. 1.1. 5G not only achieves data transfer speeds surpassing 10 Gbps but also ensures minimal latency, high reliability, and connectivity capabilities for an unprecedented number of devices. The RF spectrum, ranging from below 6 GHz to above 20 GHz, emphasizes the extensive bandwidth employed in 5G networks [12].

As 5G networks gain prominence, mobile and wireless communication takes a central role, helping interactions between humans and machines, machines and machines, and various other forms of communication. The essence of 5G's promise lies in its adaptability and integration capabilities, surpassing the constraints of its predecessors [13]. It aims not only to deliver a substantial enhancement in data performance compared to 4G but also to extend battery life, and the connection of different devices within a single cell [14]. In essence, 5G networks open doors to a range of advanced applications and services across various sectors. The evolution of cellular technologies through 5G is poised to reshape communication, introducing smart homes, healthcare solutions, and the widespread connectivity envisioned in the IoT [15].

1.2.1 Architecture

Nowadays, the 5G architecture primarily involves the coexistence of 5G NR and existing LTE networks, especially in sub-6 GHz bands [16]. 5G NR technology is designed to offer broadband connectivity, low latency, and a stable network, addressing diverse applications, including those crucial for the IoT. Next, it introduces concepts like Enhanced Mobile Broadband (eMBB), Massive Machine-Type Connectivity (mMTC), Ultra-Reliable Low-Latency Connectivity (URLLC), Machine-to-Machine Communication (M2M), and Device-to-Device Communication (D2D) [17].

As mentioned above, the 5G network predominantly operates through coexistence with the 4G network, resulting in two key network architectures: Non-Standalone (NSA) and Standalone (SA). The NSA architecture, often termed "E-UTRA - NR Dual Connectivity" or "Architecture Option 3", employs the existing 4G RAN with the new 5G NR [18]. In this configuration, the LTE radio access component of the network manages all control plane operations, while NR serves as additional capacity for the user plane. The utilization of the 4G EPC has led to higher delays than expected in dual connectivity [12].

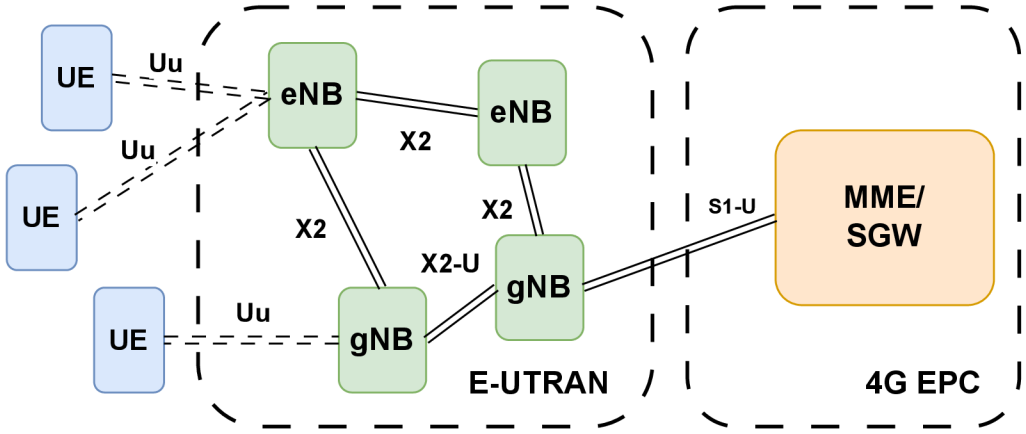

Fig. 1.5: Architecture of 5G NSA

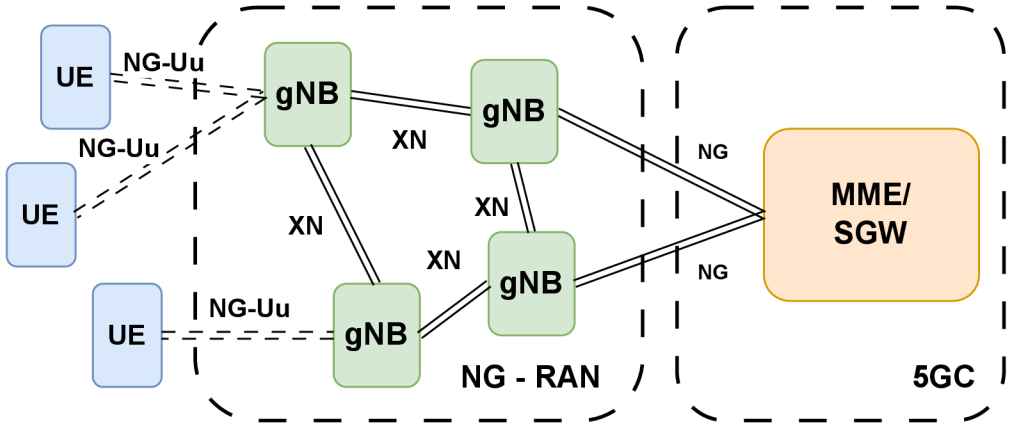

Fig. 1.6: Architecture of 5G SA

The basic structure of the 5G NSA architecture is shown in Fig. 1.5. The SA architecture, on the other hand, encompasses both the NR with Next-Generation Node B (gNB) and the new core component of the 5G core network. It supports advanced 5G services such as eMBB, URLLC, and mMTC [12]. The simplified basic structure of the 5G SA architecture is shown in Fig. 1.6.

Choosing SA 5G infrastructure over NSA 5G brings several key advantages. SA 5G offers ultra-low latency, high speed, and scalability to support over 1 million devices. It enhances the voice calling experience with Voice over New Radio (VoNR), lowers power consumption, and provides various other benefits. On the other hand, NSA 5G utilizes the existing 4G core, offering a fast and cost-effective way to implement 5G. It delivers decent download speeds and enables voice calls over LTE (VoLTE). The implementation of Dynamic Spectrum Sharing (DSS), where 4G and 5G systems can simultaneously share their RF spectrums, contributes to an overall enhancement in network performance [19].

1.2.2 Key aspects

In the PHY layer of the 5G network, when communicating from the base station to the UE in the DL, OFDM with Cyclic Prefix (CP) is employed, similar to the 4G network. Conversely, in the UL, options include OFDM or Discrete Fourier Transform (DFT) precoding, known as DFT-s-OFDM. DFT-s-OFDM is specifically used to enhance coverage in UL communication [18].

For terrestrial communications, 5G networks rely on two main frequency ranges. The first is Frequency Range 1 (FR1), which covers frequencies from 450 MHz to 7.125 GHz, and the second one is Frequency Range 2 (FR2) from 24.25 to 52.6 GHz [3], [18]. In FR1, frequencies below 1 GHz are primarily deployed because of their superior propagation characteristics, making them suitable for covering of large rural countryside areas. Frequencies above 1 GHz are deployed in urban and suburban areas as a capacitive layer to complement the base sub-1GHz frequencies. The maximum bandwidth for FR1 is typically around 100 MHz. FR2 is advantageous for achieving faster data speeds by utilizing wide bandwidths in the millimeter-wave range. However, the trade-off is a significant loss in signal coverage due to the high-frequency nature, making FR2 more suitable for crowded places like shopping centers and arenas [18].

5G NR cells utilize advanced antenna systems featuring massive MIMO technology. The primary objective is to improve the signal-to-noise ratio (SNR). To enhance data rates, a technique called Spatial or Space Division Multiple Access (SDMA) is employed. SDMA involves the simultaneous transmission of different data streams across various antennas, taking advantage of multipath propagation [20]. The main aspects of the 5G network are summarized in Table 1.2.

Table 1.2: 5G Key aspects and values [21]

Key aspects	**Values**
Peak data rate	20 Gbps
User experienced data rate	0.1–1 Gbps
Latency	1 ms over-the-air
Mobility	500 km/h
Connection density	10^6 /km^2
Energy efficiency	100 times compared with 4G
Spectrum efficiency	3–5 times compared with 4G
Area traffic capacity	10 Mbps/m^2

1.2.3 Coverage of 5G networks in the Czech Republic

As 5G SA has not been deployed in the Czech Republic yet, the higher RF bands from FR2 are not currently in use. 5G technology in the Czech Republic primarily relies on four main RF bands from FR1: Band 28 (700 MHz), Band 3 (1800 MHz), Band 1 (2100 MHz), and Band 78 (3600 MHz). Once again, Bands 1, 3, and 78 are utilized as capacitive layers for Band 28, which serves as the backbone. The RF bands used in 5G NSA technology are shown in Fig. 1.7.

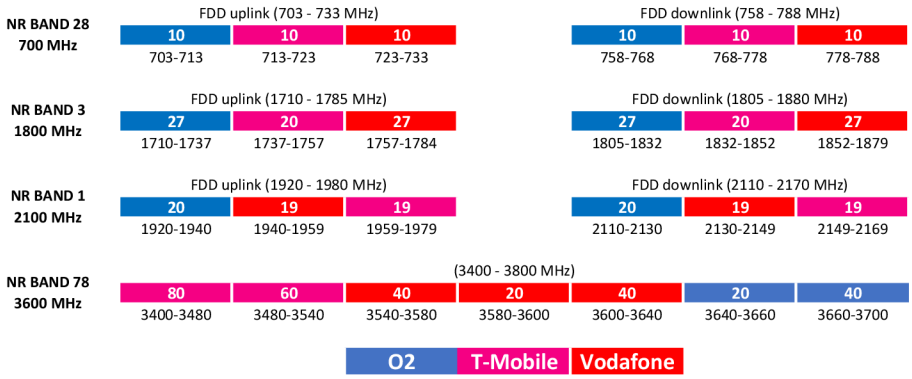

Fig. 1.7: Spectrum division of 5G NSA bands by MNOs in the Czech Republic (*valid to: 25.11.2023*) [10]

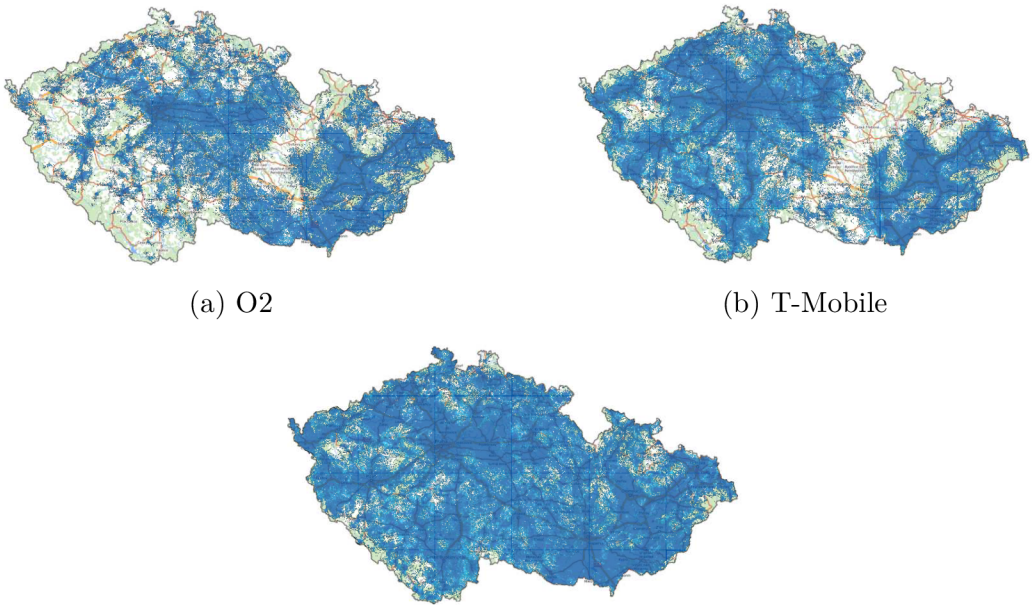

(a) O2

(b) T-Mobile

(c) Vodafone

Fig. 1.8: The 5G NSA coverage (all bands) by MNOs in the Czech Republic (*valid to: 25.11.2023*) [11]

The same principle of network coverage as in Fig. 1.4 is shown in Fig. 1.8. As evident from Fig. 1.8, the 5G NSA coverage is currently dominated by Vodafone, followed by T-Mobile and O2 based on measurements of CTO. Because O2 and T-Mobile share passive and active infrastructure for 5G technologies (RF spectrum and core of the network of each MNO remain separate) [22], they are covered quite similarly. The cooperation of O2 and T-Mobile covers the entire territory of the Czech Republic except for Prague and Brno, where each of them has its infrastructure and the coverage of 5G NSA is robust.

2 Measurement Environments

Measurements and collected data exhibit variability, primarily depending on the specific environment in which they are measured, the parameters applied, deviations of the measuring devices, and various other factors. This chapter will focus on types of environments and their impact on measurements in mobile networks. The chapter is divided into two principal types of measurement environments: indoor and outdoor (see Fig. 2.1).

Signal measurements in both outdoor and indoor environments play crucial roles in RF engineering. These environments involve drive tests and walk tests, employing specialized vehicles or individuals equipped with measurement devices to traverse geographical areas. Data collected includes signal strength, signal quality, and various performance indicators. This information is important for optimizing cell placement, adjusting antenna tilt, and mitigating interference to enhance overall network performance [23].

For 4G/5G networks, monitoring and troubleshooting end-to-end network performance are essential to ensure optimal functionality, enhance user experiences, and address performance issues promptly. Evaluating broadband infrastructure, mapping network performance across operators, and understanding the quality of experience (QoE) for Mobile Broadband (MBB) network customers enable operators to identify and address issues related to throughput, latency, loss rate, signal strength, and other performance metrics. Further discussions in this work will focus on the assessment of QoS and user experiences [24].

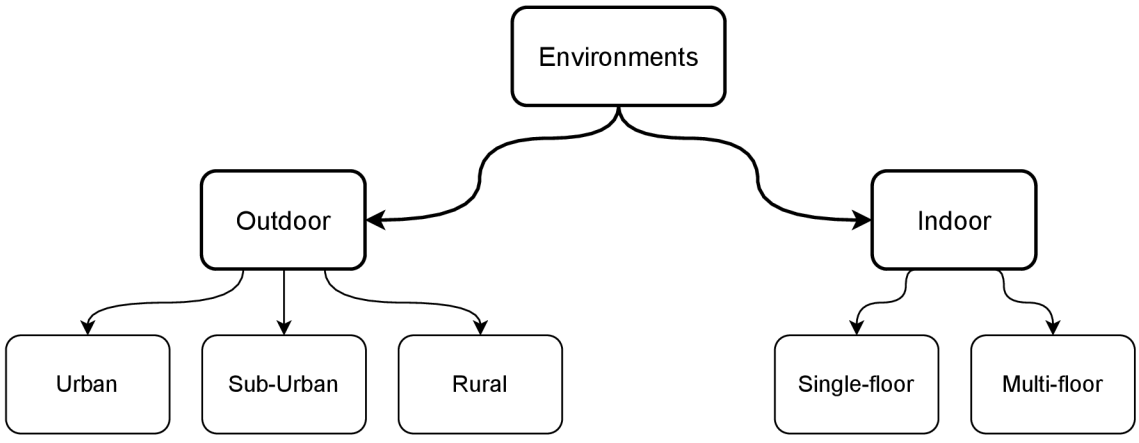

Fig. 2.1: Measurement Environments

2.1 Indoor

Indoor propagation in wireless communication introduces unique challenges, particularly in environments rich with metal structures, leading to high dispersion and a complex mix of clustered multipath components that pose challenges for broadband channels [25].

Indoor spaces, ranging from small rooms to large structures like factories and airports, exhibit diverse behavior, making simple statistical characterization challenging. Deterministic approaches such as ray-tracing or full-field methods are attractive for their simplicity but face challenges in acquiring detailed data on constituent materials and their electrical properties, especially considering dynamic factors like moving furniture and changing environments due to human presence [25].

In traditional wireless communication systems, phenomena like scattering, reflection, and diffraction by the physical environment influence radio signals transmitted in indoor environments [26]. Multipath propagation, where signals reach the receiver through multiple paths due to obstacles blocking the line-of-sight (LOS) path and reflections, is common.

The use of MIMO communication in mobile network systems further complicates indoor propagation, as each receiver antenna receives both the LOS signal and a fraction of the signal from other propagation paths. This adds to the challenges and intricacies of indoor radio signal transmission [26].

2.1.1 Positioning

Indoor environments cause challenges for positioning technologies like Global Navigation Satellite Systems (GNSS) due to signal degradation caused by obstacles and various influences [27]. Consequently, WiFi technology, based on IEEE 802.11 standards, has emerged as a widely adopted indoor positioning solution. WiFi positioning methods include triangulation, where the device measures the received signal strength from multiple access points, and fingerprinting, which matches signal-strength fingerprints to a database [28]. It is important to note that, for the scope of this work, discussions on indoor positioning techniques are exploratory, and none of them will be integrated into the final implementation.

2.2 Outdoor

In the domain of measuring radio signals for 4G/5G networks, understanding outdoor environments is vital. This necessitates a comprehensive approach to data collection [24]. Measurements are conducted in open spaces, such as city streets,

employing a precise process involving mobile driving tests with vehicles like cars, buses, or trains. Outdoor measurement scenarios are classified into urban, suburban, and rural categories, each characterized by distinct population densities and building structures. Outdoor radio signal measurements encounter challenges posed by obstacles like trees and buildings, contributing to multi-path propagation, among other factors [25].

Significant challenges persist in outdoor environments, particularly in characterizing building materials in terms of their electrical constants and surface roughness essential for modeling reflection and scattering and, consequently, the multipath environment [25].

To address these challenges and formulate effective planning schemes, a comparative analysis between modeled and measured data is imperative. Various models are employed for such comparisons, aiding the analysis between theoretically predicted signal behavior and actual measured data. Common models include path loss models, estimating signal attenuation based on distance and frequency, and ray-tracing models that simulate signal interactions with physical structures to predict propagation characteristics accurately. For instance, Fig. 2.2 shows an illustrative example of a ray-tracing model.

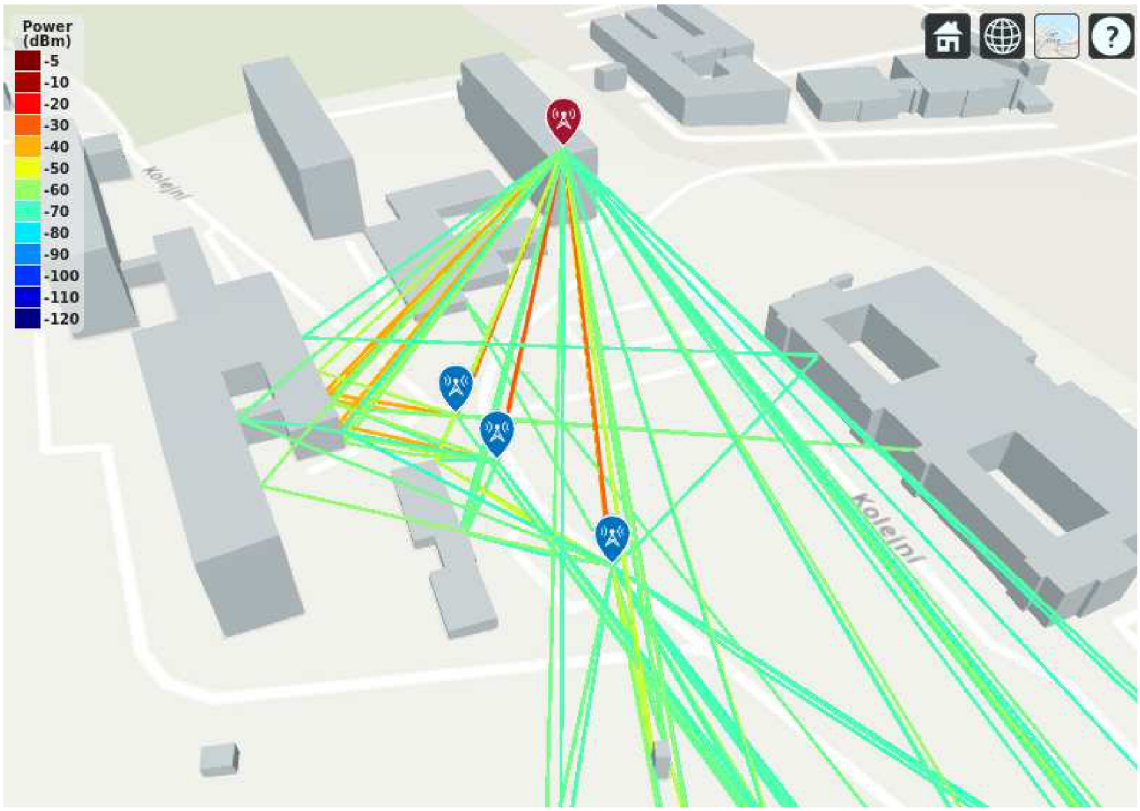

Fig. 2.2: Two-ray model on Brno Kolejní street

2.2.1 Urban areas

Cities, commonly marked by high population density and ongoing construction, typically accommodate over 50,000 people (in the Czech Republic, localities with 2,000 or more inhabitants [29]) [24]. Conducting radio signal measurements in urban areas presents challenges due to the intricate urban environment. In densely built areas, such as regional cities, general propagation models struggle to account for variations along streets and areas shielded by tall buildings, necessitating specialized treatment. Addressing these challenges is crucial for ensuring accurate radio signal measurements and predictions in diverse urban settings [25].

2.2.2 Sub-Urban areas

Situated outside city limits, sub-urban exhibits a moderate population density ranging from 2,500 to 50,000 people (again in the Czech Republic more than around 100 to 2000 inhabitants), featuring numerous houses with fewer buildings and shops. Suburban areas differ from urban centers in their vast, low-density land use [24].

2.2.3 Rural areas

Defined by their natural openness, rural areas maintain a small population density, typically fewer than 2,500 people (in the Czech Republic less than 100 inhabitants), comprising few houses and buildings compared to suburban and urban regions, reflecting a distinct rural landscape shaped by nature [24].

2.2.4 Positioning

In outdoor environments, GNSS technologies such as Global Positioning System (GPS) or Galileo leverage satellite constellations to provide accurate positioning [27]. GPS utilizes triangulation to compute positions based on signals from three or more satellites, using Time of Arrival (TOA) for distance calculation. However, GPS signals are susceptible to non-line-of-sight (NLOS) interference and climatic conditions, leading to significant positioning errors [30].

3 Measurement Setup

This chapter presents a measurement setup solution designed to comprehensively evaluate the performance of 4G and 5G networks. Careful selection of methods, equipment, and tools is essential for acquiring precise and insightful data for in-depth analysis. Examining Key Performance Indicators (KPIs), choosing appropriate network modules and processor units, considering power-saving options, and implementing effective visualization techniques are crucial factors in determining the optimal measurement setup.

3.1 Methodology

The core focus of this thesis revolves around conducting measurements utilizing various modes of transportation, including public transport, bicycles, cars, and pedestrian walks. These measurements are designed to cover extensive distances and gather a significant volume of data. Furthermore, walk tests entail affixing the measuring device to an individual, allowing for the profiling of predominantly indoor environments, while also extending to outdoor settings.

The main idea of the measurement methodology is visualized in Fig 3.1. Measured data are collected from the mobile site using a measurement device and stored in log files, which are then stored on the internal memory storage of the device (in the future preferably on the cloud). Subsequently, the data are retrieved for visualization, enabling users to analyze the measured data and deduce conclusions from the result of the measurement campaign.

This methodology closely aligns with the practices employed by most MNOs or companies specializing in benchmarking mobile networks. Most of them use approaches that involve a combination of drive tests divided into individual categories according to the environment (as outlined in subsection 2.2). Conducted measurements in this work are divided mainly into static indoor and mobile outdoor tests.

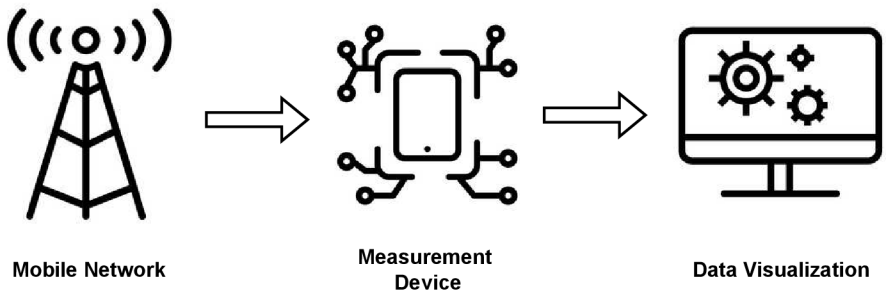

Fig. 3.1: Measurement methodology

Static indoor tests focus on assessing network performance within buildings and enclosed spaces, while mobile outdoor tests evaluate network performance in various outdoor environments, including urban, suburban, and rural areas. These assessments involve sophisticated equipment and vehicles to capture real-world scenarios accurately. Leveraging these measurements, they acquire essential input for optimization and plan subsequent steps to enhance the overall performance of the network.

3.2 Data Collection

Presently, numerous applications and devices are available to support these measurements. Examples include the Android application "G-NetTrack," employed in [24], and the "TEMS Pocket" application utilized in [31], serving as commercial phone-based mobile network measurement tools. In this work, an effort to design a novel measurement device along with its dedicated application is introduced. This approach aims to enhance flexibility and measurement efficiency, allowing for individualized settings of visualization and data manipulation. Unlike existing applications, this solution offers greater adaptability to user needs.

As mentioned and indicated in Fig 3.1, for data collection we need to design a proper measurement device that will be able to connect to the 4G/5G network, measure the necessary KPIs, and store them somewhere where they will be accessible. First, we analyze what is important for obtaining a high-quality evaluation of mobile networks and what must be taken into account during the measurement.

3.2.1 4G/5G Measurement

As mentioned in the Introduction, currently, 4G and 5G in the Czech Republic support only NSA technology. Together, 4G and 5G dynamically share resources via DSS support. For a better understanding of the following text, Fig. 3.2 shows the DSS concept of resource sharing between 4G and 5G in the time and frequency domain.

At the PHY layer, 5G is designed according to 3GPP in a similar style as 4G to support DSS with the same subcarrier spacing and a similar structure of time-domain communication [32] (though in 5G NR subcarrier spacing, number of OFDM symbols within a radio frame can vary depending on transmission numerology [33]). MNOs maintain LTE cell-specific reference signal (CRS) transmissions for backward compatibility of 4G devices, which each cell broadcasts at predefined time-frequency coordinates, and UE then can based on these CRS measure and calculate KPIs [32], [34].

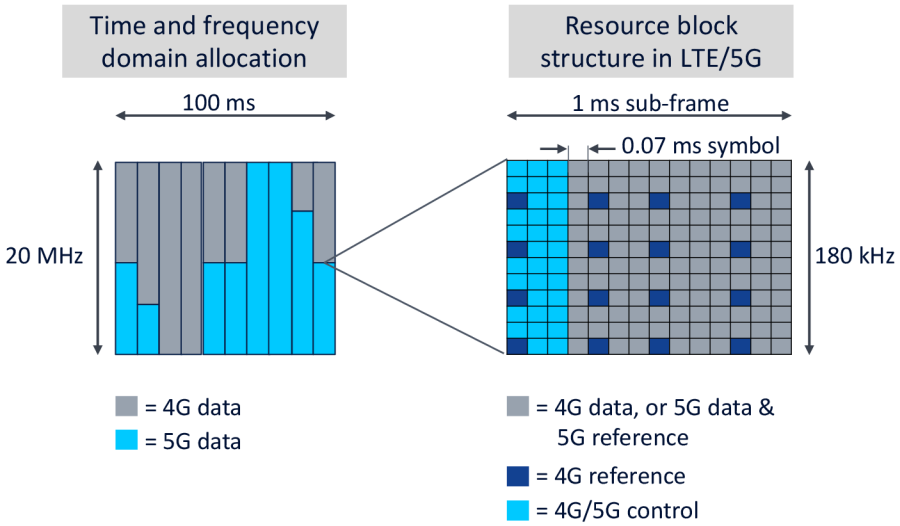

Fig. 3.2: 4G and 5G resource sharing in time and frequency domain [32]

Fig. 3.2 illustrates on the left side an allocation for 4G and 5G data and on the right side a 1 ms long sub-frame in the form of a resource grid, both in frequency and time domain. The radio resource grid is divided into time and frequency units called Resource Blocks (RBs), with a 0.7 ms duration and 180 kHz width. Each RB consists of 12 sub-carriers that are 15 kHz wide in the frequency domain both for 4G and 5G, in the time domain for 4G 7 OFDMA or SC-FDMA symbols (depending on the direction of communication) [35], and not strictly specified in the time domain for 5G [33]. As can be seen on the right in Fig. 3.2, small squares are Resource Elements (REs) which are the smallest units of the resource grid made of one subcarrier in the frequency domain and one symbol duration in the time domain.

RF Bands

Measurements on individual RF bands can differ significantly, and thus shared analysis or interpolation of all samples from mobile measurements, where there is a high chance of changing the used band in 4G or 5G technology, does not make sense. Each of the frequencies must be analyzed separately to preserve a meaningful measurement result of the subsequent interpolation of the coverage map of the measured technology in the given band. Another important element is the selection of a sufficient sample frequency of the collected data so as not to exceed the distance, which would ensure a low correlation of the measured samples and thus invalidate the data set. In [36], it was found that at frequencies above 1.8 GHz, which for example corresponds to bands 3, 1, and 7 in 4G, at a distance of around 100 meters the correlation of the measured values is around 20%, which excludes the possibility of reliable interpolation between the measured points.

3.2.2 Key Performance Indicators

To find out the important properties of mobile networks such as coverage, capacity, quality, reliability, etc., it is necessary to obtain critical KPIs. Let's analyze some of the most important measured network parameters from which analysis and deductions on how to improve QoE and QoS are collected.

Signal Measurements

- **RSSI (Received Signal Strength Indicator)** - RSSI is defined as the linear average of the aggregate received power, measured in watts. It is observed within the configured OFDM symbol and across the measurement bandwidth, encompassing N number of RBs. This comprehensive measurement accounts for signals the UE receives from various sources, including co-channel serving and non-serving cells, adjacent channel interference, thermal noise, and other contributing factors [37]. Typically, a higher RSSI value (e.g., >-65 dBm) indicates stronger signal strength and lower RSSI values (e.g., <-85 dBm) are indicative of weaker signal strengths.
- **RSRP (Reference Signal Received Power)** - RSRP is characterized as the linear average of the power contributions (measured in watts) from the RE responsible for carrying the CRS. This measurement is conducted within the designated measurement frequency bandwidth, as specified in [37]. Generally, higher RSRP values (e.g., >-80 dBm) suggest a stronger signal. Conversely, lower RSRP values (e.g., <-100 dBm) are indicative of weaker signals.
- **RSRQ (Reference Signal Received Quality)** - RSRQ is expressed as the ratio of N times the RSRP to the E-UTRA carrier RSSI, where N represents the number of RBs within the E-UTRA carrier RSSI measurement bandwidth. Both the numerator (N times RSRP) and the denominator (E-UTRA carrier RSSI) measurements are conducted over the identical set of RBs [37]. Again, higher RSRQ values (e.g., >-10 dB) suggest a stronger signal quality and lower RSRQ values (e.g., <-20 dB) are indicative of weaker signal quality.
- **SINR (Signal to Noise and Interference Ratio)** - SINR is not defined by the 3GPP specification as the metrics above (thus it is not reported to the serving cell), but it is usually defined by the vendor of UE. Mostly it is the power ratio of usable signals measured from CRS to the average interference of measured signals or channel interference signals from other cells plus noise within the measurement bandwidth. A higher SINR value (e.g. >15 dB) indicates a good separation of the signal from the noise and interference, thus the quality of the signal.

3.2.3 The 4G/5G Module

To obtain the values of all the necessary KPIs, it is necessary to choose a suitable device to measure these values. As was mentioned at the beginning of this chapter, the idea of this work is to build a solution that will be independent of any third-party application. Therefore, it is necessary to select 4G or 5G modules from the available options. Additionally, these modules should possess the capability to determine the position of device with the assistance of GNSS technology. The integration of such modules is crucial for comprehensive and accurate data collection during the measurement process.

Currently, three prominent brands in the market manufacturing 5G modules are Qualtec, Simcom, and Sierra Wireless. Each of these manufacturers provides a variety of modules with diverse parameters. However, a common feature among them is their compatibility with connecting to 4G/5G networks and even older technologies. These modules universally support satellite systems like GNSS, ensuring comprehensive connectivity and positioning capabilities for the measurement device.

Three models with the capability to connect to both 4G and 5G networks, coupled with GNSS technology, have been selected from leading manufacturers. These models include the SIM8200EA-M2 module from Simcom, the 5G RM500Q series model from Quectel, and the EM9190 model from Sierra Wireless (see Fig. 3.3).

All of them have a maximum data transfer speed of around 3 Gbps in DL and slightly different data transfer speeds in UL, with a range from 0.5 to 3 Gbps. The prices are very dependent on the merchant who offers the modules and the prices vary from 300 to 400-500 euros. More information about these modules is available in Table 3.1. Based on Table 3.1 and the availability of the module, the choice was narrowed down to two modules, a model from Simcom SIM8200EA-M2 and Quectel 5G RM500Q. These two manufacturers also offer development boards for modules, which makes working with modules much easier.

(a) Simcom SIM8200EA-M2 (b) Quectel RM500Q series (c) Sierra Wireless EM9190

Fig. 3.3: Three selected modules [38], [39], [40]

Table 3.1: Modules comparison

Key aspects	**SIM8200EA-M2** [38]	**5G RM500Q** [39]	**EM9190** [40]
5G Category	5G NSA/SA	3GPP Release 15 5G NSA/SA	5G NR Sub-6 and mmWave
5G Frequency Bands	n41, n77, n78	n38, n41, n77, n78, n79	All Supported
4G Category	Cat-20	DL Cat-16/ UL Cat-18	Cat-20
4G Frequency Bands	All Supported	All Supported	All Supported
Peak Download Rate	4 Gbps	2.5 Gbps	5.5 Gbps
Peak Upload Rate	500 Mbps	900 Mbps	3 Gbps
Satellite Systems	Supported	Supported	Supported
USB	USB 3.1	USB 3.1	USB 3.1
Price	300 €	300 €	400 €

Both of them support a sufficiently high data speed in DL/UL communication directions for benchmarking mobile networks in Czech Republic, share a similar price range, and each of them has USB 3.1 needed for potential high-speed tests, since USB 2.0 despite the limitations of 480 Mbps and USB 3.1 can transmit data with a speed up to 10 Gbps [41].

In [42], these two and other modules were tested in terms of the DL/UL using tools such as OpenSpeedTest, LibreSpeed, iPerf3 and Round-Trip-Time (RTT) in ms using the LibreSpeed tool and ping. From this module test, the clear winner between the Simcom SIM8200EA-M2 modules built into the development platform from Waveshare 5G Module and the Quectel RM500Q-GL(M2) built into the Quectel USB Modem is the module from Quactel, which had measured average download speeds of around 750 Mbps and upload 160 Mbps against Waveshare 5G. The module from Simcom had an average download speed of around 200 Mbps and upload around 100 Mbps. However, the measurement could be affected by the USB 2.0 interface, which limits the speed to 480 Mbps, but even so, the results did not reach even this theoretical limitation interface USB 2.0 [42]. In the RTT measurement, Quectel succeeded again with an average value of around 10 ms, while Waveshare achieved an average of around 13 ms [42].

Both tested modules from [42], see Fig. 3.4, underwent testing using a Subscriber Identity Module (SIM) card from T-Mobile Czech Republic. Despite the advantages offered by the Quectel Modem, the Waveshare 5G Module was selected for measurement. Unfortunately, the Quectel module yielded numerous error values during testing, and in some instances, it failed to connect to the network altogether. The GPS functionality of the Quectel module proved problematic, as it was unable to resolve locations even with reference to Quectel's documentation or support.

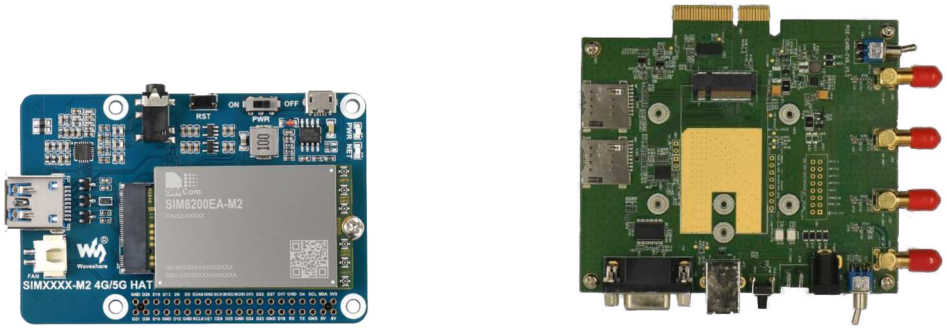

(a) Waveshare 5G Module [43] (b) Quectel USB Modem [39]

Fig. 3.4: The considered and tested modules

AT Commands

Regarding AT commands for communication and data collection from the module, Quectel stands out once again, offering a more extensive array of unique and useful commands. This broader spectrum of commands enhances the capability to collect important KPIs from the network.

However, for the reasons provided, testing was continued on the Waveshare 5G Module. It offers an AT command `"AT+CPSI?"` for basic listing of UE system information. This includes primarily signal measurements, such as RSRP, RSSI, RSRQ, and Reference Signal Signal-to-Noise Ratio (RSSNR), as defined by Simcom [38]. Additionally, this AT command provides other useful information, such as the DL frequency and RF band of the active set, Physical Cell ID, and Service-cell Identification for the next location of the base station used, as well as the transmission bandwidth configuration of the serving cell on the DL and UL.

During the measurement, additional commands are utilized to collect various data. The time and date are obtained using the `"AT+CCLK?"` command, while the name of the MNO is retrieved as a string through the `"AT+COPS?"`. Command `"AT+CSQ"` is used to obtain RSSI and Channel Bit Error Rate (BER), values defined in the Simcom documentation. Furthermore, location information is obtained with the `"AT+CGPSINFO"` command, which returns GPS fixed position data such as latitude, longitude, altitude in meters, speed in knots, and course in degrees, along with supplementary information.

During the module initialization phase, several commands are executed. `"ATI"` is used to request product information, `"ATE1"` enables command echo, `"AT+CFUN=1"` activates full functionality of the device, `"AT+CNMP"` sets the Radio Access Technology (RAT), and `"AT+CSYSSEL"` configures a specific band within the selected RAT for measurement. These initialization commands are executed only once at the beginning of the measurement.

3.2.4 Processing Unit

An essential part of the measurement setup is the processing unit, which must handle the communication with the network module, have a sufficient speed of the data rate on their interfaces, have the capability to connect to the internet for transmitting measured data to the cloud, and exhibit sufficient performance for data preparation and even basic analysis. Relatively inexpensive microprocessor units (MCUs) like ATmega, ESP32, or similar variants suffice for acquiring signal measurements alone. However, most of these MCUs do not have sufficient data transfer speed across their interfaces. For instance, ESP32 has a maximum data rate of around 100 Mbps, which is not enough for testing of the throughput in 4G/5G networks, thus the measurement would be limited.

Raspberry Pi

After thorough evaluation, the Raspberry Pi (RPi), a single-board computer (SBC) developed by the Raspberry Pi Foundation, was selected for the task. This decision was based on its consistent delivery of cost-effective, high-performance, and low-power computing capabilities. The RPi is compatible with various open-source Linux distributions, with the Raspberry Pi OS being the primary operating system utilized in this work. The most recent iteration of RPi 5 comes with a 2.4 GHz quad-core 64-bit Arm Cortex-A76 CPU, equipped with 8 GB of RAM, and supports USB 3.0 for concurrent 5 Gbps operation [44].

Despite their popularity and affordability (RPis are priced below the 90 euros threshold, even for the most powerful model), they frequently experience stock shortages and sell out within minutes when available. Therefore, the Raspberry Pi 4 Model B 2018 was selected for its practical specifications, featuring a Quad-core Cortex-A72 (ARM v8) 64-bit SoC @ 1.8 GHz, 2 GB LPDDR4-3200 SDRAM, and two USB 3.0 ports capable of transfers up to 5 Gbps [45] (see Fig. 3.5). This model, being the best available under the prevailing conditions during this project, ensures efficient throughput for high-speed tests. The quad-core ARM processor provides ample performance for rigorous data analysis. Utilizing the RPi streamlines the development process, especially with the ease of programming in Python, a language well-suited for data manipulation.

Energy saving options

Thermal testing of the RPi Model 4 in [46] revealed that in Idle mode, the RPi consumes approximately 3 W. However, under heavier loads, power consumption can escalate to 8 W. As the primary objective of this work is to maintain flexibility in movement and conduct mobile measurements in the field of interest, it's crucial to

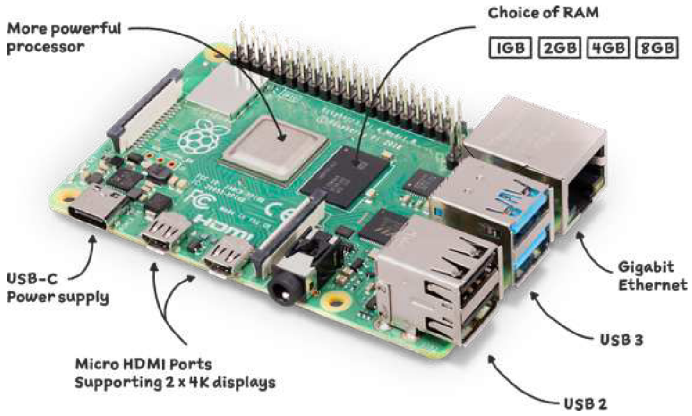

Fig. 3.5: Raspberry Pi 4 Model B 2018 [45]

equip the entire measurement setup with a portable power source. To maximize the operational time, during which the measurement setup can perform other functions like providing an internet connection to additional devices or undertaking basic data analysis, it's advisable to minimize energy consumption. This includes implementing power-saving measures within the operating system. For instance, deactivating unnecessary technologies, such as Bluetooth, which won't be utilized, and turning off peripherals like HDMI, Ethernet, etc. can significantly conserve energy. Other potential energy-saving techniques, like downclocking the processor or deactivating individual processor cores, can be explored on RPi forums.

At present, energy optimization is not a priority as a 40 Ah capacity battery is employed. This capacity ensures prolonged operation, even without implementing energy-saving measures. Under maximum RPi utilization, consuming approximately 8 W of power, the battery can sustain measurements for over a day, which is adequate for current mobile outdoor measurements. However, for future cost reduction, it would be enough to ensure a smaller capacity of the battery pack and to reduce the energy consumption of the RPi with the help of the proposed steps. Nevertheless, these solutions need thorough testing, as they may impact measurement functionalities.

3.2.5 Measurement Setting tool

In order to establish and monitor measurements accurately, an additional essential component for data collection was required. This led to the creation of an application tailored specifically for this purpose. To build the described application, a platform supporting graphical user interface (GUI) functionality is necessary, where the user can provide settings of the measurement. For this, predefined tools and Python packages are utilized.

Measurement script

The measurement script itself was implemented using the pure Python programming language, supplemented by the `pyserial` package for establishing connections with the module, along with other built-in modules for data processing and storage. To clarify the script's functionality, a simple flowchart diagram is shown in Fig. 3.6.

The script begins with the user selecting their preferred RAT and band. Subsequently, a connection is established with the module, and upon successful connection, an initialization AT command is executed. The script then checks the GPS status and sets the name, either by user input or default, typically as the start date of the measurement. Following initialization, the script enters the main loop, where it continuously acquires all measured values. Within this loop, control mechanisms associated with the module and GPS technology are engaged, and measured values are retrieved using AT commands. This process persists until the measurement time equals or exceeds the duration specified by the user.

Dash

Creating an executable application would be unnecessarily complicate and limit flexibility. Instead, the application will leverage *Dash*, a Python framework for creating low-code interactive web applications with a user-friendly interface, complemented by *Plotly* for interactive data visualizations [47]. This framework is well-suited for various complex data science and machine learning (ML) analytics.

By utilizing *Dash*, it becomes feasible to deploy a running application on the local device, primarily for debugging purposes, using a loopback address with port 8050

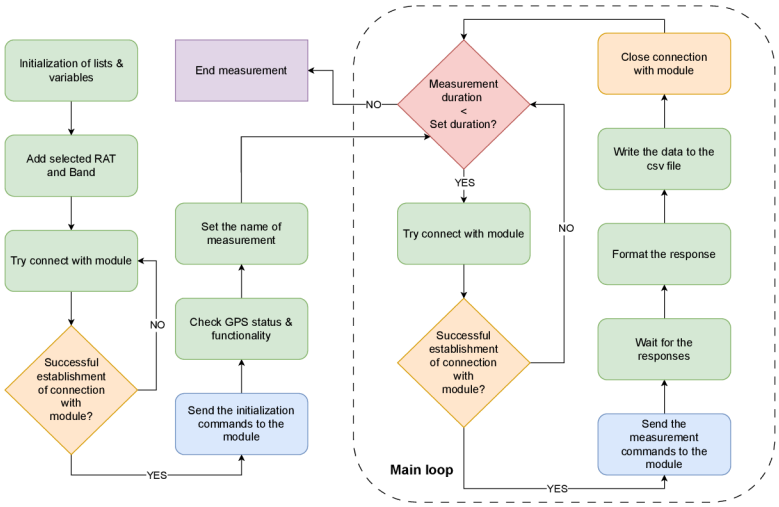

Fig. 3.6: Flowchart of the measurement script

(e.g., "http://127.0.0.1:8050/"), or by employing a pre-fork worker model like Gunicorn. Gunicorn is a Web Server Gateway Interface (WSGI) Hypertext Transfer Protocol (HTTP) server used to deploy *Dash* application at the address on the Unix device within the local network with a pre-defined port, aligning with the concept adopted in this work. The pure Python nature of *Dash* significantly simplifies the workflow, eliminating the need for other programming languages like JavaScript for web application development.

The fundamental components of the *Dash* application architecture are Layout and Callbacks. Layout defines the overall appearance of the application and comprises components in Hypertext Markup Language (HTML) and *Dash*, allowing for styling through Cascading Style Sheets (CSS). On the other hand, Callbacks are functions annotated with `@app.callback` that respond to user interactions, dynamically updating the application content based on these inputs.

Designed settings application

Leveraging the *Dash* framework enabled the creation of a user-friendly application for controlling and configuring measurements, as depicted in Fig. 3.7a, the user can specify the measurement name, duration, technology, preferred band in the specified technology, checkbox option for turning off or on GPS localization, and the trigger buttons 'START' and 'STOP'.

The application enables switching the GPS functionality for two types of specific measurements: static indoor and mobile outdoor. While GPS coordinates are essential for analyzing outdoor data, they are unnecessary for static indoor measurements, where GPS signals are often unavailable. By deactivating GPS localization, measurements become quicker as there's no need to wait for a 60-second cold start of the GPS technology on the Waveshare 5G Module before starting. Disabling safety and control mechanisms during GPS data acquisition also speeds up this process. As a result, during static indoor measurements, the device can capture up to one sample of all KPIs per second, whereas during mobile outdoor measurements, the fastest achievable sampling frequency is one sample of all KPIs per 3 seconds.

The 'START' and 'STOP' buttons employ a *Dash* Background callback, integrating the measurement script. This approach provides a scalable solution for handling lengthy callbacks on web servers. By executing these callbacks in a separate background queue, it mitigates worker overload and prevents request blocking [48]. Consequently, users terminate measurements at any point using the 'STOP' button. Moreover, real-time display of all measured data, along with a progress bar visualization as shown in Fig. 3.7b, ensures alignment with ongoing measurements.

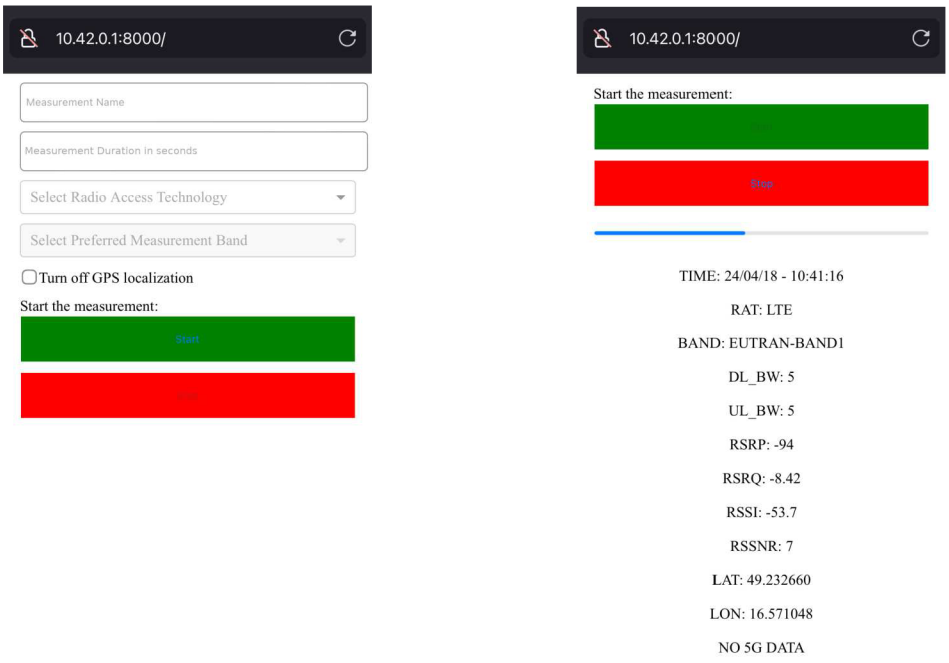

(a) Available settings for measurement (b) Tool while measuring

Fig. 3.7: Measurement setting tool on a phone via Firefox browser

Application deployment

The deployment of application is facilitated by Gunicorn, as previously mentioned. The foundation of this deployment is a bash script that executes upon the operating system's startup on the RPi. A flowchart illustrating the fundamental operation of this script is provided in Fig. 3.8 to offer insight into its functionality.

Initially, the script checks if an IP address is assigned to the module interface. If an IP address is detected, the script waits for 5 seconds before initiating the local network as a hotspot, thereby providing Internet access. Additionally, it can modify the IP address within the local network if necessary.

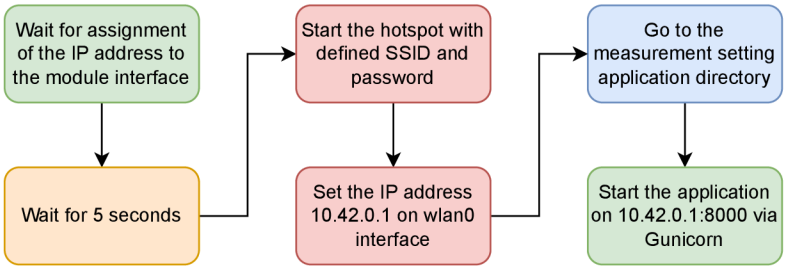

Fig. 3.8: Flowchart diagram of the startup bash script

Subsequently, the script navigates to the directory containing the *Dash* application and launches it using Gunicorn. The application is hosted at the address 10.42.0.1, which should correspond to the IP address of the RPi within the specified local network, and on the port 8000.

3.3 Data visualization

The hardware part is designed and consists of a Waveshare 5G Module, RPi 4 Model B, and a 40 Ah power bank, as can be seen in Fig. 3.9. This setup enables the initiation of data collection using a simple Python script together with the *Dash* application for setting measurements, the mentioned AT commands, and the bash script for initialization.

Another crucial aspect is the processing and visualization of the collected data. An inspiring example include the analysis and optimization tools provided by the already mentioned InfoVista, particularly software such as 'TEMS Instigation' or 'TEMS Discovery'. These tools offer insights into network performance by analyzing `log` files from devices equipped with specialized software. Users can visualize data on a map, comprehend the measured area, show individual graphs of KPIs, and extract various information from specific measured samples (see Fig. 3.10).

The visualization tool developed for this work follows a similar structure. It includes a user-friendly navigation bar, granting easy access to individual analyses of data from both mobile and static measurements. Moreover, it offers an `'About'` section that serves as a comprehensive guide for users. For instance, on the mobile

Fig. 3.9: Measurement setup

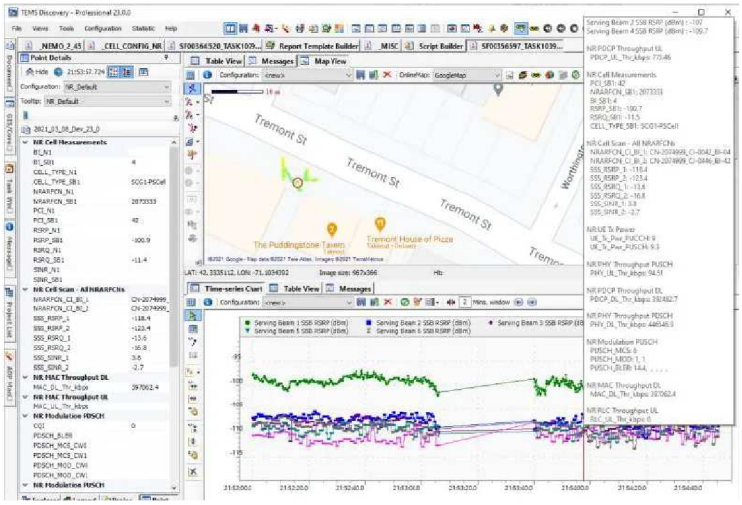

Fig. 3.10: TEMS Discovery [49]

measurement data analysis page, the tool features an interactive map enabling users to explore the measured area. Samples are color-coded based on predetermined thresholds (e.g., green for excellent signal, red for insufficient signal), allowing users to quickly identify areas of interest. Hovering over samples provides detailed information about the network. Furthermore, the tool presents graphical representations in the time domain for signal measurements, including RSRP, RSRQ, RSSI, and RSSNR. (Note: For the Waveshare 5G Module, RSSNR represents the average reference signal SNR of the serving cell, as SINR measurement is unavailable.) To ensure consistency in results, the tool incorporates integrated filtering mechanisms. These mechanisms isolate the analyzed RAT, band, operator, or other relevant parameters, facilitating focused analysis on specific criteria. Additionally, users can set individual thresholds for signal metrics, aiding in the targeted examination and detection of problematic areas.

3.3.1 Coverage Analysis tool

The final version of the analysis application is now complete, effectively fulfilling the specified requirements. Developed entirely using the *Dash* framework, the application operates system-independently, ensuring compatibility with major systems such as Windows, Mac OS, or various Linux distributions. This flexibility simplifies usage, requiring only the installation of a web browser and Python on the device. As previously mentioned, the top section of the application includes a clear navigation bar, as shown in Fig. 3.11. This navigation bar enables users to seamlessly navigate between different sections. The navigation bar includes the title `Coverage Analysis - Dashboard`, indicating the main page dedicated to mobile measure-

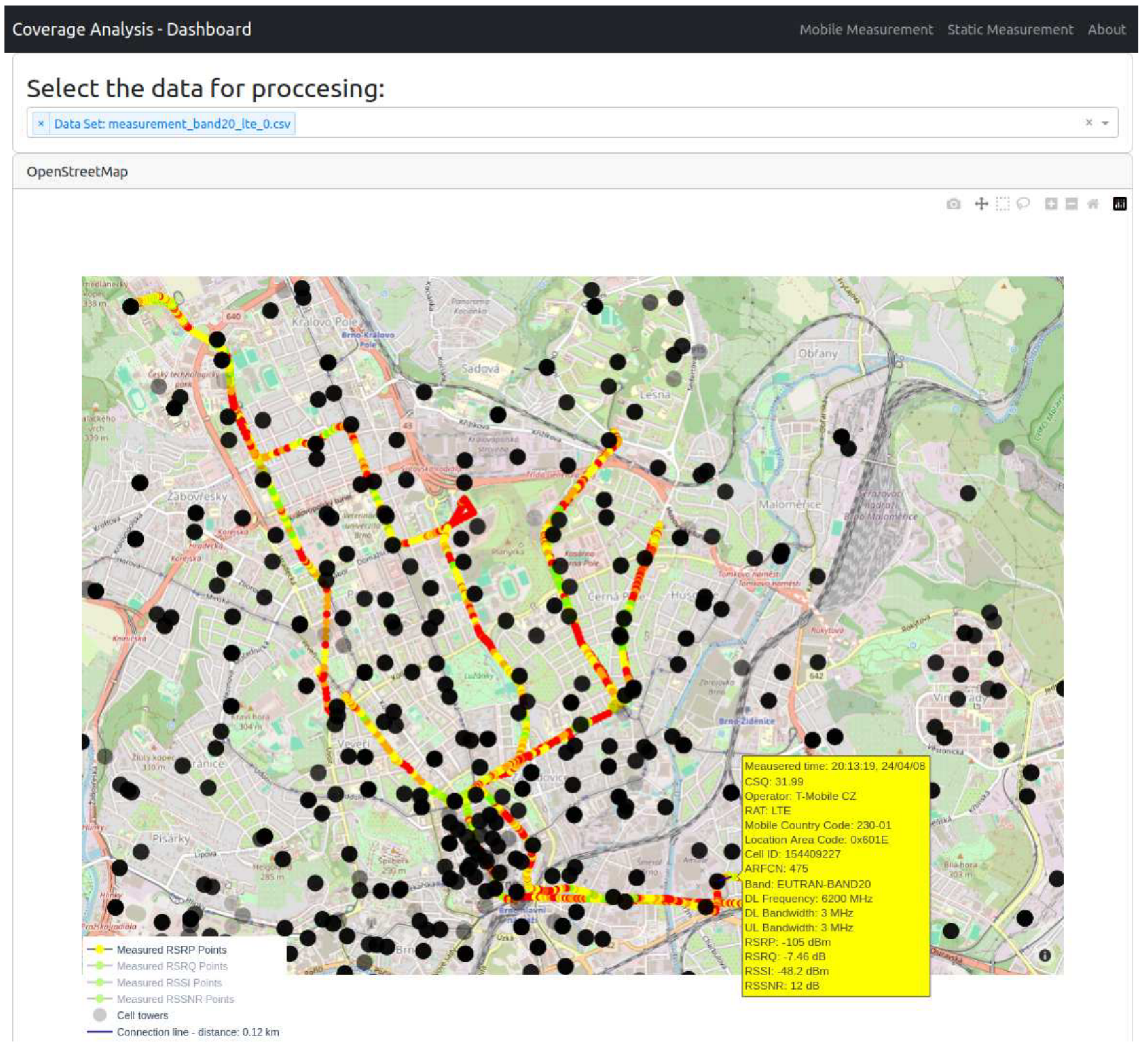

Fig. 3.11: Upper part of the application with navigation bar, dropdown data selector, and interactive map

ment analysis. Similarly, the `Mobile Measurement` section provides quick access to this main page. For static analysis, users can utilize the `Static Analysis` section. The `About` page offers detailed explanations of each feature within the application, serving as a helpful guide and documentation resource for users.

Mobile Measurement

The `Mobile Measurement` page consists of four main components. As shown in Fig. 3.11, the top section of the page is divided into two parts. The first part, labeled **Dropdown data selector**, enables users to select and process data. Users can choose multiple datasets, merge them together, or deselect them as needed. The second part is the **Interactive map**, which utilizes the OpenStreetMap API to retrieve geodata from the OpenStreetMap database. Measured points are displayed

this map, color-coded based on predefined thresholds for each KPI as shown in Table 3.2. These thresholds were determined through a combination of experimental measurements and objective assessments, considering various scenarios, including Internet connectivity status and outages on individual bands and technologies.

The eNBs or gNBs are represented by larger black circles (coordinates from [50]). Hovering over a sample on the map reveals a detailed summary of the measured sample. Clicking on individual samples generates a line connecting the sample to the corresponding cell at that moment, displaying the calculated distance in the legend. Additionally, the legend allows users to switch between different displays of individual metrics. The comprehensive functionality is depicted in Fig. 3.11.

To facilitate useful data analysis, a **Filtering** was implemented, which is also linked to the **Interpolation** setting. Through filtering dropdown menus, users can filter data based on RAT, band, and operator. Additionally, the interpolation setting enables the estimation of the coverage map over the measured data, specifying the KPI for calculation, as shown in Fig. 3.12.

The last important part for analysis is the so called **Graphs**, which display waveforms of measured KPIs, like RSRP, RSRQ, RSSI, and RSSNR, are shown in Fig. 3.13. Detailed information about each sample is displayed when hovering over it. The synchronization between the map and all graphs ensures that clicking on a point in either the graph or the map triggers the same callback in the *Dash* application, generating a line between the measured point and the corresponding cell. For various analysis scenarios, filtering values within a defined range is essential. To achieve this, a range slider is employed. This slider enables users to filter a specific metric, allowing them to, for example, isolate only very low values of the RSRP metric. This functionality aids in identifying areas with poor coverage and facilitates targeted analysis.

Table 3.2: 4G/5G NR NSA: Quality thresholds for different KPI metrics and bands

Metric	Excellent	Good	Moderate	Bad
RSRP (LTE Band 1)	> -90 dBm	-90 to -120 dBm	-120 to -140 dBm	< -140 dBm
RSRP (LTE Band 3)	> -90 dBm	-90 to -120 dBm	-120 to -140 dBm	< -140 dBm
RSRP (LTE Band 7)	> -95 dBm	-95 to -125 dBm	-125 to -145 dBm	< -145 dBm
RSRP (LTE Band 20)	> -80 dBm	-80 to -110 dBm	-110 to -130 dBm	< -130 dBm
RSRP (NR Band 78)	> -85 dBm	-85 to -95 dBm	-95 to -105 dBm	< -115 dBm
RSRQ	> -10 dB	-10 to -15 dB	-15 to -20 dB	< -20 dB
RSSI	> -65 dBm	-65 to -75 dBm	-75 to -85 dBm	< -85 dBm
RSSNR	> 10 dB	3 to 10 dB	0 to 3 dB	< 0 dB

Fig. 3.12: Filtering menu together with interpolation settings

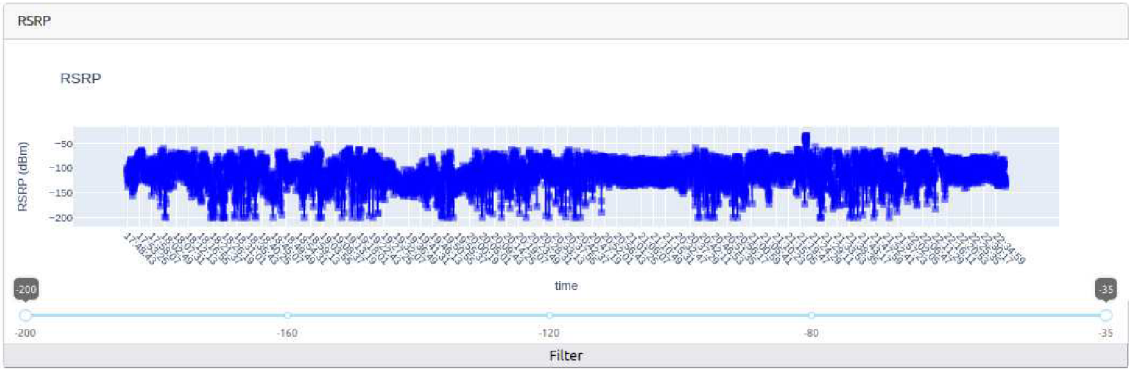

Fig. 3.13: Example of time series graph in the application

Static Measurement

The `Static Measurement` page closely resembles the `Mobile Measurement` page previously described. However, in static measurements, data are collected from a fixed location indoors, where capturing GPS signals is often not feasible. Therefore, the interactive map is removed from this page.

Essentially, the `Static Measurement` page mirrors the structure of the page designed for mobile measurements. However, instead of interactive maps, boxplots and histograms are featured, as depicted in Fig. 3.14. This similarity in layout and functionality ensures consistency across different measurement scenarios while adapting the visualization tools to suit the characteristics of static measurements. Additionally, two sections have been incorporated, crucial for analyzing large datasets with significant variability. First, a section has been introduced to set the minute rolling average, as depicted in Fig. 3.15. By averaging data over a specified window, it becomes easier to discern long-term trends or patterns while mitigating the impact of short-term fluctuations. Furthermore, another section aids in optimizing the data loading time. Given that static measurements typically entail hundreds of thousands to millions of measured samples, loading such extensive datasets on a standard computer hosting the application can impose an unnecessarily heavy burden.

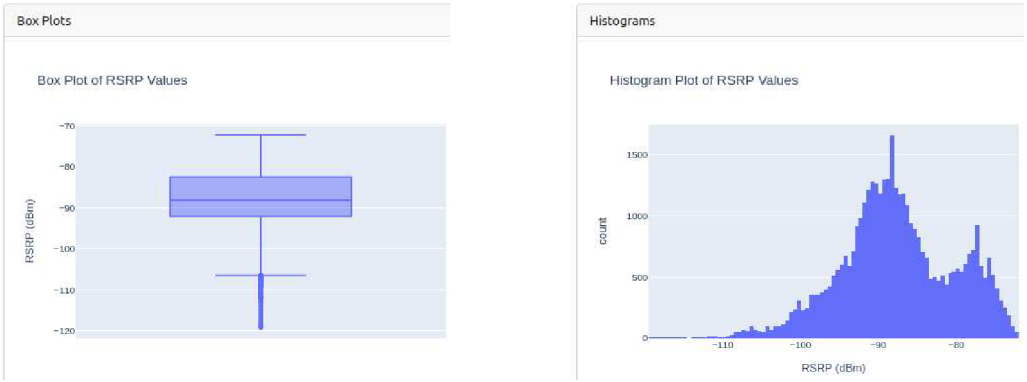

(a) RSRP Box plot (b) RSRP Histogram

Fig. 3.14: Boxplots and histograms implemented in static analysis page

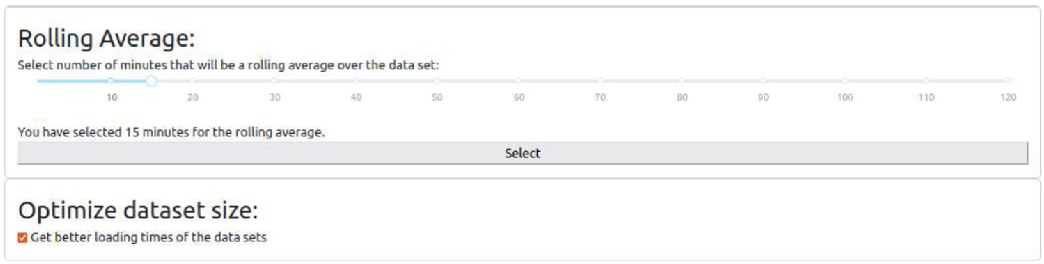

Fig. 3.15: Two added sections for averaging the static dataset and optimizing the loading time of the page

Therefore, this option allows users to reduce the dataset size, thereby alleviating the data loading strain. If this option is enabled, the dataset comprises only every nth value, based on the specified value of the slider in the 'Rolling Average' section.

About

This page serves as an introduction and user manual for individuals utilizing the application. It explains the fundamentals of measurement, outlines where to locate available data, and delineates the functionality of various features. As depicted in Fig. 3.16, the page begins with an introduction to the measurement methodology. Subsequently, it includes a user guide section, detailing the operation of individual features in mobile or static analysis and providing clarification where necessary.

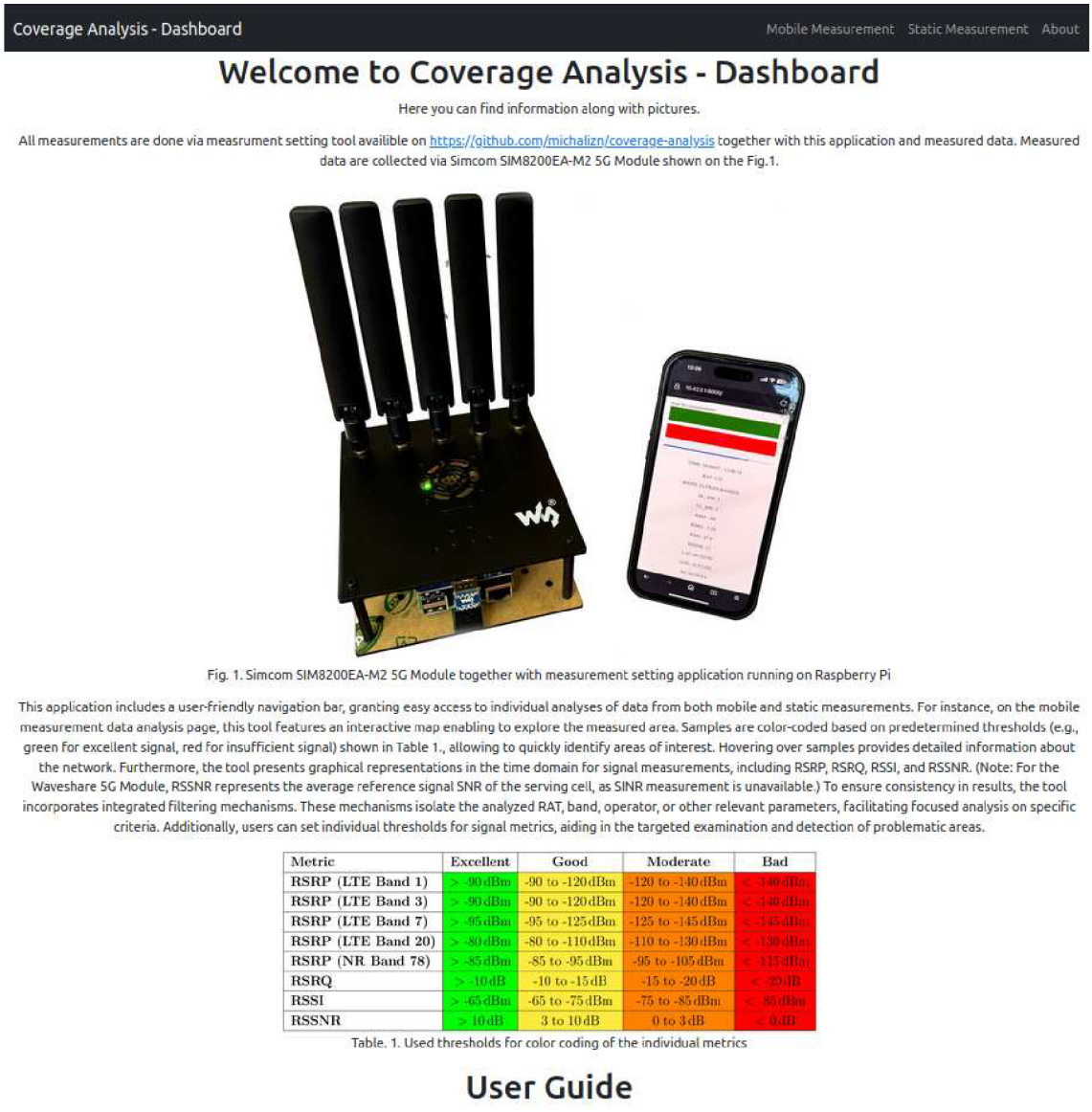

Fig. 1. Simcom SIM8200EA-M2 5G Module together with measurement setting application running on Raspberry Pi

This application includes a user-friendly navigation bar, granting easy access to individual analyses of data from both mobile and static measurements. For instance, on the mobile measurement data analysis page, this tool features an interactive map enabling to explore the measured area. Samples are color-coded based on predetermined thresholds (e.g., green for excellent signal, red for insufficient signal) shown in Table 1., allowing to quickly identify areas of interest. Hovering over samples provides detailed information about the network. Furthermore, the tool presents graphical representations in the time domain for signal measurements, including RSRP, RSRQ, RSSI, and RSSNR. (Note: For the Waveshare 5G Module, RSSNR represents the average reference signal SNR of the serving cell, as SINR measurement is unavailable.) To ensure consistency in results, the tool incorporates integrated filtering mechanisms. These mechanisms isolate the analyzed RAT, band, operator, or other relevant parameters, facilitating focused analysis on specific criteria. Additionally, users can set individual thresholds for signal metrics, aiding in the targeted examination and detection of problematic areas.

Metric	Excellent	Good	Moderate	Bad
RSRP (LTE Band 1)	> -90 dBm	-90 to -120 dBm	-120 to -140 dBm	< -140 dBm
RSRP (LTE Band 3)	> -90 dBm	-90 to -120 dBm	-120 to -140 dBm	< -140 dBm
RSRP (LTE Band 7)	> -95 dBm	-95 to -125 dBm	-125 to -145 dBm	< -145 dBm
RSRP (LTE Band 20)	> -80 dBm	-80 to -110 dBm	-110 to -130 dBm	< -130 dBm
RSRP (NR Band 78)	> -85 dBm	-85 to -95 dBm	-95 to -105 dBm	< -115 dBm
RSRQ	> -10 dB	-10 to -15 dB	-15 to -20 dB	< -20 dB
RSSI	> -65 dBm	-65 to -75 dBm	-75 to -85 dBm	< -85 dBm
RSSNR	> 10 dB	3 to 10 dB	0 to 3 dB	< 0 dB

Table. 1. Used thresholds for color coding of the individual metrics

User Guide

Fig. 3.16: About page that serves as an introduction and user guide

4 Processing Methods and Algorithms

To access individual KPIs of the 4G/5G network, various algorithms, methods, or mathematical tools must be employed. This chapter focuses on different approaches, including ML algorithms and interpolation. Through these methods, tools, and analyses, the scope of information is expanded, leading to insights into the performance of the mobile network.

4.1 Machine Learning Algorithms

With the increasing load on mobile networks, MNOs are compelled to employ advanced or new methods for detecting potential threats within the ML models to predict events, which may cause network overload, subsequently leading to various issues. Timely intervention based on these predictions allows for effective problem resolution, preventing adverse impacts on end-users. With the availability of sufficiently large sets of measured KPIs, these models can be employed to predict various scenarios. For instance, it becomes possible to estimate the future load on an individual serving cell connected to the measurement setup, identifying any irregularities in metrics and their influences. This allows for insights into expected load variations, such as lower loads at night compared to daytime.

The measured dataset is initially divided into training and testing sets, as can be seen in selected approaches for dataset division in Fig. 4.1. Using the training dataset, the ML algorithm identifies individual time patterns within the measured data. Subsequently, based on this training, the algorithm generates coefficients used in predicting the given KPI. Once the prediction is generated, the evaluation metrics such as Mean Absolute Error (MAE) or Root Mean Squared Error (RMSE) help assess the error between the created prediction and the test set, which represents the actual measurements. Analyzing this error allows for determining the suitability of the model for forecasting the given KPI of the mobile site. If necessary, more

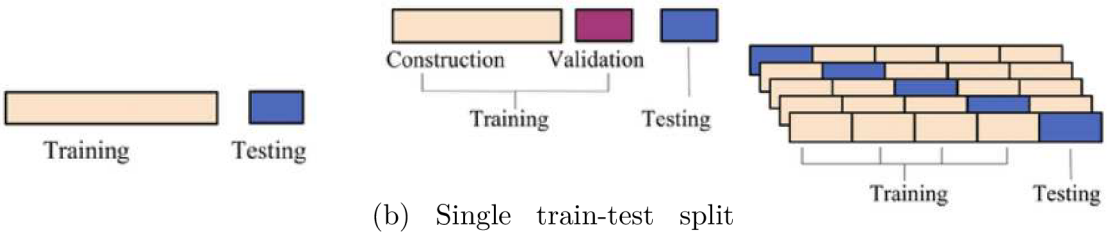

(a) Single train-test split (b) Single train-test split with an external testing set (c) Cross-validation (5-fold)

Fig. 4.1: Three selected approaches for dataset division [51]

adjustments to the parameters and coefficients of the model can be made to improve the forecasted results.

Among others, the most popular ML models are: Linear Regression, Logistic Regression, Decision Trees, Support Vector Machines (SVM), K-Nearest Neighbors (KNN), Artificial Neural Networks (ANN), Gradient Boosting Machines (GBM) – XGBoost [52]. Each of these models has its strengths and weaknesses, and the choice of model depends on the specific problem and the characteristics of the dataset. More about listed models can be found in [53].

The topic of ML is extensive and has the potential to warrant a separate study solely focused on predicting KPIs, comparing various models to select the optimal one, and explaining the necessary parameters and methods used in ML algorithms. Therefore, in this work, we will only provide a brief overview and utilize the Linear Regression model and XGBoost model, which belong under the GBM, for sequential analysis of primarily static data. This forecasting approach can prove useful when dealing with a large volume of static data and creating coverage predictions using the RSRP metric, thereby identifying potential fluctuations in the future. Further exploration and utilization of these methods can be considered for future studies.

4.1.1 Linear Regression model

Utilizing simple forecasting models like linear regression becomes beneficial for predicting values such as throughput, Physical Resource Block (PRB) utilization, the number of users, and other KPIs for individual cells. These individual indicators typically demonstrate growth over time, aligning with the increasing demands and number of users in mobile networks. This approach is computationally efficient and easy to implement, requiring minimal computing resources.

The linear regression model is used for predicting a quantitative response variable Y based on a predictor variable X. The underlying assumption is that there exists an approximately linear relationship between X and Y [54]. The Python programming language can be employed for working with this model, specifically utilizing the `LinearRegression` model from the `sklearn.linear_model` package. According to the definition provided in the documentation of this package [55], linear regression is mathematically expressed as follows 4.1:

$$Y(w, X) = w_0 + w_1 X_1 + w_2 X_2 + \ldots + w_i X_i \tag{4.1}$$

where $Y(w, X)$ is a predicted response vector, w_0 is a bias term, and w_i and X_i are the ith weight and input, respectively.

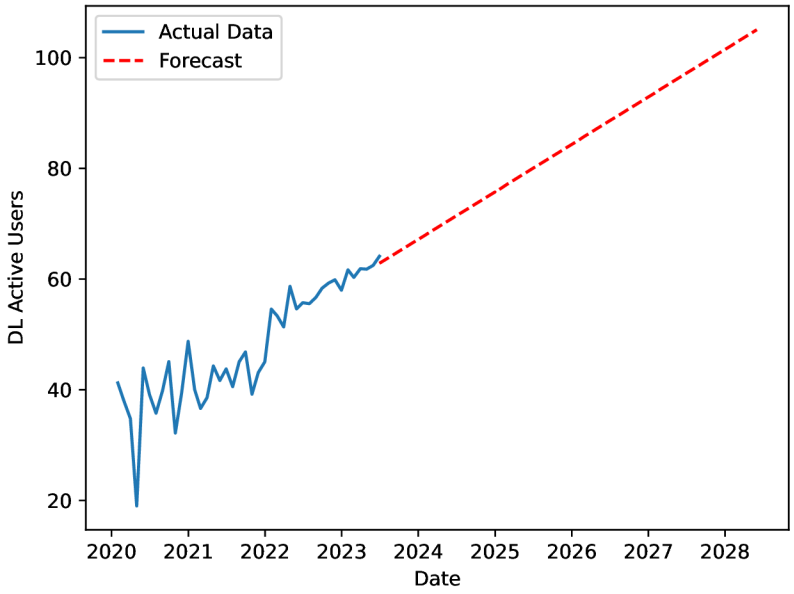

Fig. 4.2: Linear regression model forecast

An example of utilizing this model with the `sklearn.linear_model` package is illustrated in Fig. 4.2, showcasing the ascending trend of active users in DL communication (for illustrative purposes only).

4.1.2 XGBoost model

In this work, one of the top-performing out-of-the-box models, XGBoost (Extreme Gradient Boosting), has been selected for the prediction model. Compared to Linear Regression, XGBoost is much more sophisticated and is expected to yield superior prediction results. However, this comes at the expense of computational performance. The XGBoost model is readily available as a package for ML in Python. Due to its complexity, we will only provide a high-level overview of how the prediction is made.

This model belongs to the group of supervised learning models, which entails training a model based on patterns with features and leveraging these patterns in a dataset to predict new datasets with similar patterns. The model utilizes Gradient Boosting Decision Trees (GBDT), an algorithm that employs numerous relatively simple models for prediction to construct a robust prediction model [56]. GBDT constructs a model comprising multiple decision trees, where each decision tree generate a model that predicts the data by evaluating a tree structure of if-then-else true/false feature questions, estimating the minimum number of questions required to assess the probability of making a correct decision [56].

GBDTs iteratively train an ensemble of shallow decision trees, with each iteration utilizing the error residuals of the previous model to fit the next model. The final prediction is obtained by combining the predictions of all the trees with appropriate weighting [56]. An example of prediction using this model is depicted in Fig. 4.3. Cross-validation was employed, considering properties such as dependence on the hour of the day, to forecast data one day into the future based on seven days of static measurement of the RSRP metric.

By extracting relevant time-related features such as minute, hour, and day of the week from the dataset's index, the model gains insights into temporal patterns. Additionally, lag features are incorporated to capture the historical behavior of the target variable by considering past RSRP values at different time intervals.

The `TimeSeriesSplit` provided by `sklearn.model_selection` technique divides the dataset into five folds, with each fold representing a test size of one day, ensuring the evaluation of the model's predictive accuracy over varying time periods, where model within each fold involve training an XGBoost regressor on the training data while simultaneously evaluating its performance on both the training and validation sets. The evaluation metric employed was RMSE, with the score across all folds being 5.6634. The XGBoost regressor's hyperparameters were left unchanged, reflecting the default state of the model to demonstrate its capabilities. For improved prediction results, investing in hyperparameter tuning is essential. Additionally, conducting more in-depth data analysis to identify important features can further enhance the model's performance.

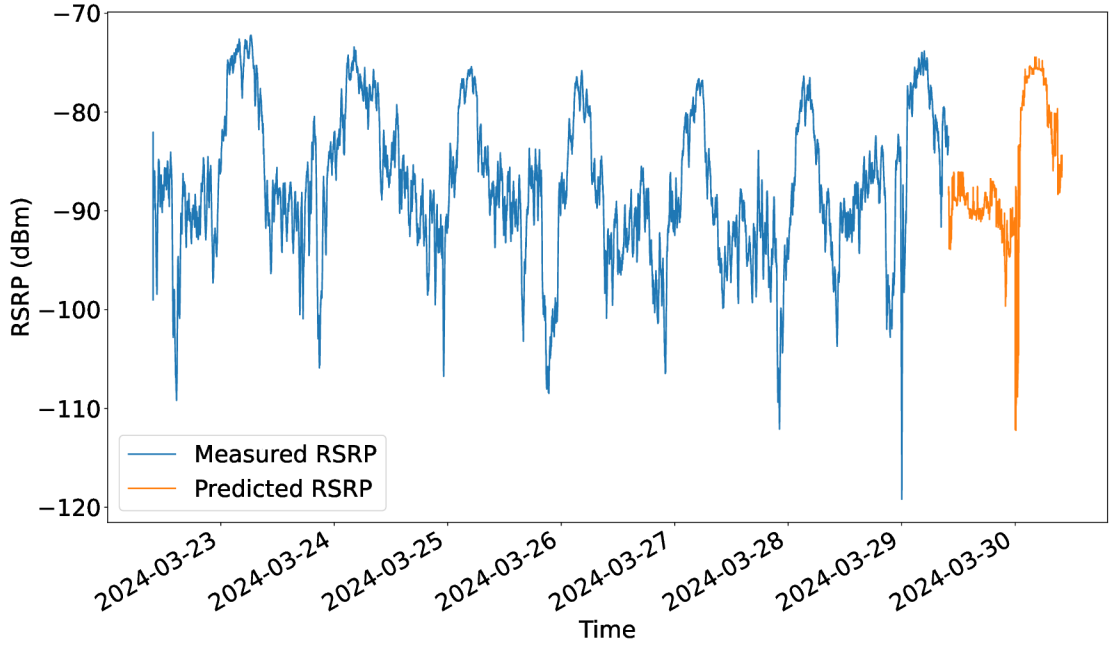

Fig. 4.3: Prediction into one day of RSRP metric with XGBoost model

4.2 Interpolation of measured data

The use of interpolation in this work has a significant impact. Through interpolation, it becomes possible to create an approximation of the coverage map for 4G or 5G technology on a specific RF band or for an individual operator. In mathematical terms, interpolation seeks the most suitable approximation of points lying between specified significant points. Therefore, with a sufficient number of points in the two-dimensional (2D) space, as illustrated in Fig 4.4, where the benchmark was conducted for testing the measurement setup and proposed functions, a coverage map between these points can be obtained through interpolation.

Python, specifically the `scipy.interpolate` package, is utilized for interpolation in this work. This package offers spline functions and classes, as well as one-dimensional (1D) and multidimensional interpolation classes [57].

4.2.1 Types of Interpolation

Determining the values of points on the 2D grid depends on the chosen interpolation method, specifically *Bilinear*, *Nearest Neighbor*, or *Cubic convolution*. The selection of the method is contingent upon the nature of the input data and its intended application after the operation. Consequently, all three methods are employed to obtain results and determine which one provides the most probable coverage for the given area.

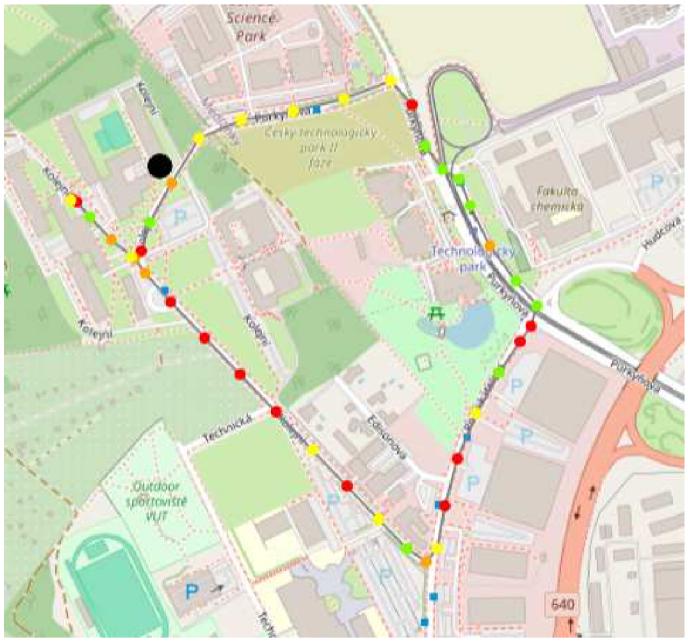

Fig. 4.4: Test measurement (RSRP points)

Bilinear interpolation

Bilinear interpolation involves calculating a weighted average of the four nearest points, where the influence of an input point increases as its proximity to the output point increases. While this method allows for deviations in output values compared to the nearest input, these deviations always fall within the same range of input values. Due to its potential to alter values, the *Bilinear* method is not suitable for categorical data but is well-suited for continuous data, such as the measured RSRP data tested in this context. The result of the *Bilinear* method is illustrated in Fig. 4.5a.

Nearest Neighbor

In the *Nearest Neighbor* method, grid values remain unchanged, preserving the accuracy of the input values. The output point values are determined by the nearest center point on the input grid. While this method can be applied to continuous data, it tends to produce blocky results, as demonstrated in the outcome when applying this method to the measured data, as shown in Fig. 4.5b.

Cubic Convolution

This method involves analyzing the 16 closest points around the specified output point and interpolating these points with a smooth curve. This method not only modifies the input values but can also yield an output value outside the input range, resembling the occurrence of a dip or peak. While *Cubic convolution* is not suitable for categorical data, it excels in smoothing continuous data, as evident in Fig. 4.5c, where the coverage map of the tested area closely resembles the most expected state.

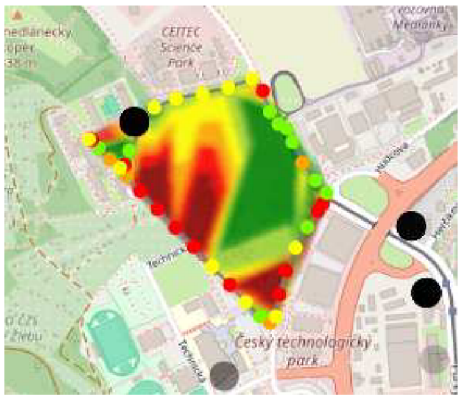

(a) *Bilinear* interpolation

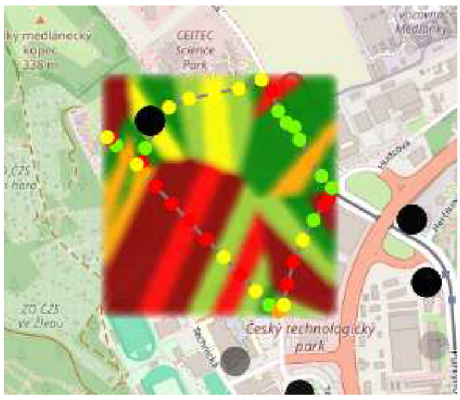

(b) *Nearest Neighbor*

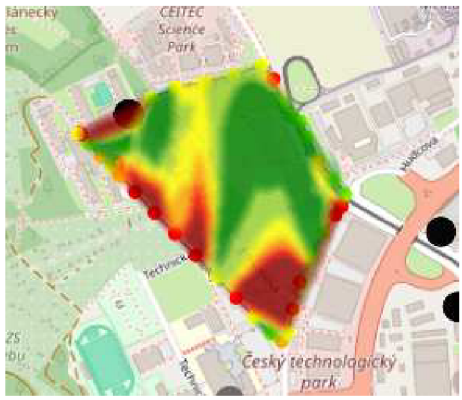

(c) *Cubic convolution*

Fig. 4.5: Interpolation methods used on measured RSRP points

5 Results and Coverage Estimation

In this part of the work, the focus is on analyzing all measured data using the proposed methodology and measurement setup. The measurement process was segmented into two main parts: static and mobile measurements, conducted in both 4G LTE and 5G NR NSA technologies.

The following text is divided into two primary sections: LTE measurement data and individual analyses of the bands deployed in the Czech Republic. Additionally, analysis is conducted in 5G NR technology, where measurement is performed on one band deployed in the Czech Republic, considering the characteristics of the utilized 5G module. All the measurements presented in this thesis were conducted in 2024.

5.1 LTE Measured data

Due to the versatility of the setup employed, supporting all bands in LTE technology, it was feasible to individually measure and analyze these bands, yielding quantitative insights. We delve into the findings from the static measurement, followed by an assessment of mobile measurements with a coverage estimation in the city of Brno.

5.1.1 Static Measurement

All static indoor measurements were conducted in the same way at Pod Palackého Vrchem dormitory on the Brno University of Technology (BUT) campus for seven consecutive days. The measurement device was positioned under a table in a second-floor room in block A04, aligning with the base station located at Brno - Královo Pole, Kolejní 2905/2, block A04 of the BUT dormitory, with Cell ID (CID) 606491, as shown in Fig. 5.1.

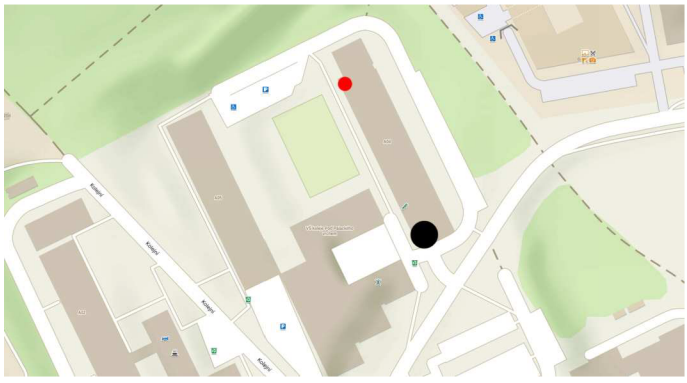

Fig. 5.1: Location of the static indoor measurement (red dot) with serving cell (black dot)

Despite being on the opposite side of the building from the cell, there was no LOS with the cell. The measurement utilized the proposed solution discussed in this work within the operational LTE network of the Czech MNO T-Mobile Czech Republic. Signal KPIs (RSRP, RSRQ, RSSI, RSSNR) were recorded approximately at a frequency of one sample per second using the provided hardware and software.

At this particular location, coverage is provided by three bands from the T-Mobile. These bands are Band 20, Band 3, and Band 1. Unfortunately, Band 7 (2600 MHz) is not available at this location, and thus no static indoor measurements were conducted on this band.

LTE Band 20 (800 MHz)

Band 20 is widely recognized as one of the most utilized bands in LTE technology globally, employed by MNOs for the deployment of LTE networks. It is distinguished as a sub-1 GHz band, offering extensive coverage in regional and rural areas as well as robust in-building coverage [58]. These characteristics have made it instrumental for MNOs in meeting regulatory coverage requirements and facilitating the launch of LTE technology [58]. Consequently, Band 20 has become one of the most utilized bands in LTE technology owing to its deep penetration and wide coverage capabilities, particularly attributable to its 800 MHz frequency.

Moreover, LTE-A or LTE-Advanced Pro technologies can leverage carrier aggregation to combine the bandwidth of Band 20 with other carriers, enhancing data throughput. Given that Band 20 coverage from the measured T-Mobile network features a 10 MHz bandwidth in the Czech Republic, carrier aggregation is frequently utilized to achieve high data rates, or users may directly connect to mid bands such as Band 3. However, due to its large wavelength, this band does not readily support advanced technologies like Massive MIMO and beamforming [58].

A static indoor measurement was conducted to assess the performance of LTE Band 20 with a module configured to the specified cell CID 606491 within the Pod Palackého Vrchem dormitory on the BUT campus. The measurement spanned from 1:00 p.m. on Monday, April 29th 2024, to 1:00 p.m. on Monday, May 6th 2024, capturing over 736,000 KPI samples, each containing RSRP, RSRQ, RSSI, RSSNR, and other relevant information.The measurement was conducted during normal college days, indicating significant user presence on weekdays, while fewer users were present during the weekend. Fig. 5.2 displays all measured samples and 15-minute averages of signal KPIs. A 15-minute interval was selected to balance data detail and presentation smoothness as in [34].

The analysis of LTE Band 20 static measurements reveals interesting patterns in KPIs, particularly in RSRP values. The observed variability underscores the

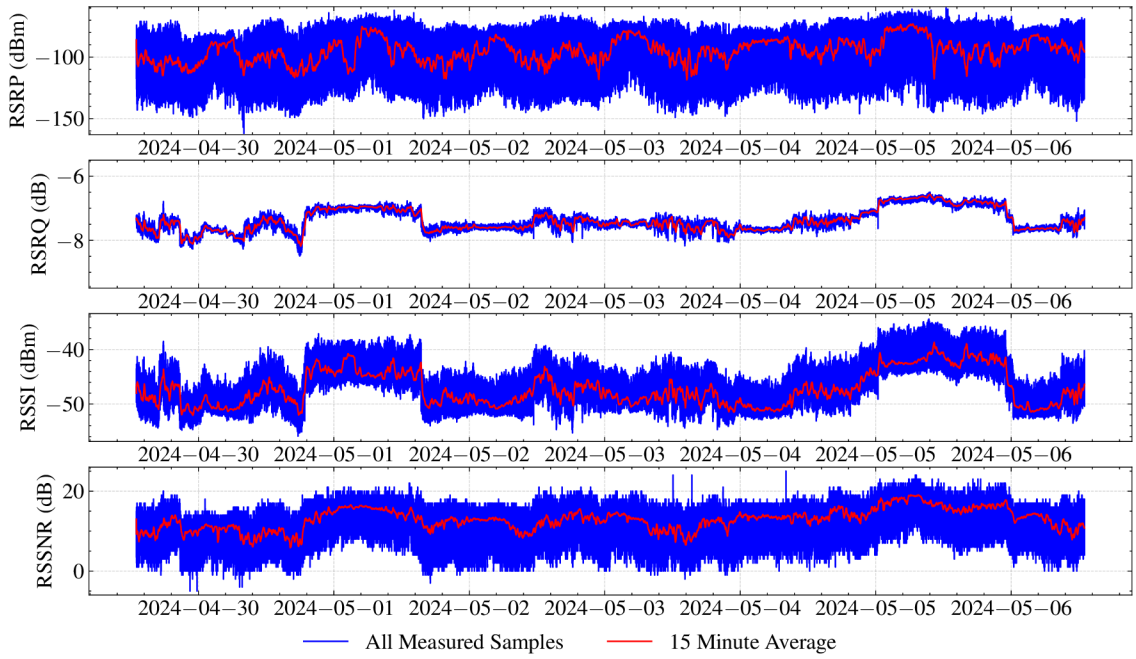

Fig. 5.2: Static indoor measurement conducted at Pod Palackého Vrchem dormitory on the BUT campus from April 29th to May 6th 2024 (LTE Band 20)

dynamic nature of network performance, influenced by factors such as time of day and network load. The periodic behavior of RSRP, as depicted in Fig. 5.2, aligns with expectations, with values decreasing during peak periods of network congestion. This trend is further elucidated in Fig. 5.3, which illustrates variations in RSRP values by hour. The early morning hours, specifically between 1:00 a.m. to 9:00 a.m., we can see an increase in RSRP values peaking around 4:00 a.m. to 5:00 a.m., likely attributed to reduced network load and improved signal conditions. Conversely, fluctuations around 3:00 p.m. and 8:00 p.m. suggest varying occupancy levels in the dormitory, impacting network usage and signal quality. These findings underscore the intricate interplay between network dynamics and signal quality in LTE Band 20.

A high positive correlation, with a correlation coefficient of 0.85, was observed between RSSI and RSRQ, indicating that higher overall signal strength correlates with better quality of the useful signal. The histogram in Fig. 5.4 illustrates the distribution of RSRP values for LTE Band 20. The histogram exhibits a roughly normal distribution, slightly skewed towards the left with RSRP values below the -100 dBm threshold. This suggests that the majority of RSRP values fall within a specific range, with fewer occurrences at the extremes. The peak of the distribution lies around -84 dBm, indicating values that were measured mostly during the morning hours when network load is lower. The median RSRP value of -92 dBm represents good overall signal strength. The distribution spans a quite large range,

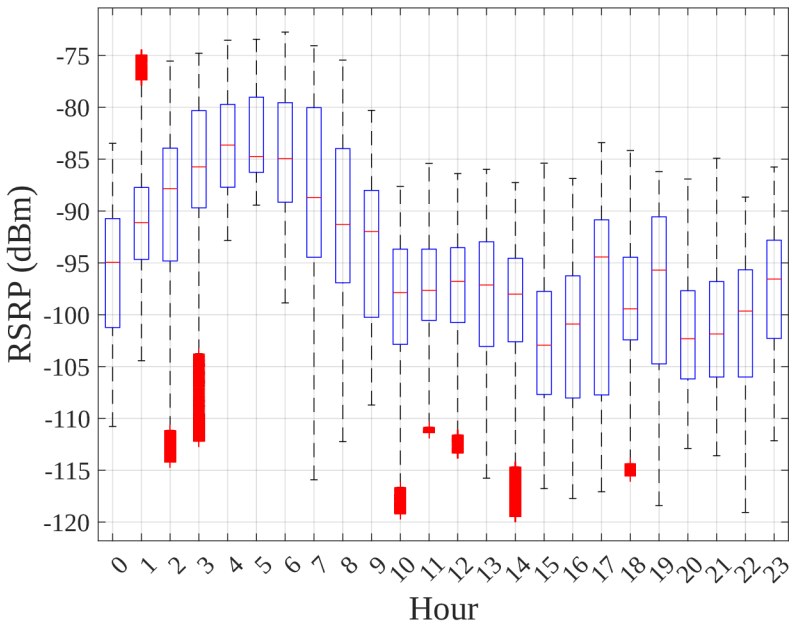

Fig. 5.3: Boxplots illustrating the variation in RSRP values aggregated by hour throughout the measurement conducted at Pod Palackého Vrchem dormitory on the BUT campus from April 29th 2024 to May 6th 2024 (LTE Band 20, data averaged over a 15-minute window)

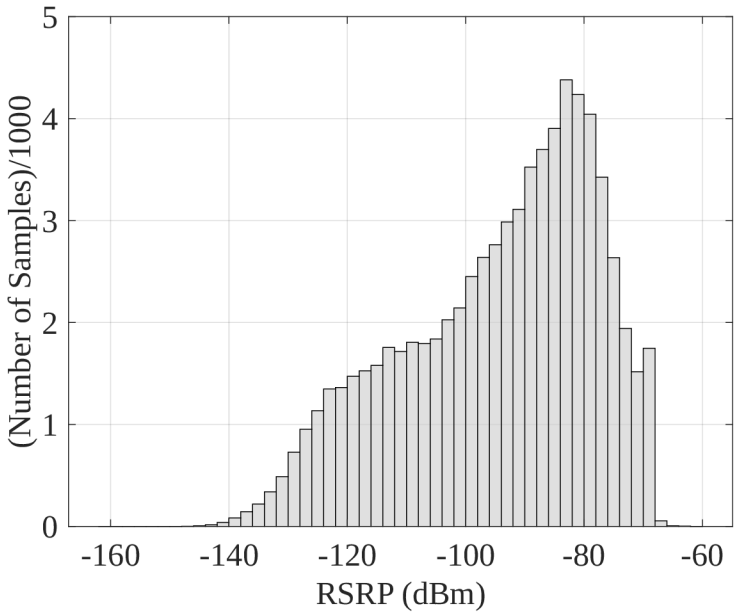

Fig. 5.4: RSRP Histogram of static measurement conducted at Pod Palackého Vrchem dormitory on the BUT campus from April 29th 2024 to May 6th 2024 (LTE Band 20). Bin size = 2 dBm.

from -144 dBm to -66 dBm, indicating significant variation in received signal strength during the measurement period.

The slightly skewed towards the left of the histogram in Fig. 5.4 is caused by increased network load during the day, leading to slightly lower RSRP values compared to the early morning hours. This phenomenon aligns with the overall trend observed in the measurement data, as shown in Fig. 5.3.

RSRP exhibited periodic behavior influenced by time of day and network load, with notable variability and a standard deviation of 16.33 dBm. Conversely, RSRQ demonstrated minimal variability, while RSSI had two big time fluctuations and RSSNR remained moderately stable. Fig. 5.5 presents more detailed distributions of individual metrics through boxplots. The observed phenomenon of large increases in RSRQ, RSSI, and RSSNR values on May 1 and May 5, each lasting for about 24 hours, is indeed interesting. However, it's challenging to definitively attribute this change to network load alone, especially considering the different occupancy patterns of the dormitory on Wednesday and Sunday. Since Wednesday typically sees higher occupancy than Sunday, it's unclear whether network usage patterns alone can explain such drastic fluctuations in these metrics. Interestingly, RSRP values exhibited more normal behavior during this period, showing typical variations in response to network load. At the same time, outlier values of around -160 dBm can be observed, indicating a very poor signal, as indicated in Table 3.2, even during

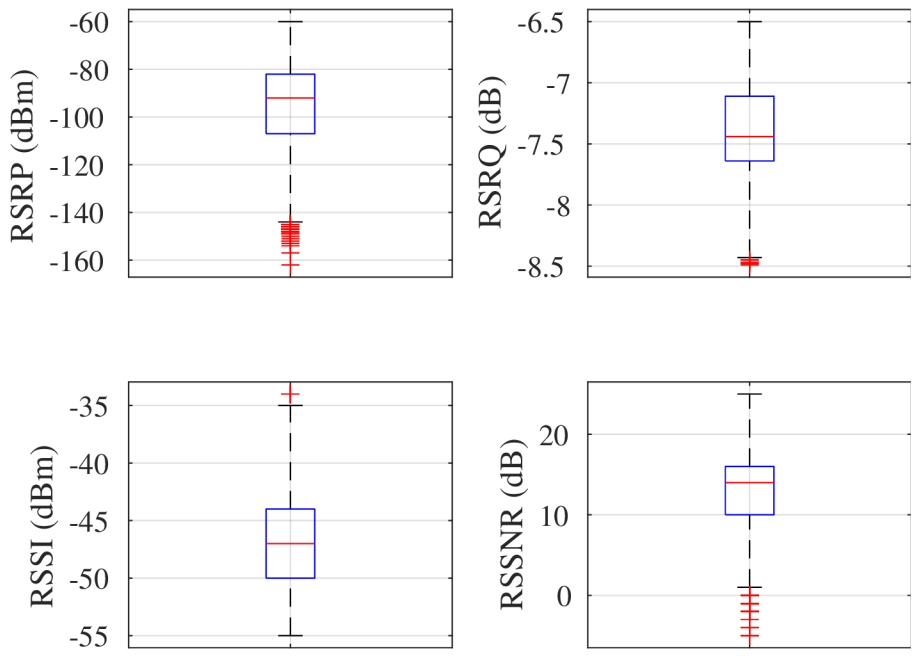

Fig. 5.5: Boxplots of a static measurement conducted at Pod Palackého Vrchem dormitory on the BUT campus from April 29th to May 6th 2024 (LTE Band 20)

the static measurement, right next to the serving cell. Further investigation may be necessary to determine the underlying cause of these sudden changes in RSRQ, RSSI, and RSSNR values.

An interesting insights to the distribution of RSRP values is provided by Fig. 5.6. The distribution of RSRP values grouped by the day of the week clearly demonstrates a strong correlation between RSRP values and the occupancy of the dormitory. This correlation allows for reasonable inference regarding the days when the dormitories are most occupied, based solely on network load indicators. On Wednesday, for instance, the median RSRP value of -100 dBm, the lowest among all days of the week, indicates the highest network load in this band. As the week progresses, the network load gradually decreases, reaching its peak on Saturday with a median of -90.2 dBm, corresponding to the fewest students in the dormitories. With the beginning of the working week, the network load increases again, continuing this cyclical trend throughout the school year.

These findings highlight LTE Band 20 as one of the most utilized bands in this location, underscoring the dynamic nature of network usage patterns influenced by student occupancy. This cyclical trend, extending from September to June, underscores the importance of considering temporal variations in network load for accurate network planning and optimization.

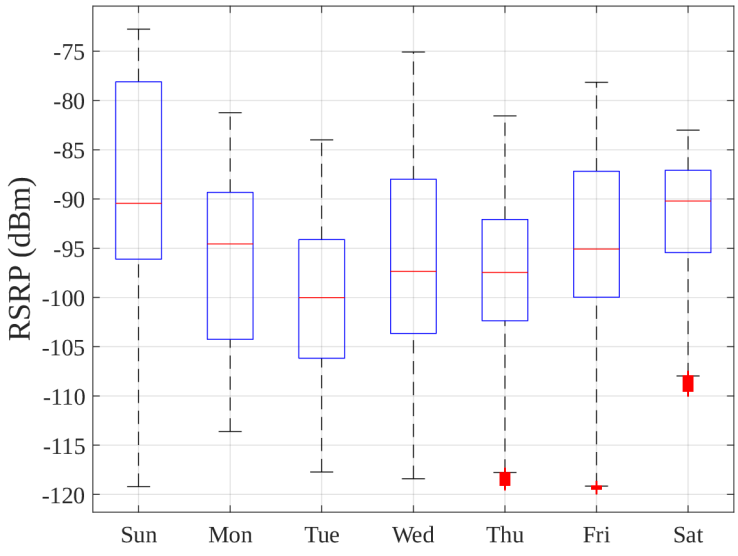

Fig. 5.6: Boxplots of the RSRP value distributions grouped by the day of the week representing the variability for a specific day of a static measurement conducted at Pod Palackého Vrchem dormitory on the BUT campus from April 29th to May 6th (LTE Band 20, data averaged over a 15-minute window)

LTE Band 3 (1800 MHz)

Band 3 serves as a capacity layer complementing the basic Band 20 facilitating rapid deployment of enhanced mobile broadband services both indoors and outdoors. This setup enables operators to accommodate more customers while enhancing user experiences [59]. Approximately 65% of devices are compatible with the Band 3 spectrum, positioning Band 3 as the primary band for LTE systems across Europe, Asia, and other International Telecommunication Union (ITU) regions [59].

A static indoor measurement was conducted again with the measurement equipment configured to the specified cell CID 606491 in LTE Band 3 (1800 MHz, FDD) at Pod Palackého Vrchem dormitory on the BUT campus from 9:40 a.m. on Friday, March 22nd 2024 to 9:40 a.m. on Friday, March 29th 2024. Fig. 5.7 illustrates all measured samples and 15-minute averages of all measured signal KPIs. Once again, a 15-minute interval was chosen as a suitable compromise between preserving data detail and ensuring smoothness in the presentation. The measurement was conducted during normal college operation, resulting in significant user presence on weekdays, while fewer users were present during the weekend. During this measurement, over 600,000 KPI samples were collected, each containing RSRP, RSRQ, RSSI, RSSNR, and other relevant information.

As depicted in Fig. 5.7, variability is evident even in the static measurement of cellular network signal metrics in this band. Notably, an intriguing pattern emerges,

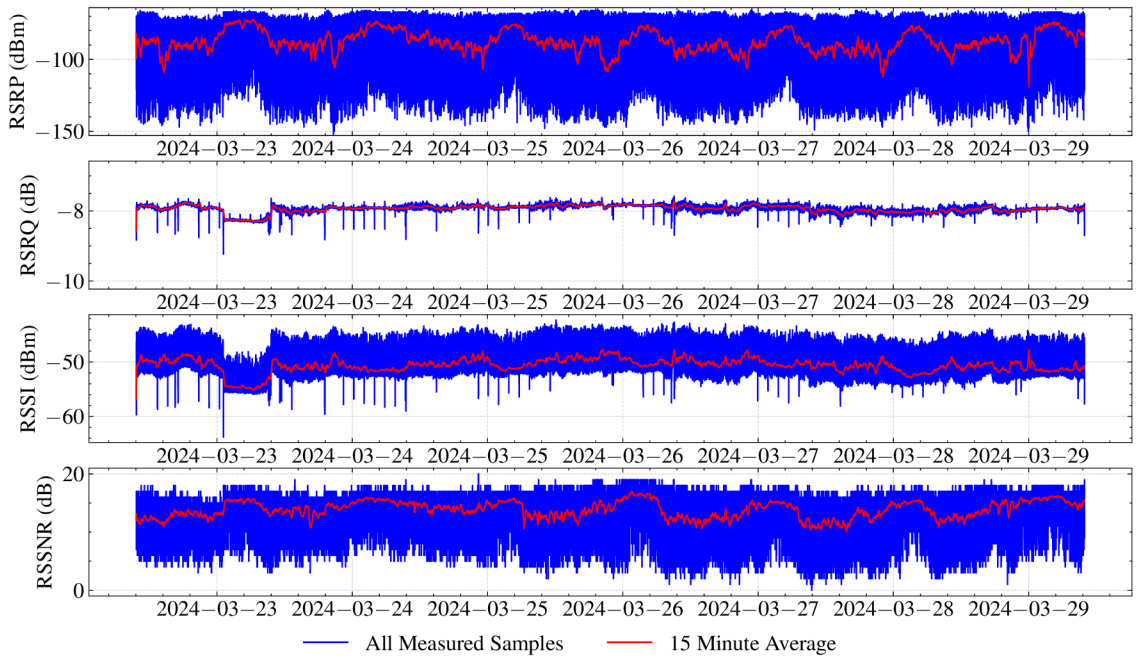

Fig. 5.7: Static indoor measurement conducted at Pod Palackého Vrchem dormitory on the BUT campus from March 22nd to March 29th (LTE Band 3)

revealing periodic behavior in the RSRP and RSSNR metrics corresponding to the time of day. During peak working hours, RSRP and RSSNR values tend to decrease due to high cell load. Conversely, in the early morning hours, typically between 1:00 a.m. to 6:00 a.m., these values increase, peaking around three to four o'clock in the morning daily.

The relationship between RSRP and RSSI demonstrates a significant negative correlation, with a correlation coefficient of -0.8. This negative correlation observed here may be attributed to the definitions of individual metrics. During night-time, RSRP increases as expected, representing the power level of the LTE serving cell specifically, focusing on the power from the reference signals in the LTE bandwidth. Conversely, RSSI measures the total received power from all sources. At night, when the network is less congested, the RSRP metric from the connected serving cell increases. The decrease in RSSI can likely be attributed to power saving efforts by T-Mobile, where in the early hours, the power of individual eNBs is reduced to conserve energy. Consequently, surrounding signals, for example, from other eNBs have less power, resulting in a smaller RSSI value.

Notable deviations are observed during peak cell load, typically occurring between 8:00 p.m. to midnight. During these periods, the RSRP data exhibits significant downward spikes, as evidenced by the bimodal distribution evident in the histogram of RSRP values in Fig. 5.8. This distribution highlights two prominent values, predominantly around -80 dBm and, during peak load hours, approximately -110 dBm. This trend is further illustrated in Fig. 5.9, which aggregates the variation

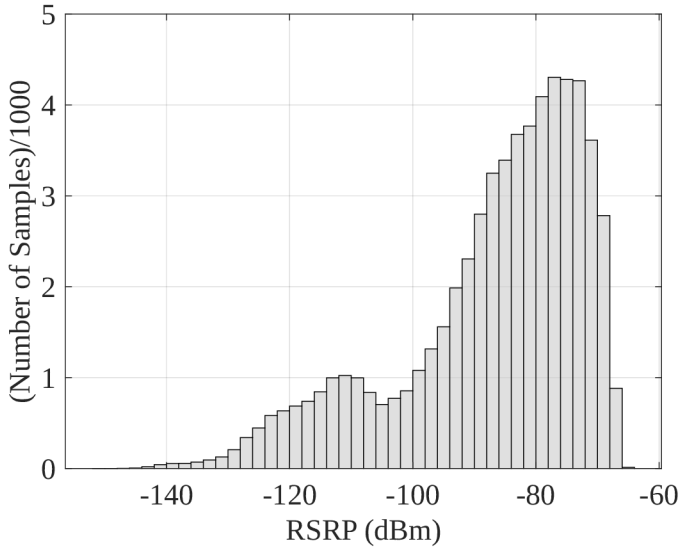

Fig. 5.8: RSRP Histogram of static measurement conducted at Pod Palackého Vrchem dormitory on the BUT campus from March 22nd to March 29th (LTE Band 3). Bin size = 2 dBm.

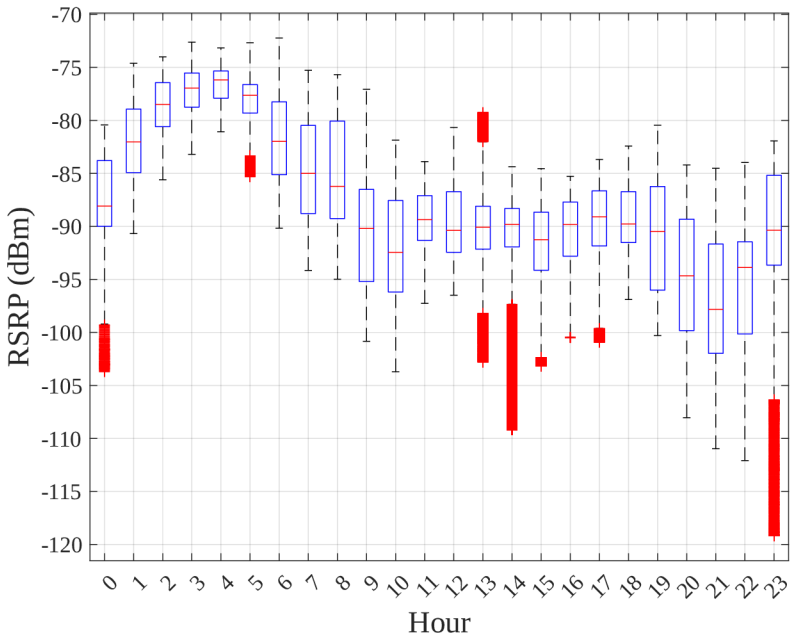

Fig. 5.9: Boxplots illustrating the variation in RSRP values aggregated by hour throughout the measurement conducted at Pod Palackého Vrchem dormitory on the BUT campus from March 22nd to March 29th (LTE Band 3, data averaged over a 15-minute window)

in RSRP values by hour throughout the measurement period with data averaged over a 15-minute window. It is notable to observe these two peaks, where RSRP acquires the highest values at 4:00 a.m. and the lowest at 9:00 p.m.

The RSRP demonstrates a substantial standard deviation of 15.145 dBm indicating significant variability in signal strength even during static measurements as it was in Band 20. In contrast, the RSRQ metric exhibits minimal variation throughout the entire duration of the measurement, with a variance of 0.012 and a standard deviation of 0.11, indicating stability at a median value of -7.92 dB. As mentioned before, the RSSNR metric demonstrates expected periodic changes, increasing during the early hours due to reduced network load and potential power saving techniques implemented by the MNO. These data suggesting a consistently clean and strong signal when measured in a static environment. Fig. 5.10 shows more detailed distributions of individual metrics through boxplots.

Interesting information can also be found in Fig. 5.11, which shows the distributions of RSRP values grouped by the day of the week. Each box again represents the variability of RSRP measurements for a specific day. The data are once again averaged over a 15-minute window to mitigate extremes and ensure data transparency. From the RSRP values depicted in the figure, it is evident that they strongly correlate with the occupancy of the dormitory. Based on this observation, we can

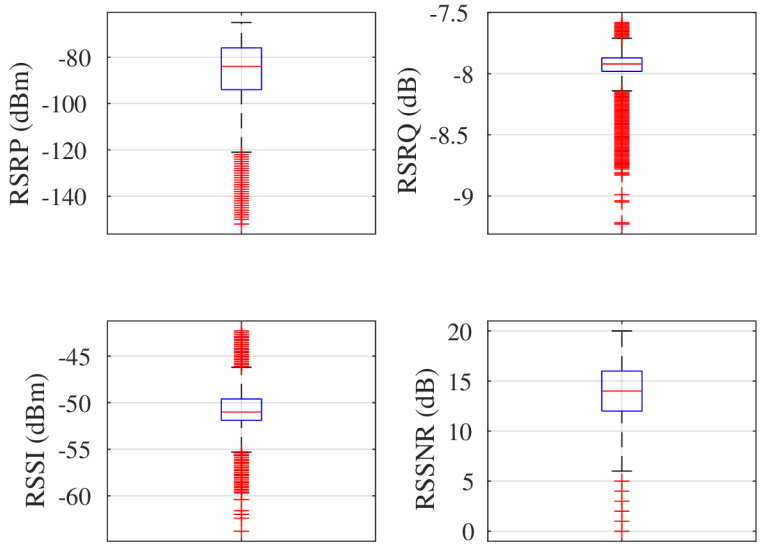

Fig. 5.10: Boxplots of a static measurement conducted at Pod Palackého Vrchem dormitory on the BUT campus from March 22nd to March 29th (LTE Band 3)

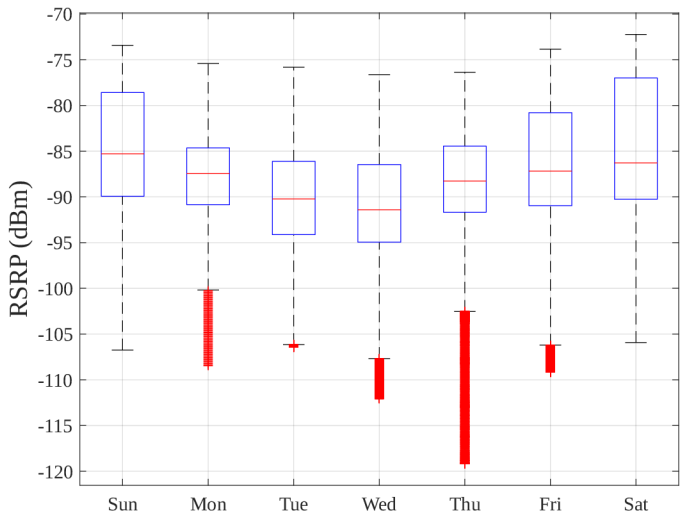

Fig. 5.11: Boxplots of the RSRP value distributions grouped by the day of the week representing the variability for a specific day of a static measurement conducted at Pod Palackého Vrchem dormitory on the BUT campus from March 22nd to March 29th (LTE Band 3, data averaged over a 15-minute window)

reasonably infer the days when the dormitories are most occupied. This trend is particularly notable on Wednesdays, where the median RSRP metric is -91.42 dBm, the lowest value among all days of the week (the highest network load on this band).

Indeed, the findings regarding the busiest days in the location offer valuable insights into network usage patterns. While Tuesday emerges as the busiest day for LTE Band 20, Wednesday takes the lead for LTE Band 3. This nuanced under-

standing of band-specific network load variations can inform network planning and optimization strategies. By identifying the days associated with the highest network load for each band, network operators can allocate resources more effectively, ensuring optimal performance and user experience during peak usage periods. This targeted approach to network management can enhance overall network efficiency and reliability, ultimately leading to improved customer satisfaction.

As mentioned before, the network load gradually diminishes as students leave the dormitories for weekend retreats, reaching its peak on Sundays with a median value of -85.29 dBm. Conversely, with the commencement of the working week, the network load increases once again. This cyclic trend is likely to persist throughout the school year, from approximately September to June in this location. Of course, these results may vary during the summer months. These findings suggest that LTE Band 3 is one of the most utilized bands in this location, mainly on Wednesday, reflecting the dynamic nature of network usage influenced by student occupancy.

LTE Band 1 (2100 MHz)

LTE Band 1 continues to function as a capacity mid-band layer, and at the location of the BUT college, it is the second most utilized band for managing user data capacity, following Band 3. A static indoor measurement was conducted with a module configured to the specified cell CID 606491 in LTE Band 1 (2100 MHz, FDD) at Pod Palackého Vrchem dormitory on the BUT campus from 10:20 a.m. on Thursday, April 11th to 8:08 a.m. on Wednesday, April 17th 2024. The measurement was not conducted in full for 7 days due to an unexpected failure of the module towards the end of the measurement period. The module began measuring only once every few minutes (approximately every 20 minutes), and eventually, on April 17th at 8:08 a.m., it completely failed. This failure is evident in the data, where no significant difference can be observed between all the samples measured and the 15-minute average, as shown in Fig. 5.12.

Another noteworthy event during the measurement period was the outage of MNO T-Mobile in the entire Czech Republic for about 1 hour on April 13th, from around 5:00 p.m. to 6:00 p.m. This incident, widely covered by various magazines [60],[61],[62], is also reflected in the measurement data, where no signal metrics were recorded. It is likely that the module could not register in the network, and consequently, the entire radio part of the network was unavailable during this time. However, as before the measurement was conducted during normal college operation, resulting again in significant user presence on weekdays, while fewer users were present during the weekend. During this measurement, over 540,000 KPI samples were collected, each containing RSRP, RSRQ, RSSI, RSSNR, and other information.

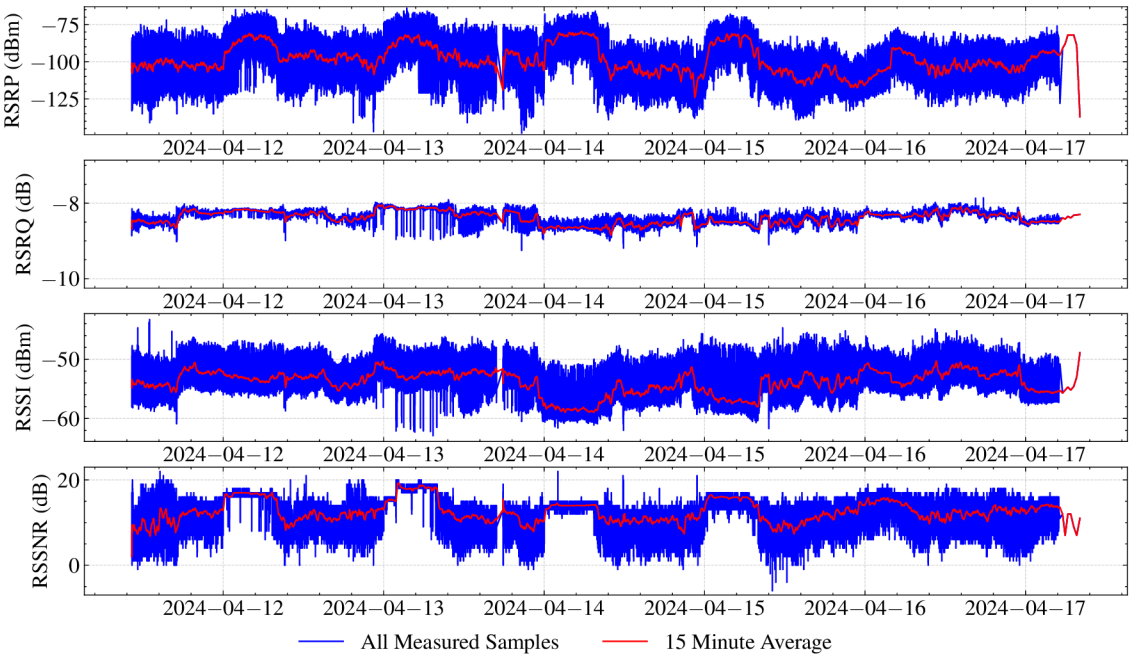

Fig. 5.12: Static indoor measurement of signal metrics conducted at Pod Palackého Vrchem dormitory on the BUT campus from April 11th to April 17th 2024 (LTE Band 1)

As depicted in Fig. 5.12, similar to the observations made for LTE Band 3, variability is evident even in the static measurement of Band 1. During peak working hours, RSRP and RSSNR values tend to decrease due to high cell load, mirroring the patterns observed for Band 3. Conversely, in the early morning hours, typically between 1:00 a.m. to 6:00 a.m., these values increase, peaking around three to four o'clock in the morning daily, with the RSSNR metric remaining stable.

Similar to Band 3, the relationship between RSRP and RSSI demonstrates a negative correlation, in this case, with a correlation coefficient of -0.44. Additionally, in this measurement, the RSSI and RSRQ metrics exhibit a relatively high positive correlation of 0.6. Deviation patterns during peak cell load, typically occurring between 8:00 p.m. to midnight, are not as dominant as those observed for Band 3, suggesting that Band 1 may be less utilized during these periods. Consequently, the distribution of RSRP values in the histogram, shown in Fig. 5.13, does not exhibit a bimodal pattern as observed for Band 3, but rather displays a normal distribution, with a median value -99 dBm. This trend is further illustrated in Fig. 5.14, which aggregates the variation in RSRP values by hour throughout the measurement period. Notable downward peaks are observed at times around 10:00 a.m. with median -103.6 dBm when network usage typically peaks after students waking up, and at 9 p.m. with -104.9 dBm when students return to their rooms.

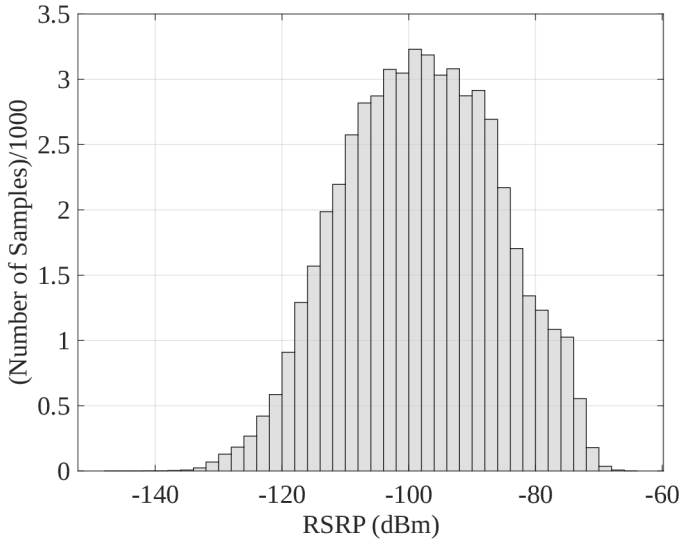

Fig. 5.13: RSRP Histogram of Static Measurement Conducted at Pod Palackého Vrchem dormitory on the BUT campus from April 11th to April 17th (LTE Band 1). Bin size = 2 dBm.

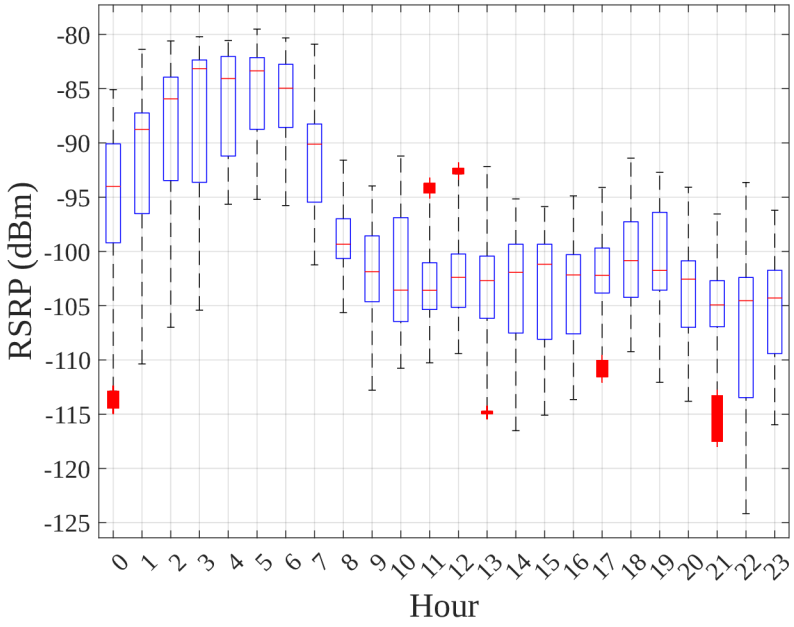

Fig. 5.14: Boxplots illustrating the variation in RSRP values aggregated by hour throughout the measurement conducted at Pod Palackého Vrchem dormitory on the BUT campus from April 11th to April 17th (LTE Band 1, data averaged over a 15-minute window)

Thanks to the utilization of a data package offering unlimited data, data measurements were conducted, presented in Fig. 5.15 illustrates the performance characteristics of an LTE Band 1 connection at the Pod Palackého Vrchem dormitory

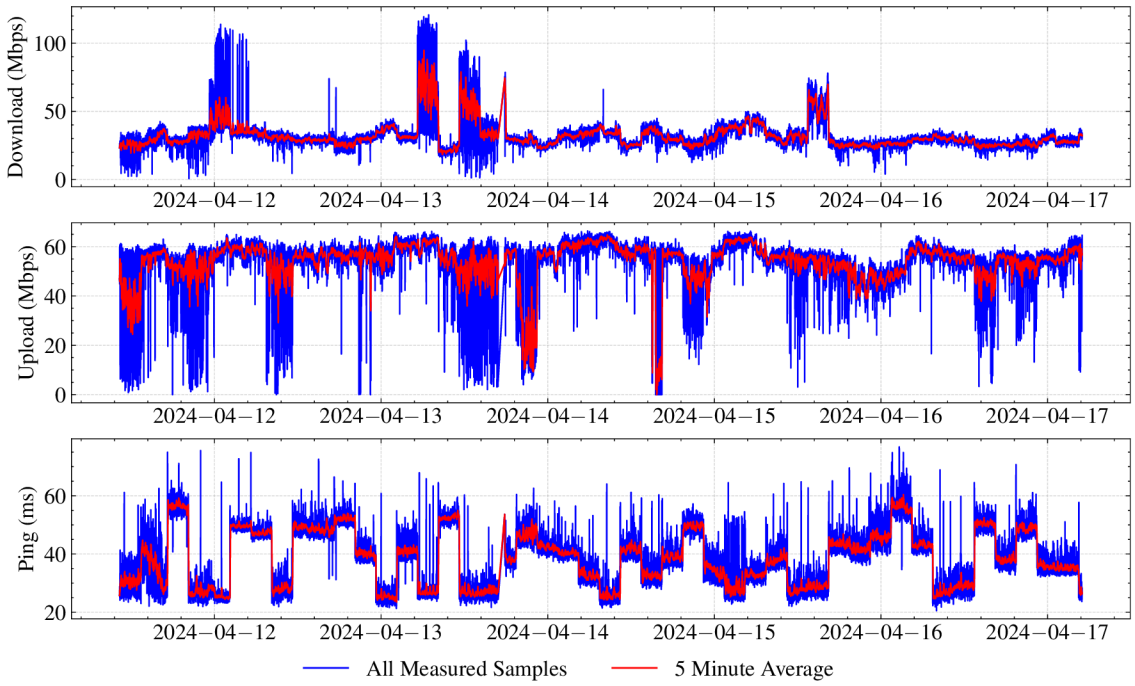

Fig. 5.15: Static indoor measurement of data metrics conducted at Pod Palackého Vrchem dormitory on the BUT campus from April 11th to April 17th (LTE Band 1)

on the BUT campus. Utilizing the `speedtest-cli` Python tool to collect download speeds (Mbps), upload speeds (Mbps), and ping times (ms) every 20 seconds. Notably, the `speedtest-cli` tool automatically selects the "best" server for each measurement based on various factors like latency and distance. This resulted in periodic server changes during the data collection process, as evident by the sharp fluctuations in ping times.

From Fig. 5.15 is visible that the download speeds exhibit considerable variability throughout the measurement period. While the median download speed sits at 29.78 Mbps, the graph reveals instances where speeds exceeded 100 Mbps, likely when the tool selected a local server in Brno. This highlights the influence of server location on download performance. Interestingly, the upload speeds demonstrate a higher median value of 56.44 Mbps compared to the download speeds. This is atypical behavior, as download speeds generally surpass upload speeds in most network scenarios. The ping times showcase significant fluctuations, primarily due to the aforementioned server changes throughout the measurement. The median ping time of 38.26 ms provides a general overview, but analyzing the distribution of ping times within specific server connections would offer a more accurate understanding of latency characteristics. In further research, it is necessary to choose a different methodology for obtaining these data than the Python tool `speedtest-cli`, which proved to be unsuitable.

The primary limitation of this dataset stems from the dynamic server selection inherent to the `speedtest-cli` tool. This makes it challenging to isolate the impact of network conditions and radio parameters on the measured performance metrics. Additionally, the tool's definition of the "best" server may not always align with the optimal server for evaluating specific performance aspects like download or upload speeds.

The Fig. 5.16 presents boxplots depicting signal strength and quality measurements collected in a static environment from April 11th to 17th using LTE Band 1. As mentioned before, the RSRP metric shows a median of -99 dBm with a fairly small interquartile range, indicating consistent signal strength. However, there are some outliers with significantly weaker signal levels down to -140 dBm. The boxplot shows a median RSRQ of approximately -8.36 dB with a compact interquartile range, suggesting consistently good signal quality. A few outliers exhibit slightly poorer quality around -9 dB. The median RSSI of -53.8 dBm with a relatively small interquartile range signifies relatively stable overall received power levels. Similar to RSRP, there are outliers with weaker signal strength down to -60 Bm. The median RSSNR is 13 dB, indicating a strong signal compared to the noise level. The tight interquartile range signifies consistent signal-to-noise ratios. Overall, the boxplots indicate a generally strong and stable LTE signal. The consistent RSRP, RSRQ, and RSSNR values suggest reliable network performance. However, the presence of outliers with weaker signals in RSRP and RSSI might point to potential signal blockages or interference issues in certain areas or at specific times.

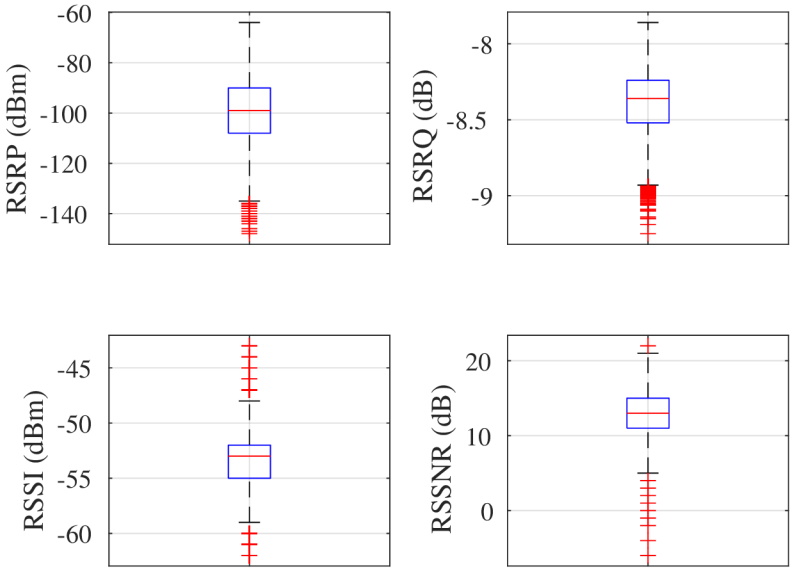

Fig. 5.16: Boxplots of a static measurement conducted at Pod Palackého Vrchem dormitory on the BUT campus from April 11th to April 17th (LTE Band 1)

Similarly to Fig. 5.6 and Fig. 5.11, which illustrates the distributions of RSRP values in Bands 20 and 3 grouped by the day of the week, with each box representing the variability of RSRP measurements for a specific day, the same representation can be observed in Fig. 5.17. As in the case of Fig. 5.6 and Fig. 5.11, the data are averaged over a 15-minute window.

However, due to an error in the measurement process, Wednesday was not the last day to be measured entirely, resulting in only around 19,000 KPI samples recorded, significantly fewer compared to the average of 94,000 KPI samples per day. Similarly, the first day of measurement, Thursday, started at 10:19 a.m. and recorded errors for more than 10 hours, resulting in approximately 54,000 KPI samples recorded on this day. Consequently, these two days are distorted, and the results from Fig. 5.17 are not as evident as for Band 20 or Band 3.

If we exclude the days of Wednesday and Thursday, a similar trend as for Band 20 and 3 is observed. Interestingly, on Tuesdays, a phenomenon occurs where the RSRP metric significantly increases compared to the expected decrease, similar to what was observed for Band 20 and 3. The reason for this phenomenon remains unknown but may be attributed to special settings from the MNO or a smaller aggregation of this band, with Band 3 taking on a larger portion of the load.

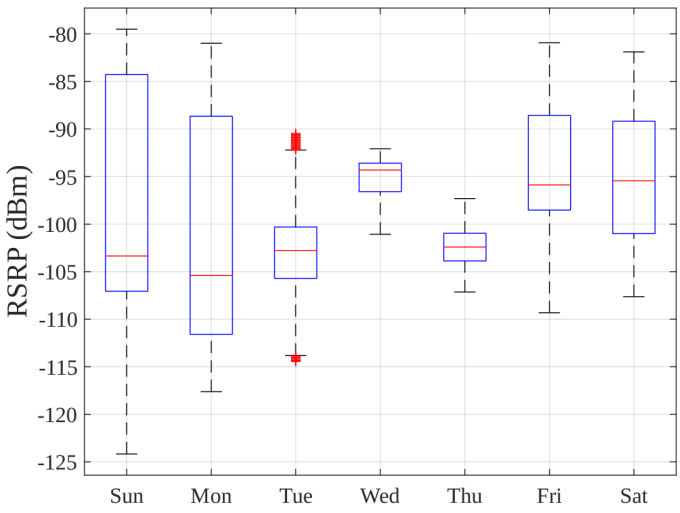

Fig. 5.17: Boxplots of the RSRP value distributions grouped by the day of the week representing the variability for a specific day of a static measurement conducted at Pod Palackého Vrchem dormitory on the BUT campus from April 11th to April 17th 2024 (LTE Band 1, data averaged over a 15-minute window)

5.1.2 Mobile Measurement

In the mobile measurement scenario, multiple walk, drive, bike and public transport tests were conducted to assess signal coverage across the city of Brno. The measuring device, locked to the individual measured LTE Band, was securely placed in a backpack. These measurements were conducted throughout the first half of 2024.

During the measurement over 46,000 KPI samples were collected, over 41 hours of measurement over 13 days with a length of 343 km in total. The primary objective of this measurement campaign is to generate an estimation of the coverage map utilizing the measured RSRP metrics. These coverage estimates are produced for individual bands employing interpolation methods such as *Bilinear*, *Nearest Neighbor*, and *Cubic convolution*. An endeavor is made to compare these methods to ascertain the optimal one for accurate estimation. Additionally, the estimated coverage maps are compared with those from the CTO to evaluate accuracy and reliability. This comparison aims to identify any potential disparities between real-world coverage and official estimates, thereby providing insights into the effectiveness of the measurement campaign and the precision of the generated coverage maps.

The selection of interpolation methods for RSRP coverage data in LTE and 5G networks was based on several key factors to ensure suitability in estimating coverage. *Bilinear* and *Nearest Neighbor* interpolation methods were chosen for their computational efficiency, making them practical for handling large datasets efficiently. These methods also offer smooth transitions between data points, resulting in visually appealing and realistic coverage maps. *Cubic* interpolation, despite being more computationally intensive, was selected for its superior accuracy, especially when dealing with complex spatial variations in signal strength. By incorporating higher-order polynomial functions, *Cubic* interpolation can more accurately capture subtle changes in signal strength, leading to more precise coverage estimates.

LTE Band 20 (800 MHz)

As discussed in the case of static measurement, Band 20 plays a fundamental role as a primary connection band to the network. Its attributes, including deep penetration and wide coverage capabilities due to its sub-1 GHz frequency, make it ubiquitous throughout the city of Brno. Fig. 5.18 shows the distribution of all measured RSRP samples across the city of Brno, where the color coding corresponds to the signal strength categories outlined in Table 3.2. In this measurement campaign, a total of 16,643 KPI samples were collected over nearly 19 hours of measurement time, spanning across 5 days of data collection. The measurement route covered a distance of 157.6 kilometers.

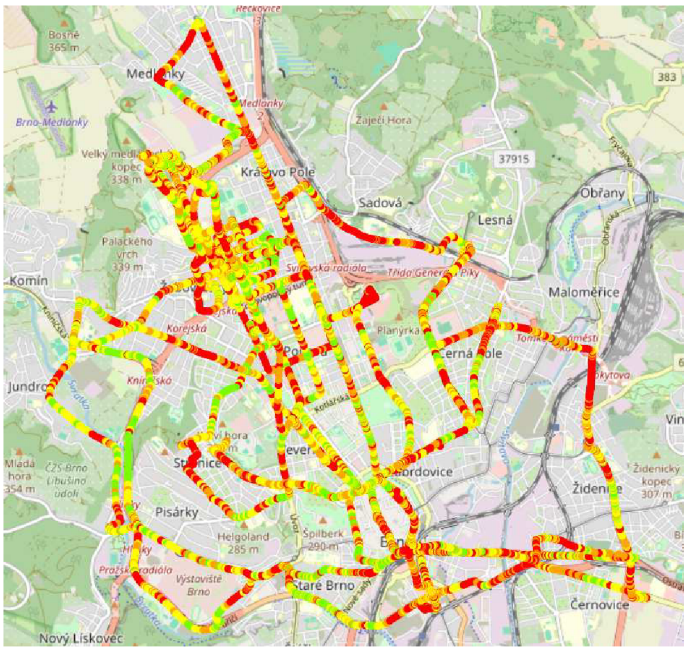

Fig. 5.18: RSRP points of a mobile measurement conducted at Brno city throughout April 2024 on LTE Band 20 (800 MHz)

The boxplots in Fig. 5.19 provide a more detailed breakdown of the distribution of KPIs across the observed days. The RSRP metric reveal a relatively stable median value around -110 to -115 dBm. This observation indicates that the RSRP metric remained relatively stable across all measured days. The consistent effect of the public transport methodology on all measured days is evident. This consistency is further supported by the Empirical Cumulative Distribution Function (ECDF) shown in Fig. 5.20, where similar curves with matching probabilities can be observed across the different days. Indeed, not only the RSRP metric but also other metrics exhibit relative stability in median values across all measured days. In the RSSNR measurement, however, slight variations can be observed. On April 7, for instance, the median RSSNR value is 10 dB, contrasting with the median values of 6-7 dB observed in the subsequent days. This discrepancy could be attributed to the conditions on April 7 being a Sunday with favorable weather, resulting in fewer people in the city and consequently less interference.

To achieve the best estimate of coverage, obtaining a larger amount of data and refining the sample grid on the map would be essential. This would result in smoother transitions between interpolated areas and reduce deviations from reality. For instance, in Fig. 5.18, certain areas such as between urban areas of Černá Pole, Židenice, and Zábrdovice, which lack easy access by public transport, were not measured, leading to gaps in coverage estimation. Similarly, in areas like the Svitavská radiála, where only a few samples were measured falling into the threshold with a

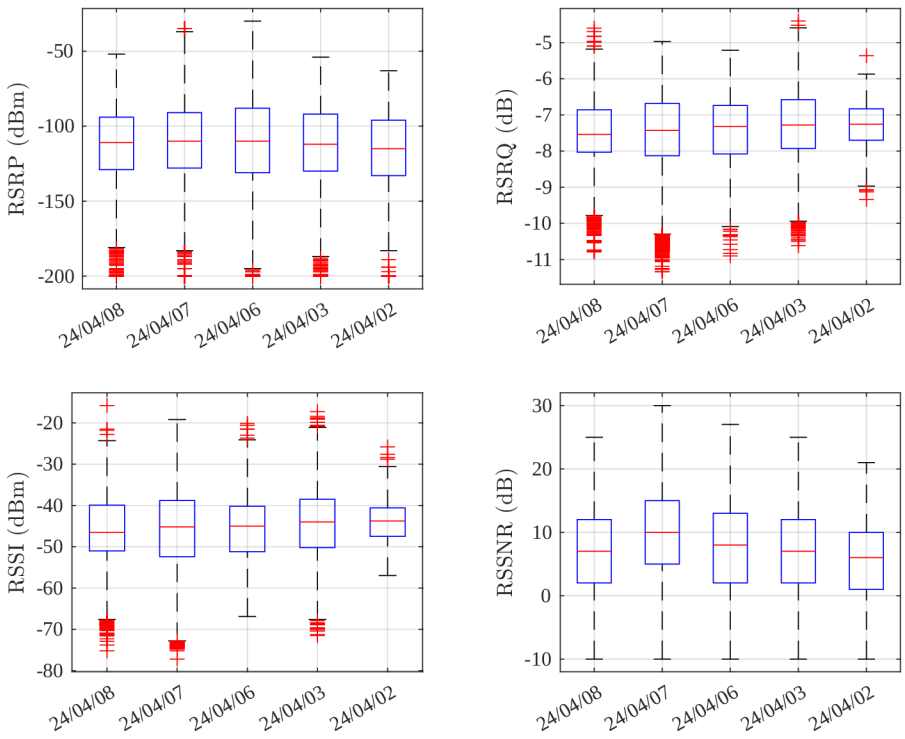

Fig. 5.19: Boxplots of signal metrics in a mobile measurement conducted at Brno city throughout April 2024 on LTE Band 20 (800 MHz)

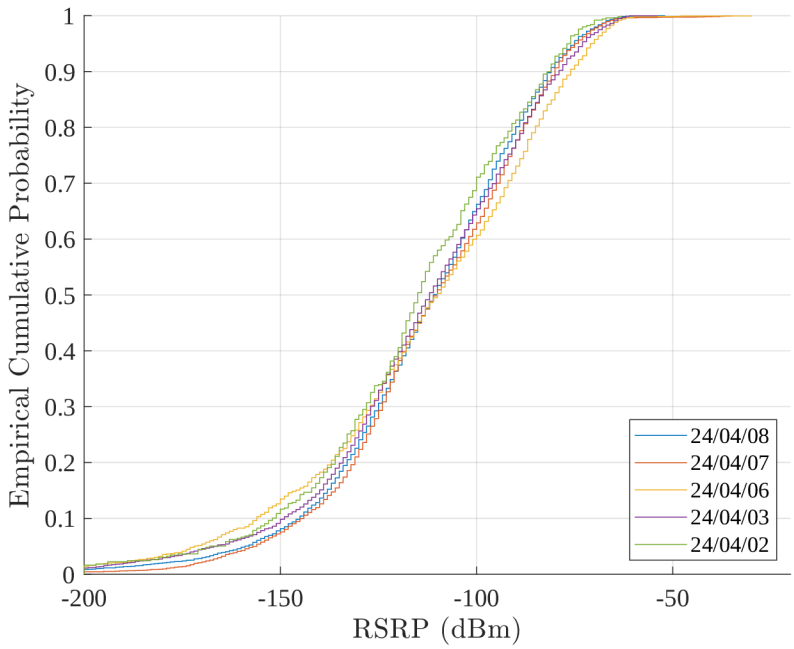

Fig. 5.20: Empirical Cumulative Distribution Functions of RSRP metric from individual measured datasets on LTE Band 20 (800 MHz)

red color, the entire area is affected, resulting in potentially inaccurate estimations. Despite these limitations, coverage estimations were made using the *Bilinear*, *Nearest Neighbor*, and *Cubic convolution* interpolation methods, graphically displayed using color coding according to Table 3.2, where good coverage is represented in green and very poor coverage in dark red, as shown in Fig. 5.21. Among these, the *Bilinear* interpolation method, shown in Fig. 5.21a, appears to be the most visually appealing and smooth, even though it can overestimate or underestimate coverage in areas with rapid changes, providing a balanced representation of coverage without being overly optimistic or pessimistic. However, it's important to note that block artifacts may still be observed in areas where not enough data points were measured, such as between Černá Pole, Židenice, and Zábrdovice or in the upper part of the estimate between Lesná and Medlánky. Overall, the coverage map depicts the expected pattern of predominantly excellent to good coverage in the inner part of Brno, with occasional areas of poorer coverage.

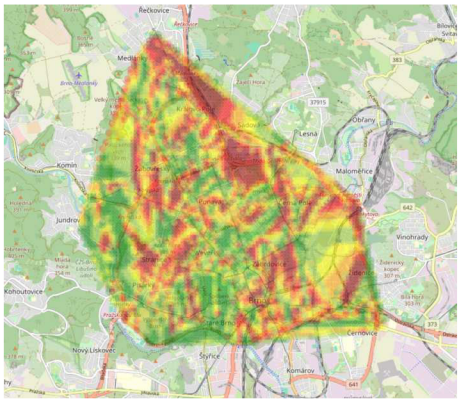

(a) *Bilinear* interpolation

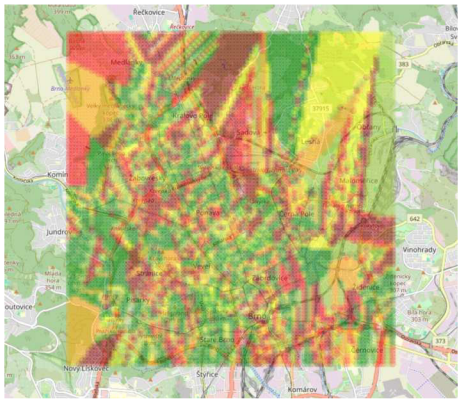

(b) *Nearest Neighbor*

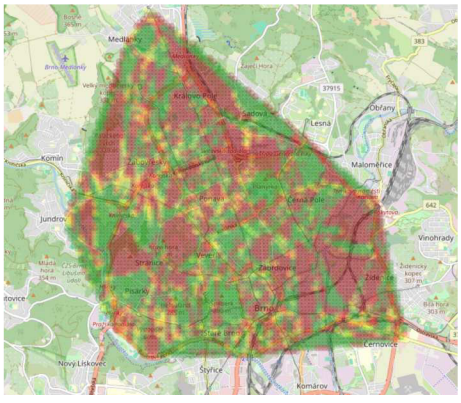

(c) *Cubic convolution*

Fig. 5.21: Coverage estimation via utilized interpolation methods for LTE Band 20 (800 MHz)

The *Nearest Neighbor* method appears to be less optimal compared to the *Bilinear* method. *Nearest Neighbor* assigns the value of the nearest data point to each area without data, which can be well observed in Fig. 5.21b, where this method creates block artifacts at the edges. On the contrary, in the inner section, the map is more detailed thanks to sharper transitions between coverage samples. The inner area essentially resembles the same estimation as the *Bilinear* method. The areas with good or bad coverage are in the same places, but with these sharp transitions on the right, thus visually it does not provide the kind of finesse that we imagine from the coverage map. While the *Nearest Neighbor* interpolation method may offer computational efficiency and preserve fast transitions, it may not always produce visually appealing results. In cases where a large amount of data is available and a quick result is needed, this method could be suitable. However, as observed in the coverage estimation for LTE Band 20, the *Nearest Neighbor* method tends to produce blocky and unnatural outcomes, especially in areas with sparse data.

The *Cubic convolution* method, although renowned for striking a balance between accuracy, detail, and smoothness, exhibited limitations in the coverage estimation for LTE Band 20. As depicted in Fig. 5.21c, this method primarily delineated coverage into two conditions: good coverage represented in green and very poor coverage in red. While intermediate levels of coverage were occasionally observed between these extremes, the result was largely dichotomous. To achieve more nuanced results with this method, extensive operational measurements covering the majority of streets and accessible places in Brno would be necessary. This would ensure a finer input matrix of values, potentially leading to more faithful coverage estimations. However, such an approach would entail significantly higher computational costs. Thus, while the *Cubic convolution* method holds promise for producing detailed and accurate coverage maps, its effectiveness hinges on the availability of comprehensive and finely sampled data.

Fig. 5.22 presents the coverage estimate provided by the CTO, calculated using the signal propagation model outlined in ITU-R P.1812 Release 5 [63]. This model employs a path-specific propagation prediction method for point-to-area terrestrial services in the VHF and UHF bands [63]. The coverage estimate indicates that T-Mobile's LTE Band 20 coverage in Brno is at a very good level. Dark blue areas represent RSRP values below the threshold of approximately -100 to -110 dBm, while lighter blue areas indicate RSRP values between -110 to -120 dBm. Areas with RSRP values less than -120 dBm are considered to have no coverage. These thresholds are more stringent than those used in this work, reflecting differences in measurement methodologies. The CTO's estimation incorporates terrain and environmental factors, which significantly influence radio wave propagation characteristics, resulting in a coverage estimate closer to reality. While the results from

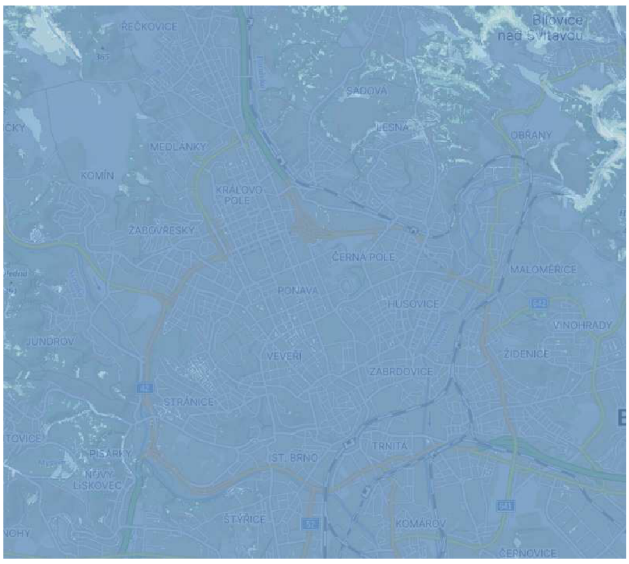

Fig. 5.22: Coverage estimation of Brno city constructed by CTO for T-Mobile Czech Republic on LTE Band 20 (800 MHz)

this estimation differ greatly from those obtained in this work, it is essential to consider the methodology used by the CTO and the basis upon which the estimate was generated. Furthermore, it is important to note that this estimate is only an approximation and should not be used as the sole basis for evaluating interpolation data and creating coverage maps. Variations in the estimated values may arise due to factors such as the measurement of values only in public transport vehicles, which can experience significant signal attenuation due to the presence of large metal parts. However, such scenarios provide valuable insights for operators, allowing them to consider worst-case scenarios and optimize network conditions accordingly.

The information depicted in Fig. 5.23, which displays samples of the RSRP metric falling below the -140 dBm threshold, is crucial for coverage optimization efforts. This map, generated using a visualization and analysis tool equipped with a filtering function, allows operators to identify areas with poor coverage that require attention for improvement. By visually identifying these areas on the map, operators can prioritize optimization efforts and implement targeted solutions to enhance coverage in regions where signal strength is insufficient. This proactive approach to coverage optimization helps ensure a better quality of service for users and enhances overall network performance. Fig. 5.23 illustrates numerous areas with signal failures and poor coverage, particularly in locations obstructed by buildings, hills, or other obstacles that impede direct line-of-sight to the eNB. These areas are characterized by longer connecting lines rather than isolated points, indicating consistent signal attenuation and degraded performance.

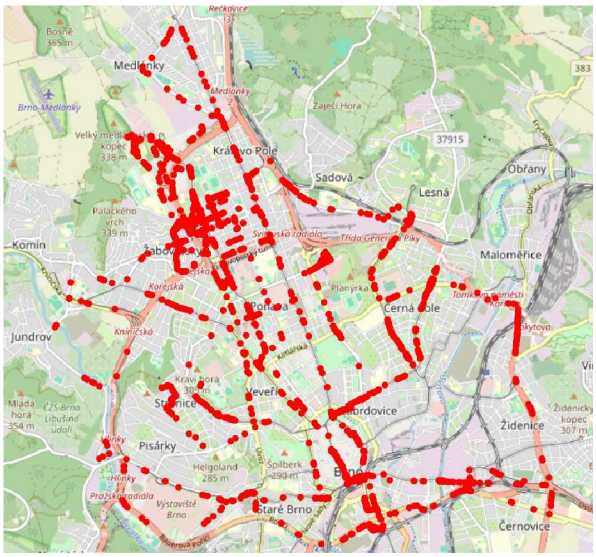

Fig. 5.23: Filtered points of RSRP metric under threshold -140 dBm

LTE Band 3 (1800 MHz)

The shift to a higher frequency band, as observed in Band 3, results in worsened propagation properties, typically leading to lower values of KPI metrics throughout the mobile measurement campaign. As was already mentioned in the static measurement of Band 3, it is one of the most used and deployed bands in LTE networks [59]. Fig. 5.24 provides an overview of the entire measurement route, showcasing all RSRP measurements color-coded according to Table 3.2. For this band, thresholds for color coding were adjusted downward due to the higher frequency, reflecting objective evaluations during the measurement, including periods of Internet connectivity and network outage. The measuring device, locked to LTE Band 3, was securely placed in a backpack. These measurements were conducted throughout March 2024. While both public transport and pedestrian tests were conducted during this campaign, the vast majority (around 95%) of the measured data originated from public transport. Over the course of 11 hours of measurement spanning four days, a total of 21,252 KPI samples were collected, covering a distance of 90 kilometers along the measurement route.

Fig. 5.25 illustrates individual distributions depicted through boxplots of respective measurements. The median values of RSRP and RSSI exhibit greater variability across different data sets compared to RSRQ and RSSNR. These changes are probably caused by different test types. For instance, on March 29th, a notable decrease in the median RSRP value to -140 dBm suggests a relatively low signal strength specifically from the RE carrying the CRS. Conversely, some of the best results were recorded on March 6th, characterized by a higher median RSRP value

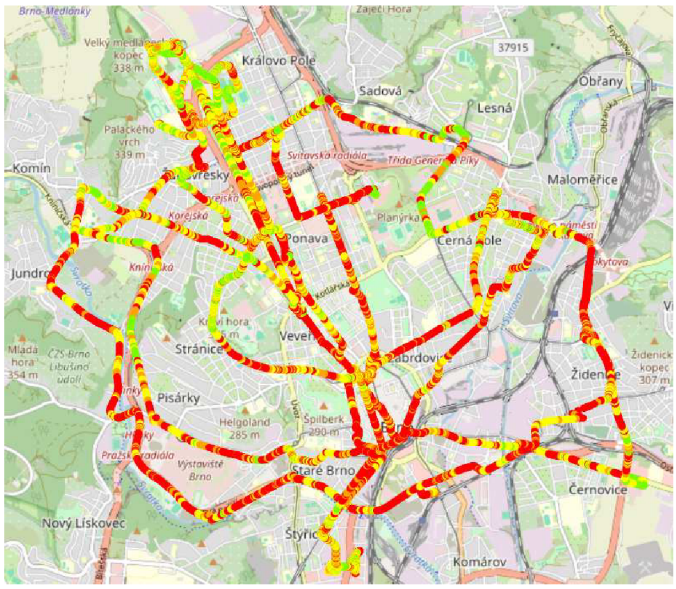

Fig. 5.24: RSRP points of a mobile measurement conducted at Brno city throughout March 2024 on LTE Band 3 (1800 MHz)

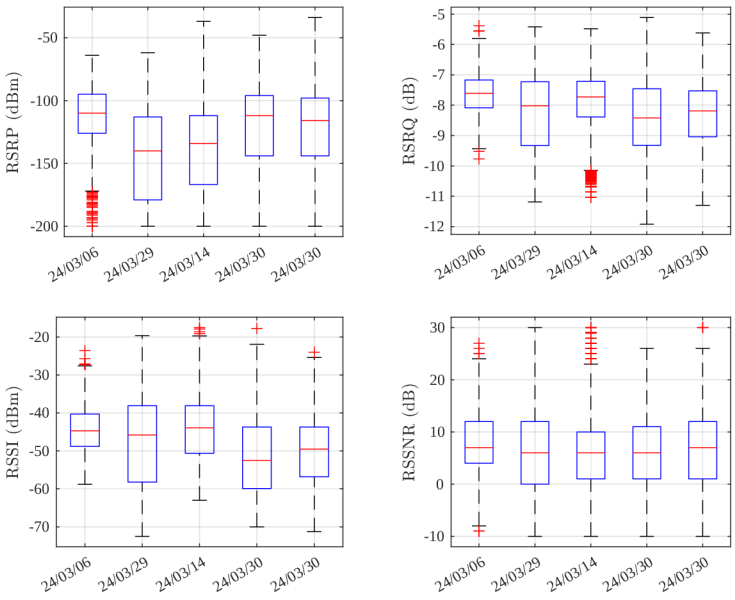

Fig. 5.25: Boxplots of signal metrics in a mobile measurement conducted at Brno city Throughout March 2024 on LTE Band 3 (1800 MHz)

of -110 dBm. Interestingly, datasets from March 30th exhibited a comparatively high median RSRP value of around -114 dBm, despite other metrics such as RSSI and RSRQ showing relatively worse performance. The RSSNR metric, however, remained stable across all datasets, maintaining a median value around 6 dB. Again, a positive correlation between RSRQ and RSSI can be seen only from the point of view of distribution, as was also the case in the static measurement.

The variability across different data sets highlights the ECDF of the RSRP samples from individually measured sets in Fig. 5.26. On Friday, March 29, approximately 50% of the sample fell below the -141 dBm limit. Similarly, on Thursday, March 14, with about 50% probability, the sample is below the -135 dBm limit. In contrast, the last dataset displays more favorable results, with only 16% of the sample below the -140 dBm threshold on March 6 and 30% on March 30. The better performance observed on March 6 is likely attributed to it being conducted as a walk test, while the others were conducted in public transport vehicles, resulting in significant attenuation.

The observed disparities between the datasets measured on March 30th and those from March 29th and 14th can be attributed to the differences in the types of public transport vehicles used for the measurements. Specifically, the datasets from March 29th and 14th, which exhibited relatively worse results, were collected in trams, whereas the two datasets from March 30th were obtained from buses. Trams typically feature larger and more robust metal components compared to buses, which can lead to increased signal attenuation and hinder signal reception. Additionally, the tram measurements may have been affected by the crowded environment, limiting access to unobstructed windows for signal reception. In contrast, measurements taken in buses may have benefited from smaller metal structures and relatively less crowded conditions, potentially resulting in improved signal reception and better measurement outcomes.

Fig. 5.27 depicts the results obtained from the interpolation methods utilized. Similar limitations can be expected as with Band 20 due to the uneven distribution

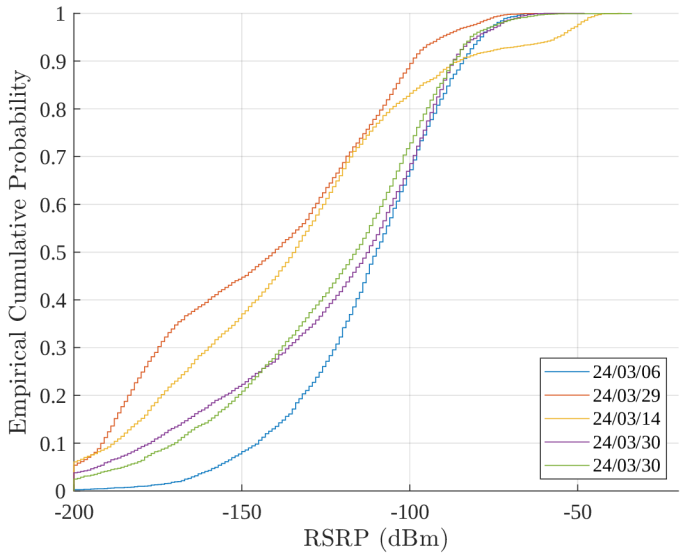

Fig. 5.26: Empirical Cumulative Distribution Functions of RSRP metric from individual measured datasets on LTE Band 3 (1800 MHz)

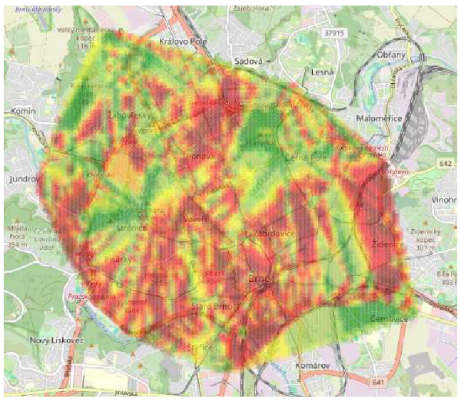

(a) *Bilinear* interpolation

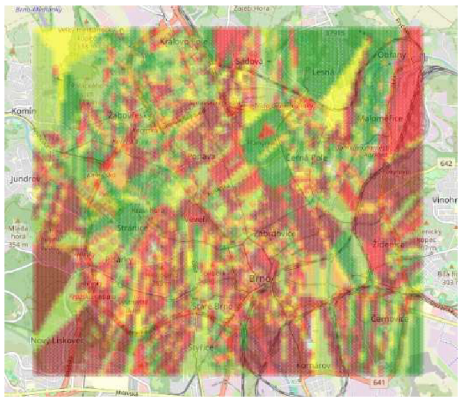

(b) *Nearest Neighbor*

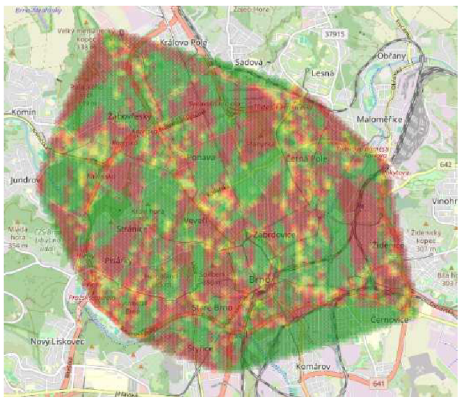

(c) *Cubic convolution*

Fig. 5.27: Coverage estimation via utilized interpolation methods for LTE Band 3 (1800 MHz)

of data in certain areas where measurements were not conducted, either due to limited accessibility via public transport or time constraints. These areas resemble those observed for Band 20, including regions between Černá Pole, Židenice, and Zábrdovice, Pisarky and Stranice, and a significant area encompassing Černá Pole, Zábrdovice, and Ponava. In these regions, the density of measurements is lower, leading to a greater potential for deviation in the interpolated RSRP metric values.

Among all three options, again the *Bilinear* interpolation method, shown in Fig. 5.27a, appears to be the most visually appealing and smooth, even with its limitations such as it can overestimate or underestimate coverage in areas with rapid changes. Once again, block artifacts are visible, particularly in the lower right portion of the interpolation above the city part of Komárov, attributable to the considerable distance between individual base points used for interpolation. In comparison to the *Bilinear* method estimation of Band 20, a greater number of red spots indicating poor coverage can be observed in this case. This outcome would

be expected given that Band 3 operates at a frequency of 1800 MHz with inferior propagation properties. However, the thresholds for color coding were adjusted to equalize the propagation properties between the bands. This suggests that Band 3 exhibits a greater number of areas with weak signals and poorer coverage.

The *Nearest Neighbor* method can be seen in Fig. 5.27b, while computationally efficient and preserving fast transitions, it is not in the mix showing visually appealing results. Compared to the *Bilinear* method, it exhibits block artifacts at edges and lacks finesse inside the interpolation area, which is the main one. Some similarities in outcomes can be observed in comparison with the *Bilinear* method within inner sections, it fails to provide the desired detail and smoothness, and overall this part seems like a lump of sum, due to the insufficient subtlety of the given method. While suitable for scenarios requiring quick results with ample data, it often results in blocky and unnatural outcomes, particularly in areas with sparse data as seen in LTE Band 20 coverage estimation.

The *Cubic convolution* method again displayed limitations as was the case with LTE Band 20 coverage estimation. Illustrated in Fig. 5.27c, it mainly categorized coverage into two conditions, as was the case with Band 20, between good (green) and very poor (red) coverage, with limited intermediate levels shown as yellow or orange . Achieving nuanced results would again require extensive operational measurements covering most streets and accessible areas in Brno to provide a finer input matrix of values, enhancing coverage estimates.

For comparison with the official coverage estimate, the CTO's coverage estimate is again presented in Fig. 5.28 (further details regarding the methodology, the model

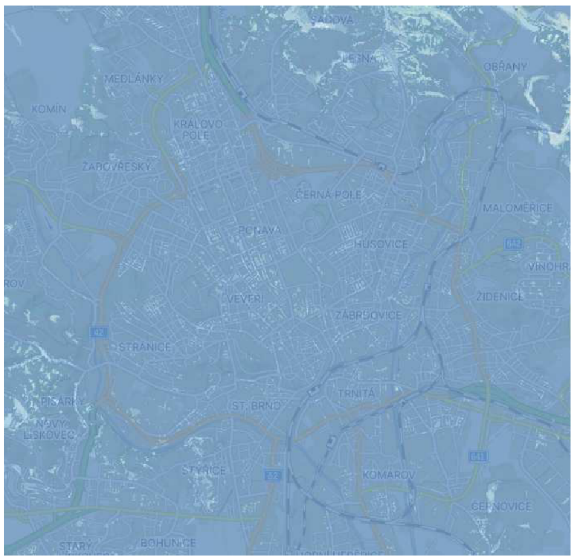

Fig. 5.28: Coverage estimation of Brno city constructed by CTO for T-Mobile Czech Republic on LTE Band 3 (1800 MHz)

utilized, and the color representation of the coverage map are provided in the analysis of Band 20). Similar to Band 20, the coverage provided by Band 3 appears to be excellent, with virtually the entire city of Brno covered. Various deviations are noticeable around building boundaries or large hills, owing to the model's utilization of terrain surface and building data. A notable disparity can be observed compared to the interpolation generated in this study, as despite adopting the same threshold for color coding, the majority of coverage estimation by the *Bilinear* method appears in red, indicating poor coverage. This discrepancy may be attributed to the measurement methodology and the mode of travel during the measurement, specifically the use of public transport vehicles. Anyway, even if the results are relatively bad in terms of coverage of this band, as previously mentioned, these data are crucial not only for understanding signal development in such conditions but also because the majority of Brno's population relies on public transportation.

Similar to the case of Band 20, Fig. 5.29 depicts the map with RSRP points falling below the signal threshold of -160 dBm. This threshold was selected experimentally based on observations during the measurement. In instances where the signal dropped below this threshold, the module often experienced difficulties connecting to the Internet or disconnected from the network entirely. As depicted in Fig. 5.29, numerous samples meet this criterion, resulting in many areas in the coverage estimation for this band being marked as very poor. Throughout the measurement, there were prolonged intervals during which the module lost network connectivity, likely due to the band's higher frequency of 1800 MHz, resulting in greater attenuation when the module connected to a more distant serving cell.

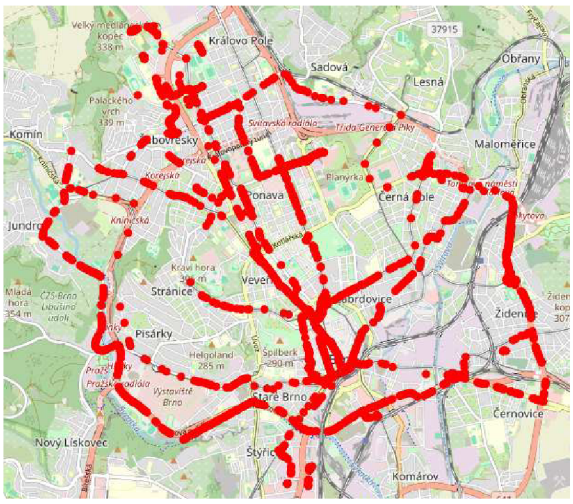

Fig. 5.29: Filtered points of RSRP metric under threshold -160 dBm

LTE Band 1 (2100 MHz)

Similar to Band 3, the higher frequency of 2100 MHz in Band 1 results in slightly diminished signal propagation properties compared to, for instance, Band 20. Consequently, this band also serves as a capacity layer providing capacity at high loads of Band 20. Fig. 5.30 displays all the measured RSRP samples, employing the same color thresholds as Band 3 due to their similarity in the frequency range. As with all measurements, the module remained locked on the measured band, thus to LTE Band 1, and securely placed in a backpack throughout the measurement. Conducted in April, the measurement followed a route similar to the previous cases of Bands 20 and 3, primarily along public transport routes. However, in addition to the public transport test, this band was also measured using measurement setup on a bicycle, allowing for a comparison between these two test types. In this measurement campaign, a total of 7,541 KPI samples were collected over nearly 10 hours of measurement time, spanning three days of data collection. The measurement route covered a distance of 87.1 kilometers.

To compare the distribution of individual metrics across different datasets, boxplots are presented in Fig. 5.31, illustrating four datasets measured in Band 1. There is noticeable variability observed in almost all metrics. However, it's important to note that the two datasets from March 27th were conducted as bicycle tests, while the datasets from March 9th and 10th were tests conducted using public transport. Hence, it's more appropriate in this case to compare datasets from the same type of test. Among the bicycle test datasets, minimal differences are observed, showing very similar RSRP values with medians of -135 dBm and -139 dBm. Interestingly,

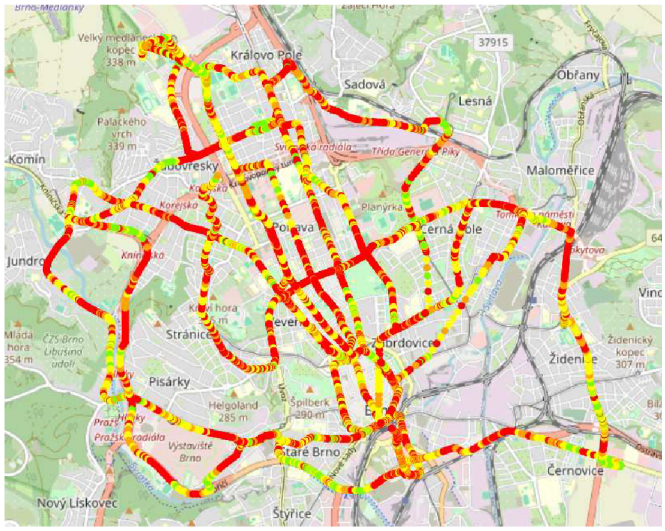

Fig. 5.30: RSRP points of a mobile measurement conducted at Brno city throughout April 2024 on LTE Band 1 (2100 MHz)

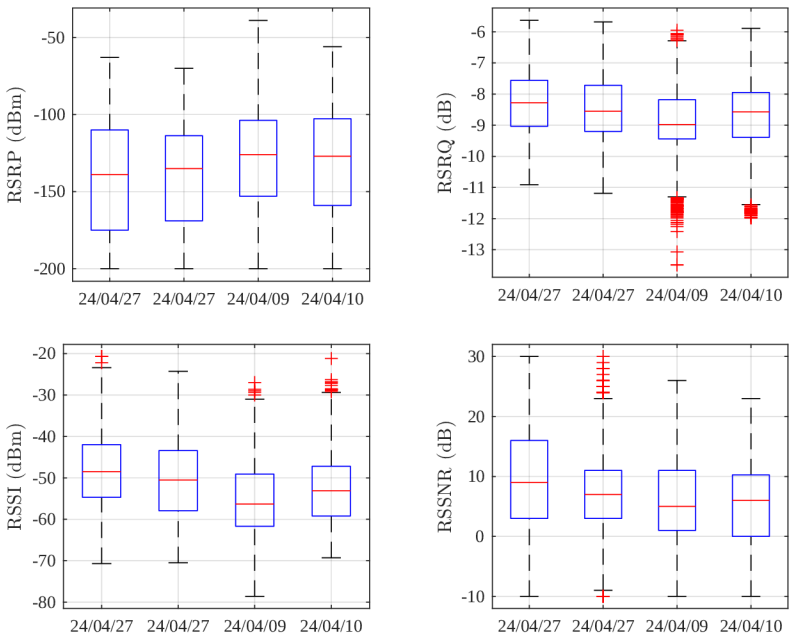

Fig. 5.31: Boxplots of signal metrics in a mobile measurement conducted at Brno city throughout April 2024 on LTE Band 1 (2100 MHz)

the tests conducted in public transport vehicles, specifically buses and trams, also exhibit consistent results with medians of -126 dBm and -127 dBm, respectively. What's intriguing is that this type of test performed better than the bicycle test, contrary to expectations based on past measurements where, for instance, walk tests outperformed public transport tests. One would expect the bicycle test to yield similar results and potentially better metrics due to the absence of metal parts causing significant attenuation, particularly in public transport. Regarding the latter metrics such as RSSI, RSRQ, and RSSNR, there is a positive correlation among them, and their distributions run in parallel. However, in contrast to RSRP, this relationship reverses, with an increase in RSRP corresponding to a decrease in all the latter metrics. This suggests that even with a relatively strong measured signal, good signal quality is not guaranteed. The decrease in the latter metrics indicates likely high interference from neighboring cells or other sources, leading to lower RSRQ and RSSNR values.

From Fig. 5.32, depicting the ECDFs of RSRP metrics from individual measured datasets, the dominance of superior values from measurements conducted in public transport over those from bicycle tests is evident once again. The public transport measurements from March 9th and March 10th 2024 exhibit a similar structure, with probabilities of individual values closely aligned. This consistency confirms the stability between these two datasets. The likely explanation for why these tests outperform the measurements on the bicycle could be attributed to specific

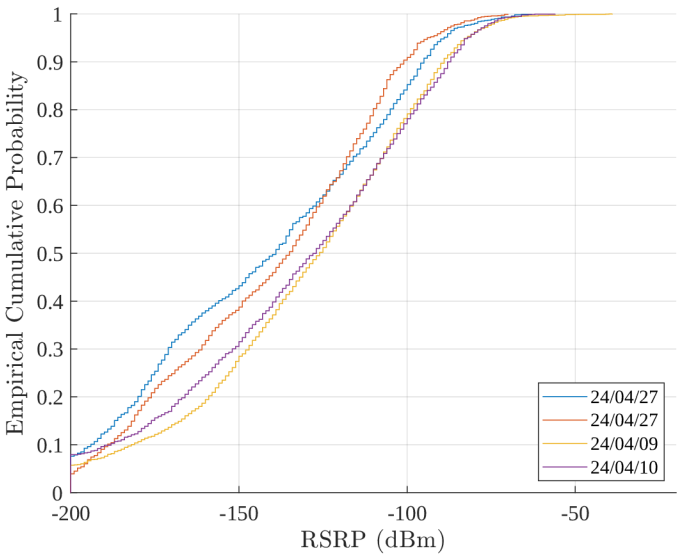

Fig. 5.32: Empirical Cumulative Distribution Functions of RSRP metric from individual measured datasets on LTE Band 1 (2100 MHz)

routes taken during public transport tests, which may have had better coverage or experienced less interference compared to the routes measured on the tests done by bicycle. Further insights could be gained through an analysis of the geographical locations and surrounding environments of each test. Such an analysis could also reveal whether specific types of public transport vehicles have a significant impact on signal quality. Based on previous measurements, it could be assumed that buses might yield better results compared to trams.

Fig. 5.33 illustrates the application of three interpolation methods used to estimate the coverage of LTE Band 1 across the Brno city area. The results closely resemble those observed in Bands 20 and 3. Each method yields a distinct visual representation of signal strength, showcasing their individual strengths and weaknesses. *Bilinear* interpolation, shown in Fig. 5.33a, produces a smooth and continuous coverage map, similar to previous cases, and appears visually the most accurate. Additionally, it avoids producing block artifacts, unlike Bands 20 and 3. Similar to Band 3, the color coding in this band is adjusted for frequency and set based on subjective evaluations of the connection during measurement. Nonetheless, most estimates still indicate red spots, signifying poor coverage with this band. *Nearest Neighbor* interpolation in Fig. 5.33b exhibits similar patterns as before, including block artifacts at the edges of the estimation. The interpolated values internally resemble clusters with unclear coverage information, resulting in a more fragmented and less smooth map. Finally, *Cubic convolution* in Fig. 5.33c aims to strike a balance between smoothness and accuracy by leveraging a weighted average of neighboring points. However, it generates a visually divided map into two

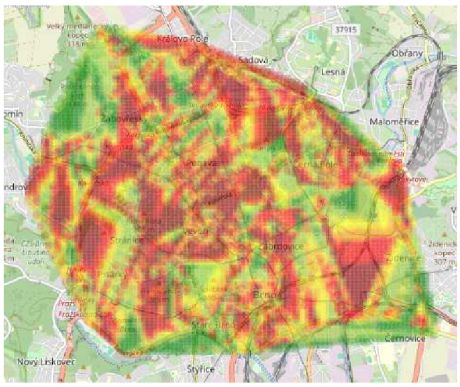

(a) *Bilinear* interpolation

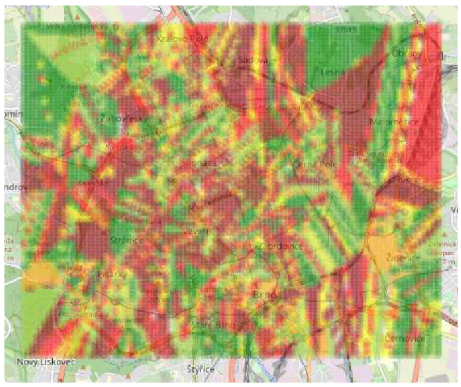

(b) *Nearest Neighbor*

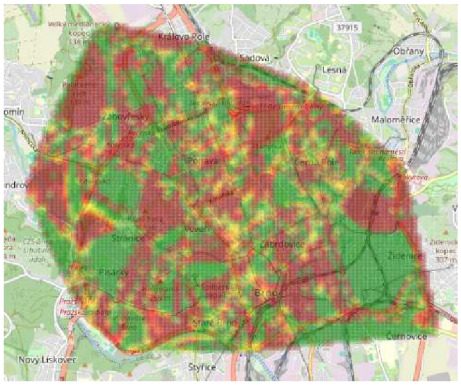

(c) *Cubic convolution*

Fig. 5.33: Coverage estimation via utilized interpolation methods for LTE Band 1 (2100 MHz)

extremes, similar to previous observations. To enhance the accuracy of the results, particularly with the *Cubic* method, it would be necessary to increase the number of measured streets and routes in Brno and adjust the measured grid of points accordingly. This would yield more optimal results across all methods and provide a more reliable representation of the coverage map closer to reality.

Fig. 5.34 captures the coverage estimation of Brno city constructed by the CTO for T-Mobile Czech Republic on LTE Band 1. According to the CTO, coverage by this operator on this band is deemed to be very good, with devices expected to connect practically anywhere in the given location. However, results in this work showed that the estimated coverage does not align with the CTO's estimate, indicating potentially worse coverage. This discrepancy may be attributed to differences in measurement methodology and the tests conducted in public transport.

Similar to the two previously analyzed bands in Fig. 5.35, the filtered RSRP metric points below the threshold of -160 dBm indicate where the signal strength was poorest during the measurement. Once again, similarly to Band 3, long lines

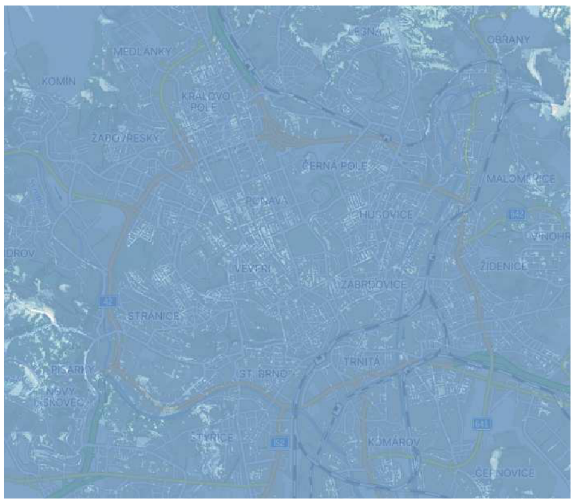

Fig. 5.34: Coverage estimation of Brno city constructed by CTO for T-Mobile Czech Republic on LTE Band 1 (2100 MHz)

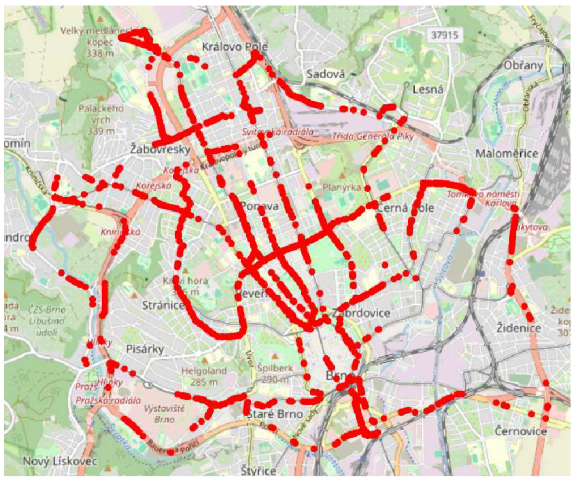

Fig. 5.35: Filtered points of RSRP metric under threshold -160 dBm

of continuous red points can be observed, indicating very poor signal along the measurement route. These signal strength drops may resemble those of Band 3 due to the band's frequency being in a similar range. Consequently, the higher frequency of 2100 MHz likely resulted in greater attenuation when the module connected to a more distant serving cell, similar to the issues encountered with Band 3.

LTE Band 7 (2600 MHz)

LTE Band 7, with its coverage area of 96.90 km^2 at -100 dBm [64], has the smallest coverage among all four deployed bands in the Czech Republic, especially considering its higher frequency. Once again, this band serves as a capacity layer and is predominantly deployed in areas with higher population density. Globally, it ranks

as the third most popular band for LTE network deployment. The entire measurement for this band was conducted via bicycle, covering only a small section where it was possible to connect the module to this band. This measured area can be seen in Fig. 5.36, where all measured RSRP points in this band are displayed, visualized using color-coded thresholds listed in Table 3.2. In this measurement campaign, a total of 982 KPI samples were collected in a little over 1 hour of measurement time, spanning across 1 day of data collection. The measurement route covered a distance of 8.3 kilometers.

As depicted in Fig. 5.37, which displays boxplots of individual signal metrics from a mobile measurement conducted in Brno center on April 24th, only one dataset was measured for LTE Band 7. Due to the challenging nature of measuring this band, attributed to its limited coverage over the entire area, the decision was made to focus the measurement in the vicinity of Svobody Square, considering the band's deployment characteristics in areas with relatively higher population density, as indicated by the coverage estimate from the CTO and the distribution of eNBs deployed by T-Mobile operator [50]. Given the relatively small size of this area, a single measurement sufficed, facilitated by using a bicycle, enabling quick coverage of most streets in the vicinity. However, from the boxplots in Fig. 5.37, it can be observed that the median RSRP value is -109 dBm, with occasional outliers reaching values as low as -200 dBm, indicating potential outages or cell edge scenarios. Despite this, the other metrics exhibit relatively stable performance, with median RSRQ values at -8.32 dB, RSSI at -51.6 dBm, and RSSNR at 11 dB.

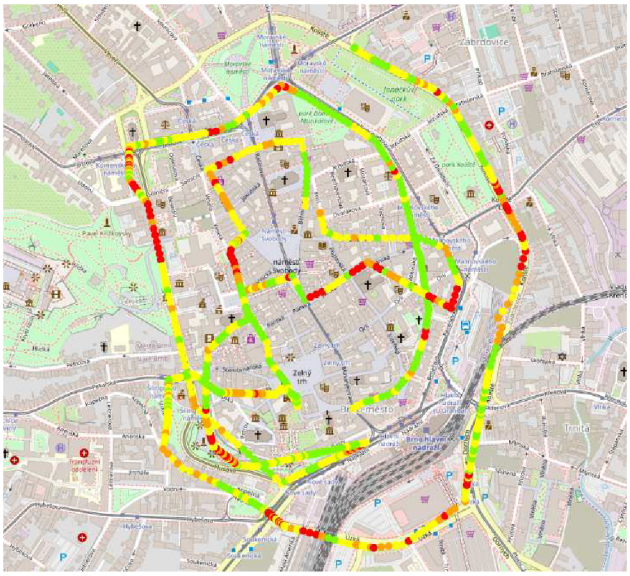

Fig. 5.36: RSRP points of a mobile measurement conducted at Brno center throughout April 24th on LTE Band 7 (2600 MHz)

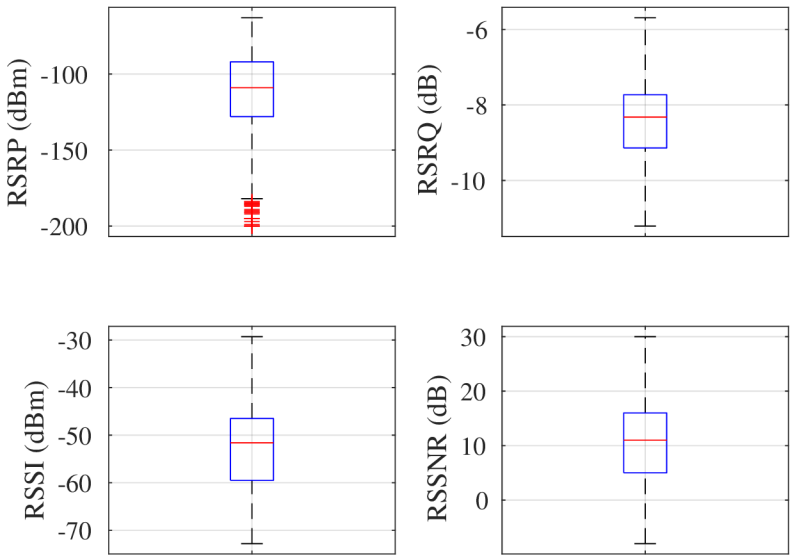

Fig. 5.37: Boxplots of signal metrics in a mobile measurement conducted at Brno center throughout April 24th on LTE Band 7 (2600 MHz)

Fig. 5.38 presents the ECDF of the RSRP metric, measured on LTE Band 7. The ECDF shows a slightly sharp increase around -120 dBm, indicating that a larger proportion of measurements fall within a relatively narrow RSRP range. This suggests a consistent signal strength measured by the measurement device within the measured dataset.

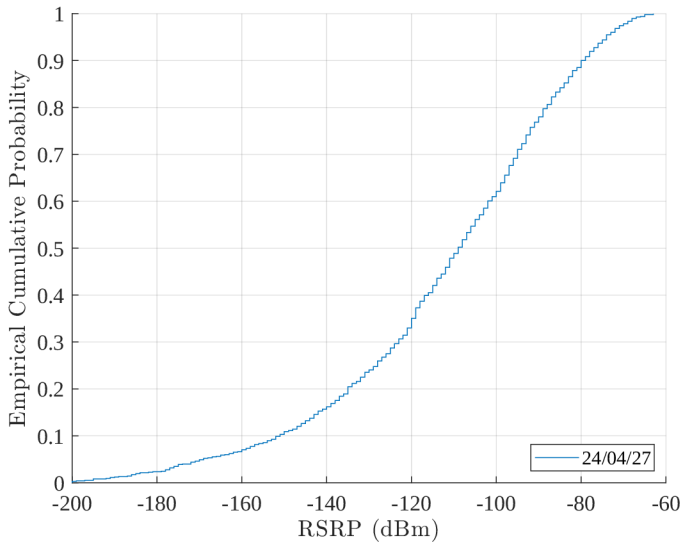

Fig. 5.38: Empirical Cumulative Distribution Function of RSRP metric from measured dataset on LTE Band 7 (2600 MHz)

As with the previous three LTE bands, three interpolation methods were employed to estimate the coverage of Band 7. Given the narrower area covered in this case, limited to the center of Brno, Fig. 5.39 presents the results of these interpolation methods. Once again, the *Bilinear* method, illustrated in Fig. 5.39a, emerges as the most optimal option, owing to its subtle transitions and ability to depict potential coverage changes between individual measured points, echoing reasons similar to those observed in the previous cases. In Fig. 5.39b, the *Nearest Neighbor* method appears less cohesive compared to Bands 20, 3, and 1, with indications of coverage resembling those of the *Bilinear* method. However, the presence of block artifacts detracts from the overall accuracy of the estimate. In Fig. 5.39c, the *Cubic convolution* method demonstrates improvement compared to previous cases, likely due to the shorter distances between measured points in this estimation. Consequently, the results are more precise. Although the estimation still predominantly oscillates between two extremes of excellent and poor coverage, there are noticeably more

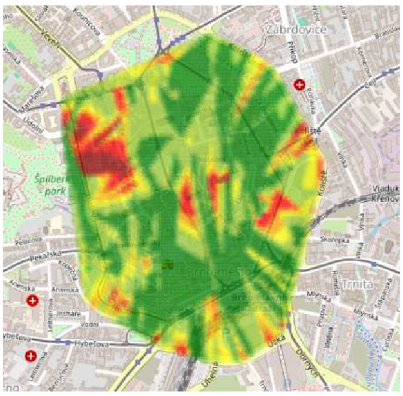

(a) *Bilinear* interpolation

(b) *Nearest Neighbor*

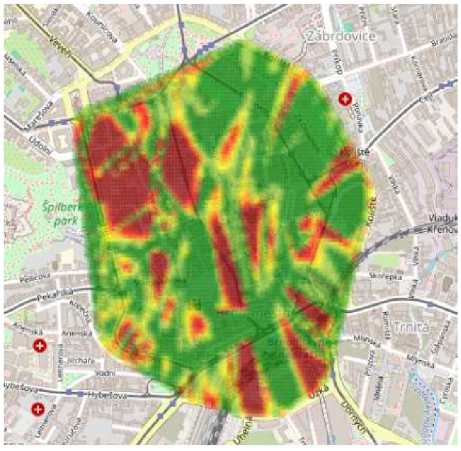

(c) *Cubic convolution*

Fig. 5.39: Coverage estimation via utilized interpolation methods for LTE Band 7

indications of transition between these states compared to estimates of previously analyzed bands. Overall, if the measured area across all four bands were extensively covered on most streets over a short period, such as during peak load scenarios, the *Cubic convolution* method could yield highly accurate results. Nevertheless, the overall estimate depicts solid coverage in the Brno area by this band, with predominantly green areas indicating very good Band 7 coverage. In Fig. 5.39a, which represents the most optimal *Bilinear* interpolation, there is only one larger area in the upper left corner of the interpolated points in red colors. This could be attributed to the module moving to the cell edge of the connected eNB in that area, followed by a handover to a better one.

For comparison with the created estimate, the official estimate provided by the CTO is shown in Fig. 5.40. As mentioned earlier, this band isn't as extensively covered as the other LTE bands, likely due to its higher frequency. Consequently, the signal propagation characteristics aren't as robust as those at lower frequencies below 1 GHz. Thus, it's expected that the CTO's estimate would depict more white spots or light blues. Nonetheless, it can be inferred that there's very good coverage in the measured area, and this is further evidenced by the CTO's estimate, which also shows a brighter area indicating strong coverage. Compared to the estimate created in this work, the estimate from CTO also shows a brighter area, i.e. not with as strong a signal as in the mentioned red area created with the help of *Bilinear* interpolation in Fig. 5.39a. From this it can be concluded that there is indeed a greater probability of a weaker coverage by this band.

Fig. 5.41 displays the filtered points of the RSRP metric below the threshold

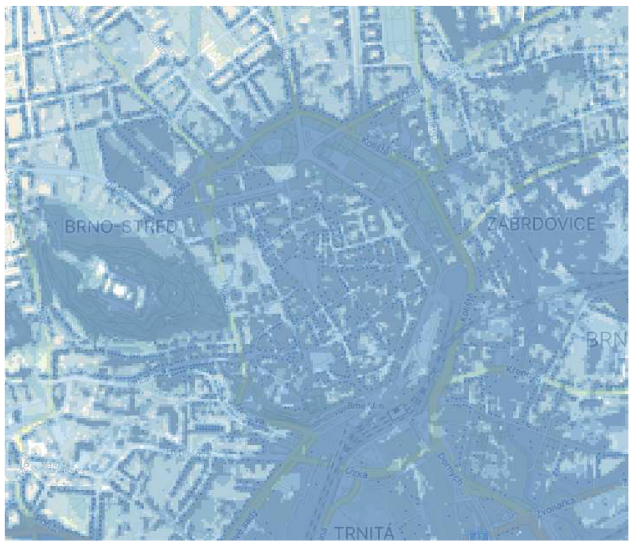

Fig. 5.40: Coverage estimation of Brno city constructed by CTO for T-Mobile Czech Republic on LTE Band 7 (2600 MHz)

Fig. 5.41: Filtered points of RSRP metric under threshold -165 dBm

of -165 dBm. This threshold was selected considering the higher frequency of this band compared to others. A concentrated section of these points can be observed in the upper left part of the map, confirming the earlier assertion about the coverage challenges posed by this band in this particular location.

5.2 5G NR Measured data

Due to limitations with the 5G module used and the unavailability of 5G SA commercially in the Czech Republic, only one band was measured: 5G NR NSA Band 78, operating at a frequency of 3500 MHz. While this band is not one of the most commonly deployed in the Czech Republic, it provides valuable insights into its coverage in the city of Brno. This band is particularly relevant for operators deploying Fixed Wireless Access (FWA) to offer internet connectivity via mobile sites. All measurements in this technology were conducted concurrently with LTE technology, as 5G currently operates in the Czech Republic only as an aggregation of LTE + NR in dual connectivity.

5.2.1 Mobile Measurement

Due to the unavailability of this band at the available locations for static measurement, only mobile measurements were conducted. The measurement setup was once again securely placed in a backpack, with measurement settings configured for both 4G and 5G networks. However, it was not possible to set up a purely 5G network due to the aforementioned dual connectivity constraints.

For the mobile measurement of 5G NR, various test types were employed, including drive, walk, bike, and public transport tests. In contrast to the LTE technology measurements, where public transport was primarily used, here the focus was on specific locations where it was feasible to measure the band. As a result, drive, bike, and walk tests were predominantly utilized to ensure detailed coverage of the target area. The measurement device, locked to 5G NR NSA Band 78, remained securely stored in a backpack throughout the measurements. These measurements were conducted throughout the first half of 2024.

During the measurement, over 852 KPI samples were collected, spanning over 10 hours of measurement conducted over 6 days, covering a total distance of 15 km. Similar to LTE measurements, the primary objective was to analyze and create an estimate of the coverage map using the collected RSRP points. The interpolation methods utilized for estimation include *Bilinear*, *Nearest Neighbor*, and *Cubic convolution*. To assess the accuracy and reliability of the results, an official estimate from the CTO is utilized as a reference for comparison.

5G NR NSA Band 78 (3500 MHz)

As the SIM8200EA-M2 module utilized for measuring KPI metrics supports only Band 78 for 5G NR NSA, measurements were solely conducted in this band at a frequency of 3500 MHz. Commonly referred to as C-band, this frequency band, as outlined in [65], is among the less utilized bands in global 5G technology. This is attributed to the relatively unoccupied spectrum in this higher frequency range around 3500 MHz compared to lower frequencies in the low and mid bands. Despite being limited by propagation characteristics inherent to its high frequency, advancements in processing techniques such as massive MIMO, beamforming, and beamtracking enable operators to overcome these limitations, thus facilitating greater coverage with this band. Additionally, the shorter wavelengths associated with higher frequencies allow for the deployment of smaller and more compact antennas, thereby facilitating easier deployment of these antennas [65].

This band was measured alongside with the LTE bands across the Brno city area. In Fig. 5.42, four locations where it was feasible to measure this 5G NR NSA technology band are depicted, along with all measured RSRP values. These values are graphically represented using color coding corresponding to the signal strength categories outlined in Table 3.2.

In the subsequent analysis, we will focus solely on the Brno location at Skácelova, depicted in Fig. 5.42a. This area allowed for the measurement of the highest number of KPIs for this band, owing to its close proximity and accessibility. Figure 5.43 presents boxplots detailing the breakdown of individual measured metrics.

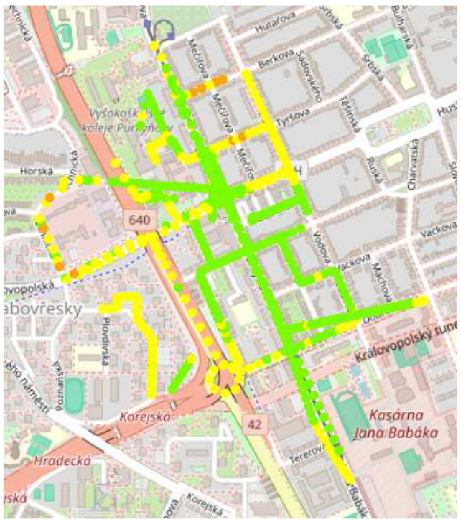

(a) Skácelova

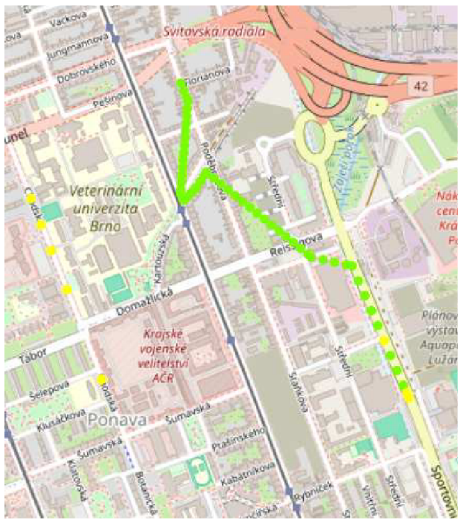

(b) Veterinární Univerzita Brno

(c) Výstaviště Brno

(d) Zvonařka, Cejl

Fig. 5.42: Coverage estimation via utilized interpolation methods at Brno – Skácelova for 5G NR NSA Band 78 (3500 MHz)

As depicted in Fig. 5.43, only RSRP, RSRQ, and RSSNR metrics were measurable in this technology, with the RSSI metric not supported by the utilized module in 5G NR NSA and thus not measured. The boxplot illustrates that while the RSRP values exhibit relatively high variability across the datasets, the RSRP medians are at a commendable level, falling below -90 dBm and even exceeding -80 dBm on April 3rd and 4th, indicating a very strong signal. Minimum values and outliers are around -110 dBm, with none surpassing -115 dBm. This threshold corresponds to the minimum level at which the module remained connected to the 5G network, with disconnections occurring below this threshold. The variability in the RSRP

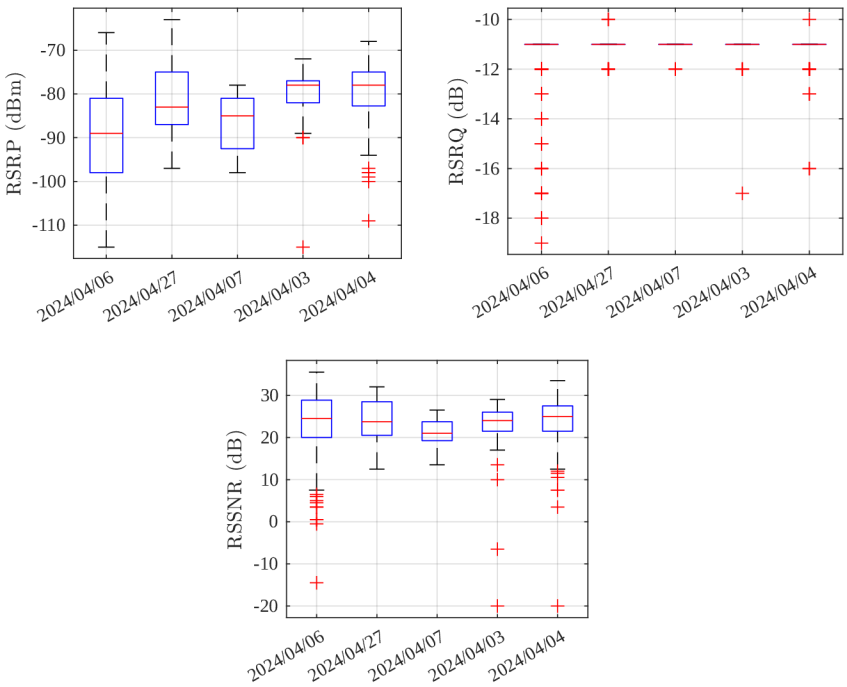

Fig. 5.43: Boxplots of signal metrics in a mobile measurement conducted at Brno - Skácelova throughout April 2024 on 5G NR NSA Band 78 (3500 MHz)

metric across datasets is likely influenced by the measurement location and possibly the speed of movement.

Regarding the RSRQ value, a stable distribution is evident, with a value of -11 dB and outliers falling below this consistent value, particularly notable in the dataset from April 6th. This discrepancy is attributed to the larger size of the dataset, comprising 523 KPI samples, resulting in increased variability and more instances where signal quality may have deteriorated.

The medians of the RSSNR metrics remain relatively stable and at a commendable level, ranging from 21 to 25 dB, indicating a robust signal quality with ample distance between the signal and noise. Outlier values around -20 dB suggest points where the measurement approached the cell edge, leading to disconnection.

Figure 5.44, illustrating the ECDFs of the RSRP samples from individually measured datasets, further confirms the notable variability in RSRP values. The plot reveals distinct transitions, particularly evident in the datasets from April 3rd and 4th, although this is attributed to the smaller sample sizes in these datasets. However, it is noteworthy that across all datasets, 50% of the samples surpass the -90 dBm threshold, indicating a consistently strong signal in half of all measured samples.

Figure 5.45 illustrates the coverage estimation via the utilized interpolation methods for 5G NR NSA Band 78 at Brno - Skácelova. In this scenario, two methods show promising results: once again, *Bilinear* interpolation and, thanks to the

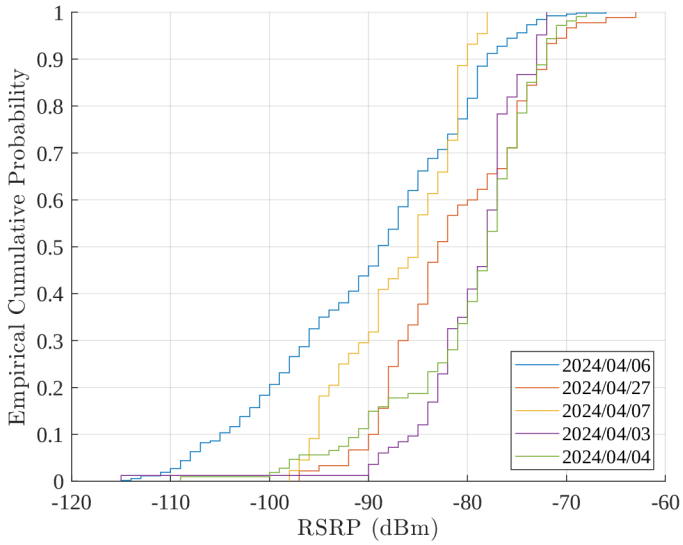

Fig. 5.44: Empirical Cumulative Distribution Functions of RSRP metric from individual measured datasets on 5G NR NSA Band 78 (3500 MHz)

higher density of the measured matrix, the *Cubic* method. *Nearest Neighbor* interpolation, shown in Fig. 5.45b, results in a more blocky, pixelated appearance with sharp transitions between coverage zones. While this method preserves some detail, it introduces a noticeable "stair-step" effect along the boundaries. The coverage area of good signal appears too large and less continuous compared to *Bilinear* interpolation, potentially overestimating actual coverage in some areas. The *Bilinear* method, depicted in Fig. 5.45a, produces a smooth, gradual transition between data points. Notice the smoothed edges of the coverage area and the gradual change in color intensity. This method is relatively simple and computationally inexpensive but can result in blurring and loss of sharp details. The coverage appears more widespread, potentially overestimating actual coverage in some areas. Meanwhile, the *Cubic* method, as shown in Fig. 5.45c, uses a more complex mathematical function to estimate values between data points. It produces a sharper image with smoother transitions than method *Nearest Neighbor*, while retaining more detail than *Bilinear* interpolation. Notice the more defined edges of the coverage area and smoother transitions within the color gradient. This method offers a good balance between detail preservation and smooth visualization but requires more computational resources than the other two methods, which is not problem in this case since the dataset includes less than thousand samples. This approach appears to deliver the most accurate representation of the coverage area. It becomes apparent that higher density and smaller distances between measured samples result in much better outcomes, especially for the *Cubic* method. In general, both the *Bilinear* and *Cubic* methods prove effective for estimating coverage in this case. However, the

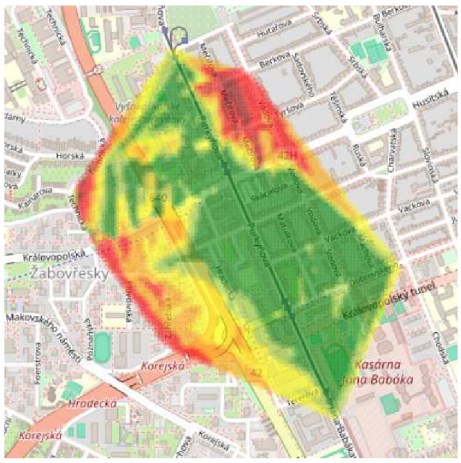

(a) *Bilinear* interpolation

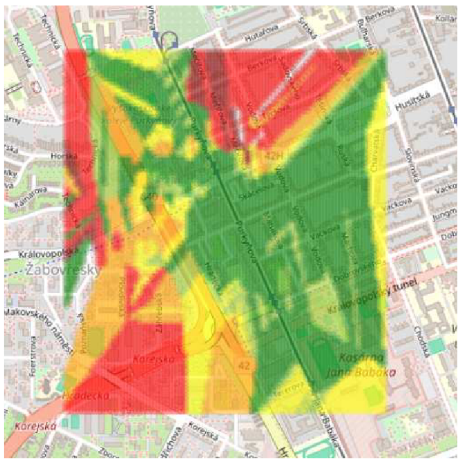

(b) *Nearest Neighbor*

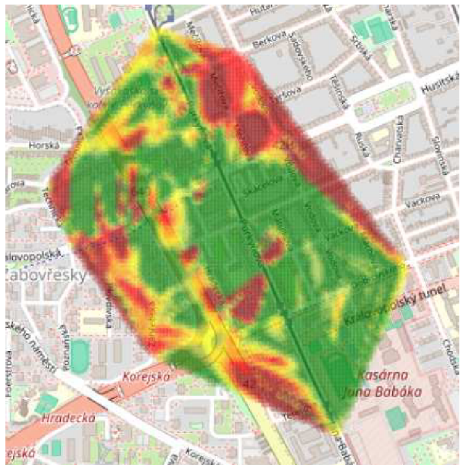

(c) *Cubic convolution*

Fig. 5.45: Coverage estimation via utilized interpolation methods at Brno - Skácelova for 5G NR NSA Band 78 (3500 MHz)

Bilinear method strikes the best balance between computational cost, appearance, and accuracy, consistently delivering optimal results across all coverage estimation scenarios.

As the only case among all estimations, the *Cubic convolution* method was chosen here as the best. For comparison with the created estimate, the official estimate provided by the CTO is shown in Fig. 5.46. It can be seen that the selected coverage estimate is very close to that of the CTO, and the most similar among all comparisons. Again, the inclusion of terrain and buildings is missing here, as can be seen in the estimate from the CTO, but essentially, the main part of the coverage around Purkyňova Street in the direction of the Kasárna Jana Babáka is very similar in both estimates, as well as the transition where the coverage is slightly weaker between Hradecká and Purkyňová and then again very good coverage on

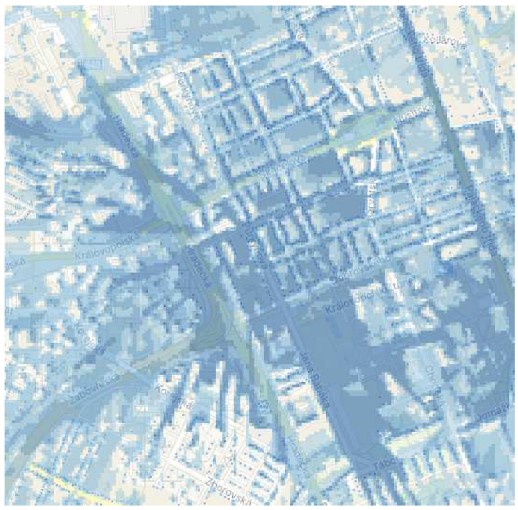

Fig. 5.46: Coverage estimation of Brno city constructed by CTO for T-Mobile Czech Republic at Brno - Skácelova on 5G NR NSA Band 78 (3500 MHz)

Hradecká Street. Compared to the CTO estimate, which shows coverage even in parts further away than the estimate in this work, no coverage was available for the used measurement module in this work. Measurements were also carried out all around, but the module was not able to connect to the network. It can be seen from both coverage estimation maps that the high frequency of 3500 MHz is crucial, where the signal has worse propagation properties. Therefore, the signal coverage in the given area is relatively small. The serving cell to which the measurement setup was connected is located on a apartment building in Svatopluka Čecha Street, and from this area, it can be seen that the coverage around is very good and gradually worsens with the distance from the cell.

Conclusion

In this thesis, the theoretical background of 4G and 5G mobile networks was presented to obtain an overview of the principles, properties, deployment, and coverage of these technologies in the Czech Republic. Additionally, a comprehensive overview of measurement environments and their impact on data collection in 4G/5G mobile networks was provided, focusing on the distinct characteristics and challenges posed by indoor and outdoor settings. This approach allowed for a deeper exploration of the methodologies and techniques for measuring, mapping, and analyzing signal coverage in these networks.

Among the main aims of the thesis was to create a portable measurement setup for assessing both indoor and outdoor network coverage. It was successfully achieved with hardware components like the SIM8200EQ-M2 5G Module, the Raspberry Pi 4 Model B, and a 40 Ah power bank, considering factors such as performance, cost-effectiveness, and power efficiency. Additionally, a custom-designed application was introduced and built using the *Dash* framework to facilitate user-friendly control and configuration of measurements. Furthermore, a methodological procedure was outlined for the long-term collection and processing of measured data, involving benchmark tests via public transport, driving, biking, or walking-based measurement, utilizing the proposed software and hardware solutions. A detailed procedure for processing and visualization was established, covering aspects like data filtering, interpolation for coverage mapping, and the use of graphical tools for analysis. This comprehensive approach ensures that the developed setup can collect high-quality network data and enables users to readily analyze and derive meaningful insights from the collected information. In addition to selecting appropriate hardware and software settings, extensive exploration of algorithmic aspects was conducted. Thorough research identified and employed suitable algorithms for processing measured data. The discussion delved into the utility of popular models like Linear Regression and XGBoost, emphasizing their effectiveness in analyzing static data and forecasting future trends. Various interpolation methods, including *Bilinear*, *Nearest Neighbor*, and *Cubic Convolution*, were employed to approximate coverage across the measured area. Each method's results were rigorously compared to determine the most suitable approach to generate a realistic coverage map.

The experimental phase of the study in this thesis involved extensive indoor and outdoor measurement campaigns to assess the impact of various transmission and environmental factors on mobile signal coverage. The focus was on evaluating 4G LTE and 5G NR NSA coverage in Brno, Czech Republic, with particular attention to the performance of T-Mobile Czech Republic. During the static indoor measurement phase, almost 2 million KPI samples were collected, each containing the

values of RSRP, RSRQ, RSSI, and RSSNR parameters, and other relevant information. These data highlighted several key findings and achievements, including the dynamic nature of network performance in LTE Bands 1, 3, and 20, with fluctuations in RSRP aligning with network load patterns throughout the day. The study also identified peak usage days for specific bands, indicating the influence of student occupancy on network usage at the measured location, Pod Palackého Vrchem dormitory. Furthermore, the impact of network congestion on various metrics such as RSRP, RSRQ, RSSI, and RSSNR was demonstrated, underscoring the importance of considering temporal variations in network planning and optimization. In the mobile outdoor measurement phase, over 46,000 KPI samples were collected during 41 hours of measurement over 13 days, covering a total distance of 343 km. These data allowed for the analysis of the coverage of LTE Bands 1, 3, 20, and 7 across Brno, revealing variability in signal strength across different locations and modes of transportation. The above mentioned interpolation methods were evaluated for estimating coverage based on the measured RSRP values. *Bilinear* interpolation consistently provided the best results. Comparisons were made between the estimated coverage maps and those from the CTO, highlighting discrepancies attributed to differences in methodology and the impact of signal attenuation in public transport. Additionally, areas with poor signal strength were identified, providing insights into opportunities for network optimization. Regarding 5G NR NSA measurements, the coverage of Band 78 in the selected location Brno - Skácelova was assessed, demonstrating that coverage in the tested area is limited due to the high frequency and its inherent propagation characteristics. Nevertheless, strong signal strength in certain areas highlights its potential for FWA deployments. The study showcased the effectiveness of the *Cubic Convolution* interpolation method in accurately capturing the coverage area, particularly in scenarios with dense measurement grids.

According to the obtained results, the answers to the posed research questions in the Introduction are as follows:

- Band 20, operating at a lower frequency, offers extensive coverage with superior in-building penetration, making it ideal for rural and regional areas. In contrast, Bands 3 and 1 provide a balance between coverage and capacity, suitable for urban and suburban areas but with somewhat reduced propagation capabilities compared to Band 20. Band 7, at the highest frequency, has the smallest coverage area and is primarily used in densely populated urban settings due to its higher susceptibility to signal attenuation. These propagation differences necessitate varying approaches to coverage estimation; lower RF bands like Band 20 require fewer measurement points, whereas higher frequency bands like Band 7 need a denser grid of samples for accurate interpolation.
- *Bilinear* interpolation emerges as the most suitable method, balancing compu-

tational efficiency, smoothness, and accuracy. It provides a visually appealing output without overly smoothing or distorting the coverage map. *Nearest Neighbor*, while computationally efficient, tends to produce blocky and less visually accurate maps due to its simplicity. *Cubic Convolution*, although highly accurate and detailed, requires a densely sampled dataset to avoid creating overly dichotomous coverage maps. Therefore, *Bilinear* interpolation is recommended for its ability to produce reliable results across various scenarios with moderate computational cost.

- Static measurements indicate that the RSRP metric is strongly correlated with network load, especially in high-usage areas like student dormitories, where signal strength improves on weekends due to lower usage. Different LTE bands show varying usage patterns, with Band 20 consistently serving as the primary connection and Bands 3 and 1 acting as capacity layers during peak hours. Mobile measurements highlight the impact of transportation modes on signal attenuation, with public transport, particularly trams, experiencing worse signal degradation compared to buses, bicycles, or walking. This underscores the importance of considering diverse transportation modes in coverage analysis. For 5G NR NSA, limited to Band 78, coverage is concentrated in specific areas with strong signal quality near serving cells but rapidly degrades at cell edges due to the high frequency.

By sharing all measured datasets alongside the open-source software developed in this study on GitHub[1], the research provided in this thesis ensures transparency and accessibility. These datasets not only validate findings but also serve as valuable resources for future research, education, and innovation in mobile network coverage analysis. Providing access to real-world data fosters collaboration, accelerates scientific progress, and empowers a diverse community to explore, learn, and advance the field. A small part of the study presented in this thesis was presented at the student conference Student EEICT 2024 [66].

[1]All recorded data, along with developed applications, are readily accessible at the following link: https://github.com/michalizn/coverage-analysis

Bibliography

[1] 3GPP, "*Introducing 3GPP*." Online, 2023. https://www.3gpp.org/about-us, [cited 2023-11-09].

[2] A. Roessler and M. Kottkamp, "*Rohde & Schwarz: White Paper 1MA232 "LTE-Advanced (3GPP Rel.11) Technology Introduction*." Online. https://scdn.rohde-schwarz.com/ur/pws/dl_downloads/dl_application/application_notes/1ma232/1MA232_1e_LTE_Rel11_technology.pdf, [cited 2023-11-10].

[3] Janeba, Matej and Lehoczký, Peter and Galinski, Marek and Milesich, Tomáš and Danko, Ján and Kotuliak, Ivan, "*Evaluation of LTE and 5G qualitative parameters for V2X use cases*," in *2022 IEEE Zooming Innovation in Consumer Technologies Conference (ZINC)*, pp. 165–169, 2022.

[4] Westbase.io, "*What is LTE-Advanced Pro?*." Online, March 2019. https://www.westbase.io/what-is-lte-advanced-pro/, [cited 2023-11-10].

[5] Artiza Networks, Inc., "*Introduction to LTE-A Pro*." Online, 2023. https://www.artizanetworks.com/resources/tutorials/lteapro.html, [cited 2023-11-10].

[6] Huawei, "*AR100, AR120, AR150, AR160, AR200, AR1200, AR2200, AR3200, and AR3600 V200R010 CLI-based Configuration Guide - Interface Management*." Online, August 2023. https://support.huawei.com/enterprise/en/doc/EDOC1100034069/f110c2e7/lte-network-architecture, [cited 2023-11-10].

[7] Sauter, Martin, *From GSM to LTE-Advanced Pro and 5G An Introduction to Mobile Networks and Mobile Broadband*. John Wiley & Sons, Ltd., 4 ed., 2021.

[8] Roy, Jibendu Sekhar and Mishra, Subhra Surochita, "*Performance of SC-FDMA for LTE Uplink Under Different Modulation Schemes*," in *2019 International Conference on Mechatronics, Robotics and Systems Engineering (MoRSE)*, pp. 202–206, 2019.

[9] Vaclav Raida, "*Deriving a Network Perspective of Cellular Mobile Networks Based on Crowd Sourced Benchmark Tests. Diploma Thesis, Technische Universität Wien*." Online, November 2017. https://doi.org/10.34726/hss.2017.32149, [cited 2023-11-12].

[10] Spectrum Tracker, "*Frequency spectrum database, Czech Republic*." Online, July 2023. https://www.spectrum-tracker.com/Czech-Republic, [cited 2023-11-15].

[11] Český telekomunikační úřad, "*Veřejné širokopásmové pokrytí mobilní sítě 4G a 5G v pásmech 700MHz, 800MHz, 1800MHz, 2100MHz, 2600MHz a 3600MHz*." Online, September 2023. https://digi.ctu.cz/pokryti/, [cited 2023-11-15].

[12] Gavrić, Radana and Ilišević, Dijana and Ćurguz, Nataša Banović and Budimir, đurađ, "*Comparison of basic characteristics of 4G/LTE and 5G NR technology*," in *2019 27th Telecommunications Forum (TELFOR)*, pp. 1–4, 2019.

[13] Osseiran, Afif and Monserrat, Jose F. and Marsch, Patrick, *5G Mobile and Wireless Communications Technology*. Cambridge University Press, 2016.

[14] Sun, Haijian and Hu, Rose Qingyang and Qian, Yi, *5G and Beyond Wireless Communication Networks*. Wiley-IEEE Press, 2023.

[15] Singh, Radheshyam and Jepsen, Jes H. and Ballal, Kalpit D. and Nwabuona, Stanley and Berger, Michael and Dittmann, Lars, "*An Investigation of 5G, LTE, LTE-M and NB-IoT Coverage for Drone Communication Above 450 Feet*," in *2023 IEEE 24th International Symposium on a World of Wireless, Mobile and Multimedia Networks (WoWMoM)*, pp. 370–375, 2023.

[16] Levanen, Toni and Ranta-Aho, Karri and Kaikkonen, Jorma and Nielsen, Sari and Pajukoski, Kari and Renfors, Markku and Valkama, Mikko, "*5G new radio and LTE uplink coexistence*," in *2018 IEEE Wireless Communications and Networking Conference (WCNC)*, pp. 1–6, 2018.

[17] Mustofa, Ali and Edy Purnomo, Muhammad Fauzan and Talcha Krusbeek Orrilia Audre, A.P.S., "*Optimization of 5G NR Network Based on Performance of 4G LTE Network in Area of Universitas Brawijaya Malang*," in *2022 11th Electrical Power, Electronics, Communications, Controls and Informatics Seminar (EECCIS)*, pp. 229–233, 2022.

[18] 3GPP, "*5G System Overview*." Online, August 2022. https://www.3gpp.org/technologies/5g-system-overview, [cited 2023-11-16].

[19] Arjun Sha, "*5G SA vs NSA: Difference Between Standalone and Non-standalone 5G Architecture*." Online, August 2022. https://beebom.com/sa-vs-nsa-5g/, [cited 2023-11-16].

[20] Kún, Gergely and Varga, Péter János and Wührl, Tibor and Wührl, Dóra and Gyányi, Sándor and Nádai, László and Kovács, Róbert, "*"Opened" or "Closed" RAN in 5G*," in *2022 IEEE 20th Jubilee World Symposium on Applied Machine Intelligence and Informatics (SAMI)*, pp. 000347–000352, 2022.

[21] Wei Xiang, Xuemin (Sherman) Shen, and Kan Zheng, *5G Mobile Communications*. Springer International, 2017.

[22] Jan Láska, "*O2 a T-Mobile mohou pokračovat ve sdílení sítí. Musí ale dodržovat pravidla, která si sami navrhli*." Online, July 2022. `https://mobilmania.zive.cz/clanky/o2-a-t-mobile-mohou-pokracovat-ve-sdileni-siti-musi-ale-dodrzovat-pravidla-ktera-si-sami-navrhli/sc-3-a-1355568/default.aspx`, [cited 2023-11-20].

[23] MyMobi Force, "*Telecom Drive Testing Optimization Using GIG Workforce*." Online, May 2023. `https://mymobiforce.com/blog/mmf-field-services/telecom-drive-testing-optimization-using-GIG-workforce.html`, [cited 2023-12-02].

[24] El-Saleh, Ayman and Abdullah Al Jahdhami, Majan and Alhammadi, Abdulraqeb and Shamsan, Z.A. and Shayea, Ibraheem and Hassan, Wan, "*Measurements and Analyses of 4G/5G Mobile Broadband Networks: An Overview and a Case Study*," *Wireless Communications and Mobile Computing*, vol. 2023, 04 2023.

[25] Haneda, Katsuyuki; Rudd, Richard; Vitucci, Enrico; He, Danping; Kyösti, Pekka; Tufvesson, Fredrik; Salous, Sana; Miao, Yang; Joseph, Wout; Tanghe, Emmeric, "*Radio propagation modeling methods and tools*." Online, January 2021. `https://acris.aalto.fi/ws/portalfiles/portal/8196834/Haneda_Radio_propagation_modeling.pdf`, [cited 2023-12-08].

[26] Liyanage, Mohan and Chang, Chii and Srirama, Satish and Loke, Seng, "*Indoor people density sensing using Wi-Fi and channel state information*," *Advances in Modelling and Analysis A*, vol. 61, pp. 37–47, 03 2018.

[27] Belakbir, A. and Amghar, Mustapha and Rechiche, A., "*An Indoor-Outdoor positioning system based on the combination of GPS and UWB sensors*," vol. 31, pp. 1155–1159, 03 2014.

[28] Wenzhong Shi, Michael F. Goodchild, Michael Batty, Mei-Po Kwan, Anshu Zhang, *Urban Informatics*. Springer, 2021.

[29] Demographic Yearbook, "*DEFINITION OF "URBAN".*" Online, 2005. https://unstats.un.org/unsd/demographic/sconcerns/densurb/defintion_of%20urban.pdf, [cited 2023-12-10].

[30] Sheng-Cheng Yeh and Wu-Hsiao Hsu and Ming-Yang Su and Ching-Hui Chen and Ko-Hung Liu, "*A study on outdoor positioning technology using GPS and WiFi networks*," in *2009 International Conference on Networking, Sensing and Control*, pp. 597–601, 2009.

[31] Minovski, Dimitar and Ögren, Niclas and Mitra, Karan and Åhlund, Christer, "*Throughput Prediction Using Machine Learning in LTE and 5G Networks*," *IEEE Transactions on Mobile Computing*, vol. 22, no. 3, pp. 1825–1840, 2023.

[32] Nokia, "*Nokia Dynamic Spectrum Sharing for Rapid 5G.*" Online, April 2020. https://onestore.nokia.com/asset/207265, [cited 2024-01-01].

[33] 3GPP, "*5G; NR; Physical channels and modulation (3GPP TS 38.211 version 16.3.0 Release 16).*" Online, November 2020. https://www.etsi.org/deliver/etsi_ts/138200_138299/138211/16.03.00_60/ts_138211v160300p.pdf, [cited 2024-01-02].

[34] Raida, Vaclav and Svoboda, Philipp and Rupp, Markus, "*Real World Performance of LTE Downlink in a Static Dense Urban Scenario - An Open Dataset*," in *GLOBECOM 2020 - 2020 IEEE Global Communications Conference*, pp. 1–6, 2020.

[35] 3GPP, "*LTE; Evolved Universal Terrestrial Radio Access (E-UTRA); Physical channels and modulation (3GPP TS 36.211 version 14.2.0 Release 14).*" Online, April 2017. https://www.etsi.org/deliver/etsi_ts/136200_136299/136211/14.02.00_60/ts_136211v140200p.pdf, [cited 2024-01-02].

[36] Weitzen, J. and Lowe, T.J., "*Measurement of angular and distance correlation properties of log-normal shadowing at 1900 MHz and its application to design of PCS systems*," *IEEE Transactions on Vehicular Technology*, vol. 51, no. 2, pp. 265–273, 2002.

[37] 3GPP, "*LTE; Evolved Universal Terrestrial Radio Access (E-UTRA); Physical layer; Measurements (3GPP TS 36.214 version 14.2.0 Release 14).*" Online, April 2017. https://www.etsi.org/deliver/etsi_ts/136200_136299/136214/14.02.00_60/ts_136214v140200p.pdf, [cited 2024-01-01].

[38] Simcom, "*SIM8200EA-M2.*" Online, 2024. https://www.simcom.com/product/SIM8200EA_M2.html, [cited 2024-01-05].

[39] Quectel, "*5G RM50xQ series*." Online, 2024. https://www.quectel.com/product/5g-rm50xq-series, [cited 2024-01-05].

[40] Sierra Wireless, "*EM9190 5G NR Sub-6 GHz and mmWave Module*." Online, 2024. https://www.sierrawireless.com/iot-modules/5g-modules/em9190/, [cited 2024-01-05].

[41] Anker, "*USB 2.0 vs 3.0: A Comparative Guide for Beginners 2023*." Online, August 2023. https://www.anker.com/blogs/hubs-and-docks/usb-2-vs-usb-3, [cited 2024-01-07].

[42] Lackner, Thorge and Hermann, Julian and Dietrich, Fabian and Kuhn, Christian and Angos-Mediavilla, Mario and Jooste, Wyhan and Palm, Daniel, "Measurement and comparison of data rate and time delay of end-devices in licensed sub-6 ghz 5g standalone non-public networks," *Procedia CIRP*, vol. 107, pp. 1132–1137, 01 2022.

[43] RPishop.cz, "*Waveshare SIM8200EA-M2 5G HAT pro Raspberry Pi s podporou 5G/4G/3G, Snapdragon X55, Multi Mode Multi Band*." Online, August 2024. https://rpishop.cz/iot-karty/4346-waveshare-sim8200ea-m2-5g-hat-pro-raspberry-pi-s-podporou-5g4g3g-snapdragon-x55-multi-mode-multi-band.html, [cited 2024-01-07].

[44] Raspberry Pi, "*Raspberry Pi 5*." Online, 2024. https://www.raspberrypi.com/products/raspberry-pi-5/, [cited 2024-01-07].

[45] Raspberry Pi, "*Raspberry Pi 4*." Online, 2024. https://www.raspberrypi.com/products/raspberry-pi-4-model-b/, [cited 2024-01-07].

[46] Alex Bate, "*Thermal testing Raspberry Pi 4*." Online, 2024. https://www.raspberrypi.com/news/thermal-testing-raspberry-pi-4/, [cited 2024-01-07].

[47] Plotly, "*Dash Documentation and User Guide | Plotly*." Online, 2024. https://dash.plotly.com/, [cited 2024-04-29].

[48] Plotly, "*Dash Documentation and User Guide | Background Callbacks*." Online, 2024. https://dash.plotly.com/background-callbacks, [cited 2024-04-29].

[49] Commselect, "*Tems Discovery Device 23.01 Released*." Online, April 2021. https://www.commselect.net/2021/04/13/tems-discovery-device-23-01-released/, [cited 2024-01-09].

[50] GSMweb.cz, "*Seznamy BTS*." Online, January 2024. https://gsmweb.cz/, [cited 2024-01-09].

[51] Mathai, Neann and Chen, Ya and Kirchmair, Johannes, "*Validation strategies for target prediction methods*," *Briefings in bioinformatics*, vol. 21, 04 2019.

[52] Chen, Tianqi and Guestrin, Carlos, "*XGBoost: A Scalable Tree Boosting System*," *Proceedings of the 22nd ACM SIGKDD International Conference on Knowledge Discovery and Data Mining*, vol. 22, no. 3, p. 785–794, 2016.

[53] T. Hastie, R. Tibshirani, and J. Friedman, *The elements of statistical learning: data mining, inference and prediction*. Springer, 2 ed., 2009.

[54] James, Gareth and Witten, Daniela and Hastie, Trevor and Tibshirani, Robert and Taylor, Jonathan, *Linear Regression*. Cham: Springer International Publishing, 2023.

[55] Scikit-learn Contributors, "*Linear Models (scikit-learn documentation)*." Online, 2024. https://scikit-learn.org/stable/modules/linear_model.html, [cited 2024-01-12].

[56] Nvidia, "*XGBoost*." Online, 2024. https://www.nvidia.com/en-us/glossary/xgboost/, [cited 2024-05-01].

[57] The SciPy community, "*Interpolation (SciPy v1.11.4 Manual)*." Online, 2024. https://docs.scipy.org/doc/scipy/reference/interpolate.html, [cited 2024-01-12].

[58] Halberd Bastion RF, "*B20 (800 MHz)*." Online, 2024. https://halberdbastion.com/technology/cellular/4g-lte/lte-frequency-bands/b20-800-mhz, [cited 2024-05-04].

[59] Halberd Bastion RF, "*B3 (1800 MHz)*." Online, 2024. https://halberdbastion.com/technology/cellular/4g-lte/lte-frequency-bands/b3-1800-mhz, [cited 2024-05-02].

[60] iDNES.cz, "*T-Mobile postihl masivní výpadek. Problémy hlásili lidé po celém Česku*." Online, 2024. https://www.idnes.cz/zpravy/domaci/cesko-t-mobile-operator-vypadek.A240413_174414_domaci_svm, [cited 2024-05-02].

[61] iROZHLAS, "*Síť T-mobile čelila masivním výpadkům. Zákazníkům operátora nefungovaly klasické hovory ani internet* ." Online, 2024. https://www.irozhlas.cz/zpravy-domov/t-mobile-internet-volani-telefon-vypadek_2404131924_jud, [cited 2024-05-02].

[62] TNCZ, "*T-Mobile postihl masivní výpadek. Lidé napříč Českem neměli signál.*" Online, 2024. https://tn.nova.cz/zpravodajstvi/clanek/550872-t-mobile-ma-masivni-vypadek-lide-napric-ceskem-nemaji-signal, [cited 2024-05-02].

[63] International Telecommunication Union - Radiocommunication Sector, "*A path-specific propagation prediction method for point-to-area terrestrial services in the VHF and UHF bands.*" Online, 2014. https://www.itu.int/dms_pubrec/itu-r/rec/p/R-REC-P.1812-3-201309-S!!PDF-E.pdf, [cited 2024-05-08].

[64] Halberd Bastion RF, "*B7 (2600 MHz).*" Online, 2024. https://halberdbastion.com/technology/cellular/4g-lte/lte-frequency-bands/b7-2600-mhz, [cited 2024-05-10].

[65] Halberd Bastion RF, "*n78 (3500 MHz).*" Online, 2024. https://halberdbastion.com/technology/cellular/5g-nr/5g-frequency-bands/n78-3500-mhz, [cited 2024-05-13].

[66] M. Baranek, L. Polak, J. Kufa, "*Mapping and analyzing of signal coverage of 4G/5G mobile networks. Proceedings of the 30 th Conference STUDENT EEICT 2024.*" Online, 2024. https://www.eeict.cz/download#proceedings, [cited 2024-05-15].

Symbols and abbreviations

3GPP	3rd Generation Partnership Project
4G	Fourth-Generation
5G	Fifth-Generation
ANN	Artificial Neural Networks
API	Application Programming Interface
BER	Bit Error Rate
BUT	Brno University of Technology
CA	Carrier Aggregation
CID	Cell ID
CN	Core Network
CRS	Cell-Specific Reference Signal
CP	Cyclic Prefix
CSS	Cascading Style Sheets
CTO	Czech Telecommunication Office
D2D	Device-to-Device Communication
DFT	Discrete Fourier Transform
DL	Downlink
DSS	Dynamic Spectrum Sharing
ECDF	Empirical Cumulative Distribution Function
eMBB	Enhanced Mobile Broadband
eNB	E-UTRAN NodeB
EPC	Evolved Packet Core
E-UTRAN	Evolved Universal Terrestrial Radio Access Network
FDD	Frequency Division Duplex

FR1	Frequency Range 1
FR2	Frequency Range 2
FWA	Fixed Wireless Access
GBDT	Gradient Boosting Decision Trees
GBM	Gradient Boosting Machines
GNSS	Global Navigation Satellite Systems
GPS	Global Positioning System
gNB	Next-Generation Node B
GUI	Graphical User Interface
HTML	Hypertext Markup Language
HTTP	Hypertext Transfer Protocol
HSS	Home Subscriber Server
IEEE	Institute of Electrical and Electronics Engineers
IoT	Internet-of-Things
IP	Internet Protocol
ITU	International Telecommunication Union
KNN	K-Nearest Neighbors
KPIs	Key Performance Indicators
LOS	Line-of-Sight
LTE	Long-Term Evolution
LTE-A	LTE-Advanced
MAE	Mean Absolute Error
MBB	Mobile Broadband
M2M	Machine-to-Machine Communication
MCU	Microprocessor Unit

MIMO	Multiple Input Multiple Output
ML	machine learning
mMTC	Massive Machine-Type Connectivity
MNO	Mobile Network Operator
MME	Mobility Management Entity
NLOS	Non-Line-of-Sight
NR	New Radio
NSA	Non-Standalone
OFDMA	Orthogonal Frequency Division Multiple Access
PAPR	Peak-to-Average Power Ratio
PGW	Packet Data Network Gateway
PHY	Physical Layer
PRB	Physical Resource Block
QoE	Quality of Experience
QoS	Quality of Service
RAN	Radio Access Network
RAT	Radio Access Technology
RBs	Resource Blocks
REs	Resource Elements
RF	Radio Frequency
RNC	Radio Network Controller
RPI	Raspberry Pi
RMSE	Root Mean Squared Error
RSSI	Received Signal Strength Indicator
RSRP	Reference Signal Received Power

RSRQ	Reference Signal Received Quality
RSSNR	Reference Signal Signal-to-Noise Ratio
RTT	Round-Trip-Time
SA	Standalone
SBC	Single-Board Computer
SC-FDMA	Single-Carrier Frequency Division Multiple Access
SDMA	Space Division Multiple Access
SGW	Serving Gateway
SIM	Subscriber Identity Module
SINR	Signal-to-Noise and Interference Ratio
SNR	Signal-to-Noise Ratio
SoC	System on a Chip
SVM	Support Vector Machines
TDD	Time Division Duplex
TOA	Time of Arrival
UE	User Equipment
UL	Uplink
URLLC	Ultra-Reliable Low-Latency Connectivity
USB	Universal Serial Bus
VoLTE	Voice over LTE
VoNR	Voice over New Radio
WiFi	Wireless Fidelity
WSGI	Web Server Gateway Interface

A Laboratory Assignment focused on analyzing the Coverage of Mobile Networks

1. Measurement and Analysis of the LTE Mobile Network

Abstract
This laboratory exercise focuses on measuring key performance indicators (KPIs), including RSRP (Reference Signal Received Power), RSRQ (Reference Signal Received Quality), RSSI (Received Signal Strength Indicator), and RSSNR (Received Signal-to-Noise Ratio) in mobile networks. The aim is to perform measurements using the SIM8200EA-M2 module with the software developed for this exercise and subsequently conduct a quantitative analysis. The goal is to assess signal coverage and reliability, particularly in the context of mobile networks. Through this process, students develop the ability to evaluate network performance and extract essential metrics from 4G networks.

Keywords
Mobile Networks – LTE – RSRP – RSRQ – RSSI – RSSNR – SIM8200EA-M2 – Quantitative Analysis of LTE Coverage

Assignment

1. Familiarize yourself with the SIM8200EA-M2 module and the relevant software for measuring key performance indicators in mobile networks.
2. Understand the significance of the measured parameters, such as RSSI, RSRP, RSRQ, and RSSNR.
3. Perform measurements on three different LTE bands (Band 1, Band 3, Band 20) for 5 minutes at three defined locations.
4. Analyze the impact of frequency band and location on signal quality using the measured data.
5. Evaluate network coverage and reliability based on the obtained data and other relevant information.
6. Present the results of the analysis and coverage in a clear measurement report.

1. Introduction

In today's world, mobile networks have become an integral part of the daily lives of most of the world's population. Within mobile networks, the fundamental concept is the division of extensive areas into smaller cells. Each cell has its own base station (BS), and devices (user equipment - UE) connect to the nearest station in their current location. As users move and transition between cells, the network ensures their uninterrupted connection by connecting them to the most suitable nearby base stations. These approaches and technologies ensure continuous and seamless connectivity for mobile devices.

Among the most widely used networks today are fourth-generation networks (4G). 4G LTE (Long Term Evolution) or E-UTRAN (Evolved Universal Terrestrial Access Network), introduced in 3GPP Rel. 8, is the radio access component of the Evolved Packet System (EPS) - a purely IP-based mobile network standard. As an evolution of 3G UMTS, 4G LTE shares many similarities, such as harmonized frequency bands, but also many significant technological advancements [4]. Using the Orthogonal Frequency Division Multiple Access (OFDMA) multiple access scheme and combining it with higher modulation orders (up to 256QAM), large bandwidths (up to 100 MHz aggregated), and spatial multiplexing techniques (MIMO), very high data transfer rates can be achieved [4]. LTE is developed to support a range of frequency bands - E-UTRA operational bands - which currently range from 450 MHz to 6 GHz. Available bandwidths are also flexible, ranging from 0.2 MHz to 20 MHz. LTE is developed to support both Time Division Duplex (TDD) and Frequency Division Duplex (FDD) duplexing technologies [4].

Every mobile network consists of two basic parts. The first part includes the physical layer (PHY) and the Radio Access Network (RAN). The RAN section coordinates transmissions, assigns channels, and performs other coordination functions. The second part is the Core Network (CN), which connects all access networks. It provides global services such as authentication, roaming, and billing, while also establishing connections with external networks such as the internet [6]. Fig. 1 illustrates the simplified architecture of the LTE network and its basic elements. The network is structured into two main components: the E-UTRAN and the Evolved Packet Core (EPC), as shown in Fig. 1. E-UTRAN is responsible for supervising the radio interface between UE and the network. Conversely, the EPC handles call coordination and data routing between UE and external networks.

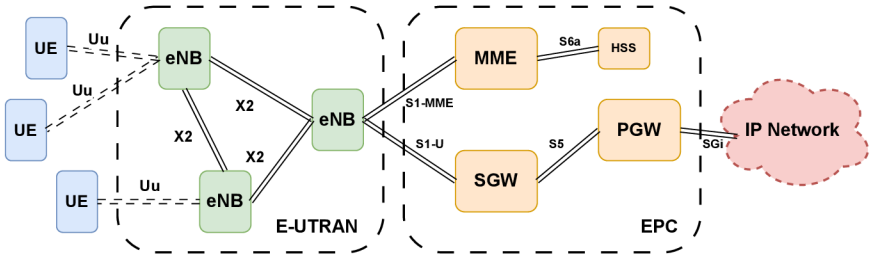

Figure 1. LTE network architecture

Unlike traditional 3GPP networks, the LTE network adopts a unified architectural structure by combining Radio Network Controller (RNC) and NodeB into E-UTRAN NodeB (eNodeB). These eNodeBs handle circuit switching at base stations, optimize the network, reduce system latency, and minimize costs associated with creation and maintenance [5]. LTE primarily relies on an IP-based core network. The use of all-IP network architecture significantly simplifies the design and operation of LTE air interface, radio network, and CN [8].

Fig. 1 illustrates the connections (via interfaces) between various network elements. These connections include the *Uu* interface, which connects UEs to eNBs, the *X2* interface, which interconnects eNBs, the *S1-MME* interface, which connects eNBs to the Mobility Management Entity (MME) entity, the *S6a* interface, which connects MME to the Home Subscriber Server (HSS), the *S1-U* interface, which provides connectivity between eNBs and the Serving Gateway (SGW) responsible for routing data traffic between UEs via the *S5* connection to the Packet Data Network Gateway (PGW), and the *SGi* connection linking to other IP networks such as the internet. In 4G networks, UEs include various types of devices, including mobile phones, smart terminals, multimedia devices, and streaming devices [5].

1.1 4G network coverage in the measurement location (Technická 12)

In the Czech Republic, three main mobile network operators (MNOs) - O2, T-Mobile, and Vodafone - provide comprehensive mobile signal coverage across the country. 4G network coverage varies depending on the specific radio frequency band. 4G technology in the Czech Republic primarily relies on four radio bands (Bands): Band 20 (800 MHz), Band 3 (1800 MHz), Band 1 (2100 MHz), and Band 7 (2600 MHz). Bands 1, 3, and 7 are strategically utilized as capacity layers in areas with high population density, such as large cities, ensuring robust coverage and high data transmission speeds. Band 20 serves as a backbone band, excelling in providing broader coverage in less populated and rural areas. Fig. 2 illustrates the coverage of all bands by the T-Mobile operator at the Technická 12 location (other operators are practically the same) based on measurements conducted by the Czech Telecommunication Office (CTO) [3].

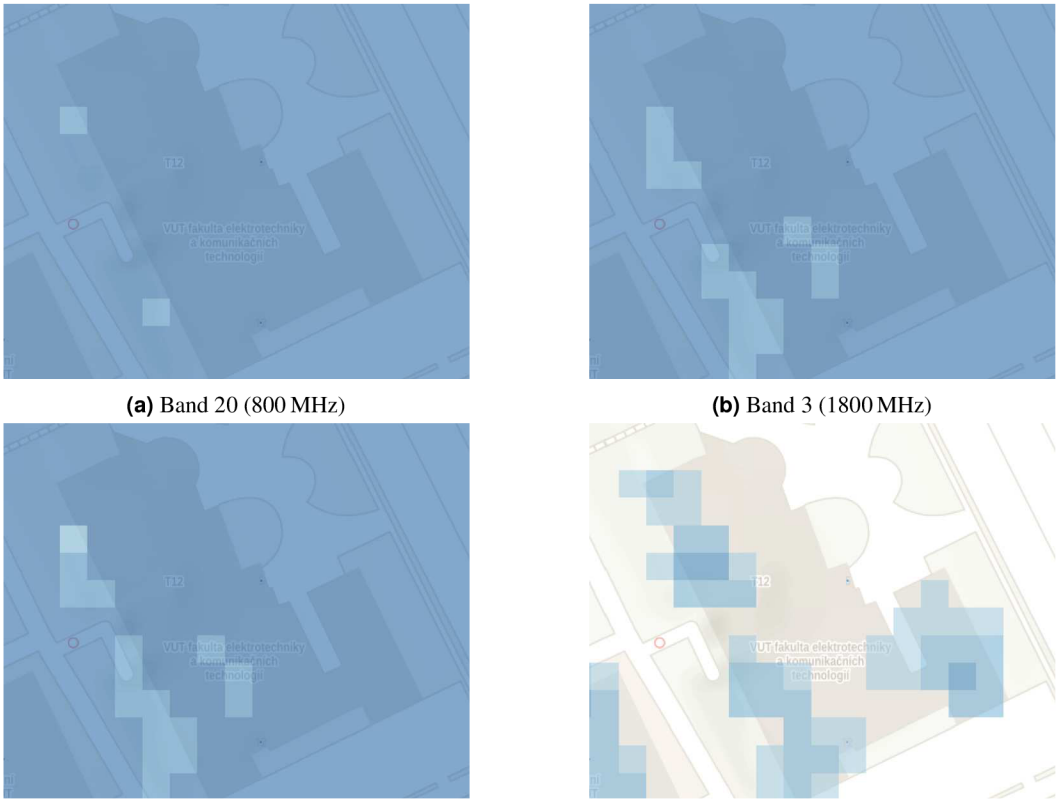

(a) Band 20 (800 MHz)

(b) Band 3 (1800 MHz)

(c) Band 1 (2100 MHz)

(d) Band 7 (2600 MHz)

Figure 2. 4G LTE coverage (all bands) of the T-Mobile operator in the Technická 12 locality (*valid on : 06.05.2024*)[3]

As seen from Fig. 2, coverage at Technická 12 address is available for Bands 1, 3, and 20, therefore, only these bands are measured in this task using Subscriber Identity Module (SIM) card from T-Mobile operator.

1.2 Key Performance Indicators (KPIs)

To determine important characteristics of mobile networks such as coverage, capacity, quality, reliability, etc., it is essential to obtain Key Performance Indicators (KPIs).

Before defining individual KPI metrics, it is appropriate to look at the physical layer of LTE (FDD). The Radio Resource Grid, depicted in Fig. 3, is divided into time and frequency units called Resource Blocks (RBs), with a duration of 0.7 ms and a width of 180 kHz. Each RB consists of 12 subcarriers, which are 15 kHz wide in the

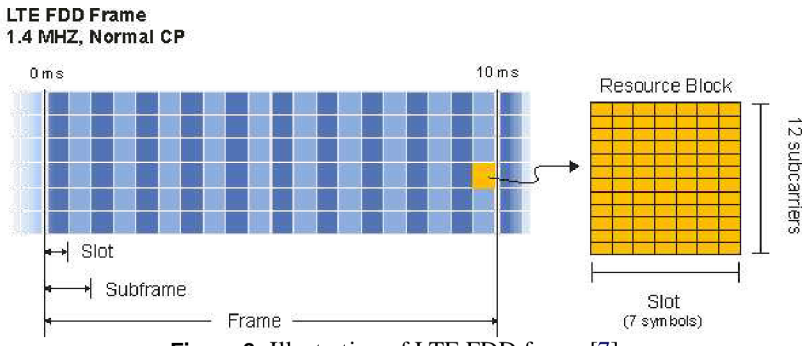

Figure 3. Illustration of LTE FDD frame [7]

frequency domain, and 7 OFDMA or SC-FDMA symbols (depending on the communication direction) in the time domain [1]. The small yellow squares represent Resource Elements (REs), which are the smallest units of the resource grid composed of one subcarrier in the frequency domain and one symbol in the time domain.

Let's analyze some of the most important measured network parameters, from which data is collected for analysis and conclusions on how to improve service quality and reliability.

- **RSSI (Received Signal Strength Indicator)** - RSSI is defined as the linear average of the aggregated received signal power, measured in watts. It is observed within the configured OFDM symbol and over the measuring bandwidth, including N number of RBs. This comprehensive measurement takes into account signals received by UE from various sources, including serving and non-serving cells in the same channel, interference from adjacent channels, thermal noise, and other contributing factors [2]. Typically, higher RSSI values (e.g., >-65 dBm) indicate stronger signal strength, and lower RSSI values (e.g., <-85 dBm) indicate weaker signal strength.

- **RSRP (Reference Signal Received Power)** - RSRP is characterized as the linear average of power contributions (measured in watts) from REs responsible for transmitting cell-specific reference signals (CRS). This measurement is performed within the designated frequency measurement bandwidth as specified in [2]. Usually, higher RSRP values (e.g., >-80 dBm) indicate stronger signals. Conversely, lower RSRP values (e.g., <-100 dBm) indicate weaker signals.

- **RSRQ (Reference Signal Received Quality)** - RSRQ is expressed as the ratio of N times RSRP to the RSSI of the E-UTRA carrier, where N represents the number of RBs within the E-UTRA carrier RSSI measurement bandwidth. Both the numerator (N times RSRP) and the denominator (RSSI of the E-UTRA carrier) are measured over the same set of RBs [2]. Again, higher RSRQ values (e.g., >-10 dB) indicate higher signal quality, and lower RSRQ values (e.g., <-20 dB) indicate poorer signal quality.

- **RSSNR (Reference Signal Signal to Noise Ratio)** - RSSNR is not defined by the 3GPP specification as the above metrics (and therefore is not reported to the serving cell), but is typically defined by the UE manufacturer (in this case, SIMCom). RSSNR is the ratio of the power of usable signals measured from CRS to the average noise within the measurement bandwidth. A higher RSSNR value (e.g., >15 dB) indicates good signal-to-noise separation, hence signal quality.

1.3 SIM8200EA-M2 Module

This module is manufactured by SIMCom Wireless Solutions. The baseboard of this module is equipped with a standard M2 connector, which allows connection to various 4G or 5G communication modules with M2. It also features a built-in USB3.1 port, audio connector and decoder, SIM card slot, etc. Combined with a configuration script and, for example, the AT command "`AT+CPSI?`", basic system UE information can be obtained. This mainly includes signal measurements such as RSRP, RSSI, RSRQ, and RSSNR. Additionally, this AT command provides

Table 1. SIM8200EA-M2 Specification

Key Aspects	SIM8200EA-M2
5G Category	5G NSA/SA
5G Frequency Bands (NSA)	n78
4G Category	Cat-20
4G Frequency Bands	All supported
Max. Download Speed	4 Gbps
Max. Upload Speed	500 Mbps
Max. RF Output Power	23 dBm
Satellite Systems	Supported
USB	USB 3.1
Price	300 €

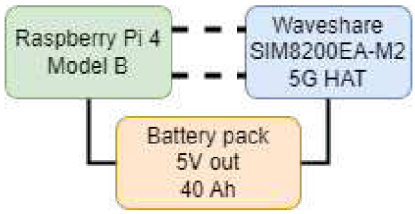

Figure 4. Connection of individual components of the measurement device

other useful information such as DL frequency and active set RF band, Physical Cell Identity (PCI) identification, and identification of the cell serving the next location used by the base station, as well as bandwidth configuration for both downlink and uplink channels.
Important parameters and specifications of the used module are in Table 1.

In Fig. 4, a block diagram of the entire measurement device is displayed. The setup includes a Raspberry Pi 4 Model B, a 5G HAT from Waveshare, and a battery pack with a 5V output and a capacity of 40Ah.

In Fig. 5, a simple application for network performance measurement is shown. The application allows users to name the measurement, specify its duration in seconds, and select the preferred measurement band. There are two buttons: "Start" (green), which initiates the measurement process, and "Stop" (red), which terminates the measurement process. Real-time information is displayed below the button to obtain an overview of the measurement start, and a status bar visually indicates the progress of the measurement. The application runs locally directly on the measurement device and can be accessed via a web browser at the 'loopback' address with port 8050 (i.e., "http://127.0.0.1:8050/").

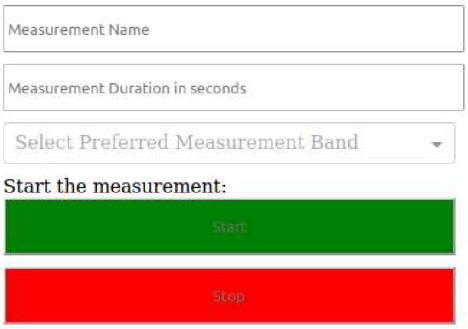

Figure 5. Application for measurement settings

2. Measurement procedure

3. Take the prepared cable (with USB Type C - USB Type C connectors) at your workstation and connect the battery pack to the Raspberry Pi. Using the second cable (with USB Type A - USB Micro connectors), connect the SIM8200EA-M2 module to the Raspberry Pi, or to the output from the battery pack (according to the block diagram on Figure 4). If everything is connected correctly, the **LED indicators** on both devices should light up. Next, use an HDMI cable (with HDMI Standard - HDMI Micro connectors) to connect the Raspberry Pi to the monitor at your workstation. Ensure that the monitor is turned on. The monitor should automatically detect the signal from the HDMI cable. **Wait for the operating system to start**.

In the top left corner of the screen, you will find the icon for the Firefox web browser. Click on it to start the browser. Be patient with loading the applications (due to the Raspberry Pi's performance, these tasks are not the fastest, so they may take some time). Once the web browser loads, enter the following address into the search bar: `127.0.0.1:8050` and press Enter on your keyboard. This will connect you to the application running on the Raspberry Pi, which is used to configure the measurements. If the application does not start, restart the Raspberry Pi by disconnecting and reconnecting the USB-C cable, and repeat the process.

If the application loads successfully and you see all the elements as shown in Figure 5, you can proceed further. Before setting up and starting the measurements, it is necessary to **restart the SIM8200EA-M2 module** using the reset button on the side of this module. The white reset button is located on the side, along with the USB Micro connector, the ON/OFF switch, and the headphone jack connector. After pressing the button, the module's green LED, indicating connection to the network, should stop flashing. Wait a few seconds until the module starts flashing the green LED again, indicating that it is connected to the network and ready for measurements.

Now it's time for the measurement part. The measurements will take place at **three locations**:

- The first one is located **directly at the workstation**, so you don't need to move anywhere.
- Perform the second measurement in a room **closest to one of the windows**.
- The third one **in the corridor near the emergency exit** facing the Pod Palackého Vrchem dormitory.

The procedure for all measurements will be similar:

First, set up the measurement using the application in the browser, i.e., choose a suitable measurement name in the Measurement Name section, for example, location1_band1 (for subsequent measurements, you can proceed similarly, i.e., location1_band3, location1_band20, location2_band1...). In the second section Measurement Duration in seconds, select the measurement duration in seconds. For the first measurement at the workstation, enter a value of 300. For subsequent measurements, where you will be moving, choose a slightly larger value, taking into account the movement to the respective location, so for example 320. In the next section Select Preferred Measurement Band, select the band to be measured. At each location, perform measurements for all three LTE bands (EUTRAN-BAND1, EUTRAN-BAND3, and EUTRAN-BAND20), totaling approximately 15 minutes of measurement at each location. After selecting the band, click on the green Start button, and a status bar and information indicating the start of the measurement should appear.

If the measurement is at a location other than directly at the workstation, disconnect the HDMI cable and move with the measuring device to the respective location. Wait for the measurement to complete (about 5 minutes). If you are measuring somewhere other than the workstation, return to the workstation, reconnect the HDMI cable to the Raspberry Pi, and check that the measurement has been completed. Then follow the same procedure for the other two bands. Be careful to change the name of measurement, so you don't overwrite the measured data with the new measurement.

4. After measuring all LTE bands at all three locations, prepare a USB flash drive and connect it to one of the USB ports on the Raspberry Pi. Using the icon named Files, navigate to the file explorer. In the left sidebar, navigate to the following path: Home > Desktop > MeasuredData. Select all the measured CSV files you

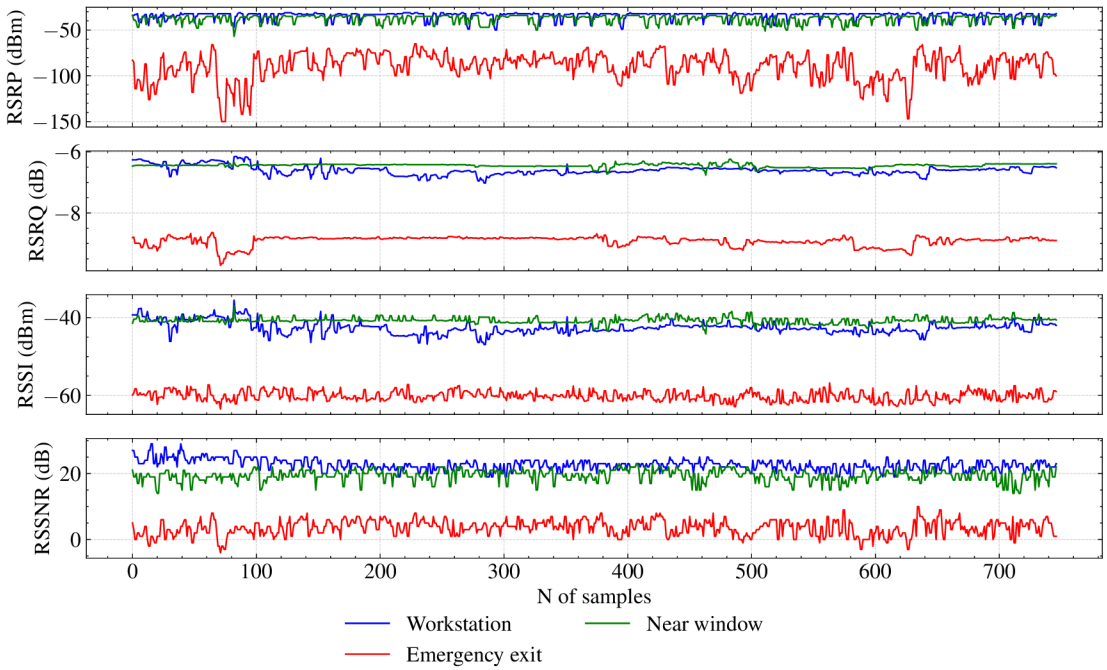

Figure 6. Measured values depicted graphically over time at individual stations for LTE Band 1

have recorded, then right-click on the selected files. Choose the option Copy to... . Another window with the file explorer will open, where you should see your USB flash drive in the left sidebar. Click on it (or create a new folder for the measured data if necessary) and click on the green Select button in the top right corner of the window. Remove all the measured data using the option Move to Trash and eject your USB flash drive from the Raspberry Pi. Disconnect all connections and return everything to its original state.

Create three graphs illustrating all the measured metrics (RSRP, RSRQ, RSSI, and RSSNR) over time for each measured band. To create these graphs, you can proceed as follows. Use suitable data visualization software such as Python with libraries like `Matplotlib` or `Seaborn`, or MATLAB. Create three graphs, each containing four subplots, with each subplot displaying one of the measured metrics over time. These graphs can be arranged in columns, where each column represents one metric. The graphs should be labeled with axis labels, legends, and other relevant information for proper understanding of the data. An example of such a graph for Band 1 is shown in Figure 6.

Next, create boxplots for each measured band, which are useful for visualizing the distribution and variability of data sets. They help quickly identify the median, quartiles, and potential outliers. When analyzing signal strength, boxplots can provide an overview of how values differ between different locations or bands. Boxplots allow easy comparison of multiple data sets on one graph, facilitating the identification of differences and trends. An example of boxplots for Band 1 is shown in Fig. 7.

5. From the created graphs, such as those in Fig. 6 and Fig. 7 for individual bands, perform a simple analysis and evaluate network coverage and reliability. Consider and observe fluctuations in **RSRP, RSRQ, RSSI, and RSSNR** over time at each location. Then compare the signal strength metrics at the workstation, emergency exit, and window to identify clear differences in average signal strength or variability. What might be the reason for weak signal in a given location or, conversely, the reason for strong signal? Recall the conditions during the measurements, and try to spot an eNodeB from the window if there is one. Analyze how different metrics correlate with each other (you can use the *corr()* function in MATLAB or in Python with the `pandas` and `numpy` libraries) and determine

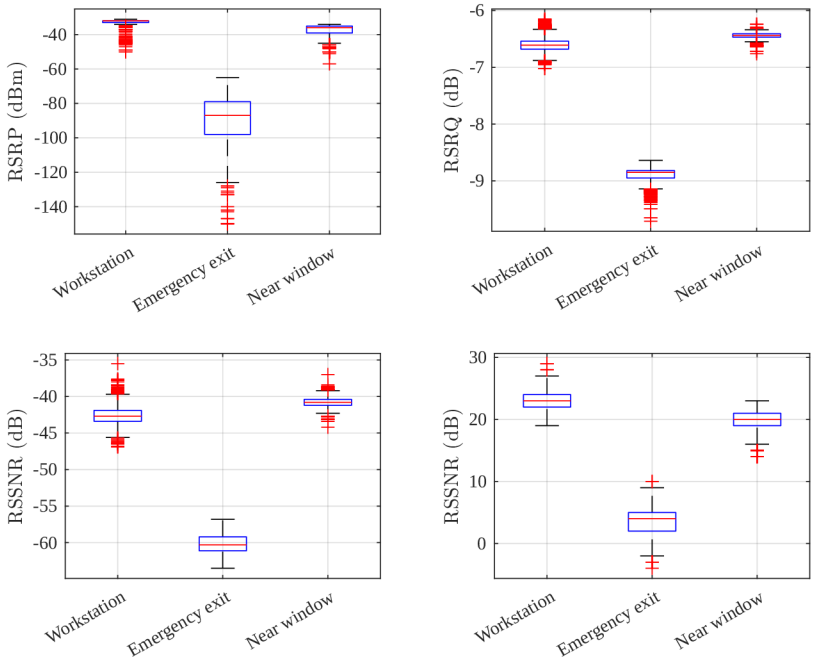

Figure 7. Measured values depicted graphically in boxplots at individual stations for LTE Band 1

whether they usually increase and decrease together or if there are situations where one metric is strong and the other is weak. Use visual inspection to observe trends and patterns on the graphs, supplemented by statistical analysis to calculate average signal strength, standard deviation for variability, and correlation coefficients between metrics. When comparing bands, take into account the frequency used by the band and the signal propagation characteristics at that frequency.

3. Reference, recommended literature

[1] 3GPP. *LTE; Evolved Universal Terrestrial Radio Access (E-UTRA); Physical channels and modulation (3GPP TS 36.211 version 14.2.0 Release 14)*. Online. `https://www.etsi.org/deliver/etsi_ts/136200_136299/136211/14.02.00_60/ts_136211v140200p.pdf`, [cited 2024-05-06]. Apr. 2017.

[2] 3GPP. *LTE; Evolved Universal Terrestrial Radio Access (E-UTRA); Physical layer; Measurements (3GPP TS 36.214 version 14.2.0 Release 14)*. Online. `https://www.etsi.org/deliver/etsi_ts/136200_136299/136214/14.02.00_60/ts_136214v140200p.pdf`, [cited 2024-05-06]. Apr. 2017.

[3] Český telekomunikační úřad. *Veřejné širokopásmové pokrytí mobilní sítě 4G a 5G v pásmech 700MHz, 800MHz, 1800MHz, 2100MHz, 2600MHz a 3600MHz*. Online. `https://vportal.ctu.gov.cz/mobile/mapa`, [cited 2024-05-06]. 2024.

[4] Halberd Bastion RF. *4G LTE*. Online. `https://halberdbastion.com/technology/cellular/4g-lte`, [cited 2024-05-06]. 2024.

[5] Huawei. *AR100, AR120, AR150, AR160, AR200, AR1200, AR2200, AR3200, and AR3600 V200R010 CLI-based Configuration Guide - Interface Management*. Online. `https://support.huawei.com/enterprise/en/doc/EDOC1100034069/f110c2e7/lte-network-architecture`, [cited 2024-05-06]. Aug. 2023.

[6] Janeba, Matej and Lehoczký, Peter and Galinski, Marek and Milesich, Tomáš and Danko, Ján and Kotuliak, Ivan. "*Evaluation of LTE and 5G qualitative parameters for V2X use cases*". In: *2022 IEEE Zooming Innovation in Consumer Technologies Conference (ZINC)*. 2022, pp. 165–169. DOI: `10.1109/ZINC55034.2022.9840619`.

[7] Keysight. *LTE Physical Layer Overview*. Online. https://helpfiles.keysight.com/csg/89600B/Webhelp/Subsystems/lte/content/lte_overview.htm, [cited 2024-05-06]. 2024.

[8] Sauter, Martin. *From GSM to LTE-Advanced Pro and 5G An Introduction to Mobile Networks and Mobile Broadband*. 4th ed. John Wiley & Sons, Ltd., 2021, p. 617. ISBN: 9781119714705.

4. Used devices and tools

- Waveshare 5G HAT with SIM8200EA-M2 module
- Raspberry Pi 4 Model B
- Battery pack 40 Ah
- Monitor
- USB, HDMI cables